

Faculty of Engineering and Science

**Matrix Characteristics Influence on Mechanical Performance
of Oil Palm Filler Reinforced Nanocomposite**

Wong Hwan Liang Dominick

0000-0001-7973-4012

**This thesis is presented for the Degree of
Master of Philosophy (Mechanical Engineering)
of
Curtin University**

September 2022

I declare that this thesis entitled “*MATRIX CHARACTERISTICS INFLUENCE ON MECHANICAL PERFORMANCE OF OIL PALM FILLER REINFORCED NANOCOMPOSITES*” is the result of my own research except as cited in the reference. The thesis has not been accepted for any degree and is not concurrently submitted in the candidature of any other degree.

Signature :

Name : WONG HWAN LIANG DOMINICK

ID : 18594999

Date : 23rd June 2022

“I hereby declare that I have read this thesis and in my opinion, this thesis is sufficient in terms of scope and quality for the degree of Master of Philosophy (Mechanical Engineering).”

Signature : _____
Supervisor : DR. MAHMOOD ANWAR
Date : 23rd June 2022

Signature : _____
Co - Supervisor : DR. SUJAN DEBNATH
Date : 23rd June 2022

"I as a Co-Author, declare that Wong Hwan Liang Dominick, developed the methodology, performed the experimental work, analysed data and wrote the following manuscripts that have been included as part of this thesis."

1. *"Degassing Process Influence on Tensile Strength of Neat E132 Epoxy Polymeric Materials"*
2. *"A Review: Recent Development of Natural Fiber-Reinforced Polymer Nanocomposites"*
3. *"Tensile Strength and Morphological Behavior of Treated Oil Palm Empty Fruit Bunch Particle Reinforced Polymeric Composite"*
4. *"The Influence Matrix Density on The Weibull Modulus of Natural Fiber Reinforced Nanocomposites"*
5. *"Composite Matrix Density Influence on The Morphological and Tensile Behavior of Natural Fiber Reinforced Nanocomposites"*

Signature : _____
Co-Author : DR. MAHMOOD ANWAR
Date : 23rd June 2022

Signature : _____
Co-Author : DR. SUJAN DEBNATH
Date : 23rd June 2022

Signature : _____
Co-Author : MR. ABDUL HAMID
Date : 23rd June 2022

Signature : _____
Co-Author : PROF DR. IZMAN BIN SUDIN
Date : 24th June 2022

“I as a Co-Author, declare that Wong Hwan Liang Dominick, developed the methodology, performed the experimental work, analysed data and wrote the following manuscripts that have been included as part of this thesis.”

1. *“Degassing Process Influence on Tensile Strength of Neat E132 Epoxy Polymeric Materials”*
2. *“Tensile Strength and Morphological Behavior of Treated Oil Pam Empty Fruit Bunch Particle Reinforced Polymeric Composite”*

Signature :
Co-Author : DR. ALOKESH PRAMANIK
Date : 27th June 2022

Signature :
Co-Author : DR. ANIMESH BASAK
Date : 27th June 2022

ACKNOWLEDGEMENT

Throughout the writing of this MPhil thesis, I have received a great amount of support and assistance from a variety of people. I would like to place on record, my sense of gratitude to one and all, who have directly or indirectly, lent their hands to me in this venture, especially during the height of the COVID-19 pandemic.

I would first like to give the utmost credit to my esteemed supervisor, Dr. Mahmood Anwar, for his invaluable supervision, support, and tutelage throughout the course of my studies. His emphasis on the learning process and the pursuit of knowledge has left a profound mark on me. Additionally, I would like to express my gratitude to Dr. Sujan Debnath for his treasured support from the very beginning and critiques of my methodologies and data. My sincere thanks also go to Mr. Michael Ding for his relentless training, insights and assistance throughout my experimental stage. These three individuals were instrumental in the completion of my experiments.

I would like to acknowledge the contribution of oil palm fibers from Sarawak Oil Palm Berhad and Mr. Martin Nguen for this assistance with its preparation.

It is my privilege to thank Ms. Fianita Anthony, Mr. Yap Zhi Wen and Ms. Wong Shin Yi for their wonderful companionship, encouragement, and support throughout my research period.

I would like to express my deep and sincere gratitude to Curtin Malaysia Graduate School and the Ministry of Higher Education Malaysia for their financial support and opportunities.

Last but not the least, my appreciation also goes out to my family. I thank them for their sacrifices and understanding.

ABSTRACT

Oil palm empty fruit bunch (OPEFB) fibers fillers have shown to exhibit good mechanical properties that can be used to produce environmentally friendlier composites. Studies have found that OPEFB and carbon nanoparticles can impart various mechanical improvements in polymer composites. Nevertheless, poor dispersion of the fillers in the composite is currently identified as one of the major challenging issues, resulting in deteriorated mechanical performances. However, the dispersion of nanoparticles is greatly influenced by the characteristics of the composite matrix, particularly the density of the fluidized epoxy matrix. Despite the reporting by several researchers, such issues as the polymer matrix characteristics influence on dispersion of nanoparticles as well as mechanical performances are yet to be established. In this research work, the influence of degassing processes, effects of sonication parameters, filler loadings, size and geometry of nanoparticles with respect to tensile performance were studied. Furthermore, the morphological and tensile behaviour was evaluated using epoxy matrices of varying densities. Neat epoxy resins were subjected to hot water, ultrasonic bath and vacuum to remove microvoids; it was found that the vacuum degassing method was the most effective, it displayed the least microvoids via optical microscopy and resulted in the highest average tensile strength at 48.8 MPa. It was also found that epoxy is more sensitive toward heat energy degradation compared to mechanical forces degradation. In addition, OPEFB composites with up to 10 wt% were fabricated; It was revealed that the addition of 0.3125 wt% - 2.5 wt% has a reinforcing effect, observing improvement up to 17.4% compared to its neat condition. Polymer matrices were subjected to various sonication parameters in terms of durations and amplitudes; it was found that the presence of ice helped reduce the formation of bubbles substantially. In addition, higher sonication amplitude and longer duration have been shown to impart greater intensity of chromatic alteration. With the addition of nanofillers, it was found that the filler combination of 0.3125 wt% OPEFB and 0.25 wt% nanofiller resulted in the most effective tensile strength at 57.9 MPa. In addition to that, it was found that there is a threshold limit of nanofiller size. Composites consisting of carbon nanotubes < 10nm were found to have a

drastic reduction in their tensile strength, by up to 34.5% decrease when compared to its larger variants. It was also revealed that the decrease in nanofiller dimensions (Tube > Platelets > Spherical) yielded greater tensile strength reinforcement. This indicated that instead of aspect ratio, the geometry and total surface area per volume fraction of the nanofiller plays a larger role in the efficiency of stress transfer under high-stress load. By investigating the influence of matrix density, it was discovered that the increase in matrix density increases the ductility and reliability of the composites. Further supported through SEM micrographs, it is revealed that the failure mode transitioned from brittle to intermediate to ductile for low, medium and high density respectively. The micrographs also showed that the tensile strength alongside the interfacial bonding between filler and matrix is greatly affected by the matrix density. Additionally, while it was observed that all polymer matrices displayed good dispersion, the use of high-density matrix presented a poorer distribution of fillers. Such findings would facilitate the development of effective matrix-based nanocomposite materials.

TABLE OF CONTENTS

ACKNOWLEDGEMENT	I
ABSTRACT	II
TABLE OF CONTENTS	IV
LIST OF TABLES	VII
LIST OF FIGURES	VIII
NOMENCLATURE	XII
PUBLICATIONS	XIII
CHAPTER 1 INTRODUCTION	1
1.1 Background	1
1.2 Researched Problem Statement	3
1.3 Research Questions	4
1.4 Objectives	4
1.5 Scope	5
CHAPTER 2 LITERATURE REVIEW	6
2.1 Composite	6
2.1.1 Matrix (Polymer)	8
2.1.2 Hand Lay-up	9
2.2 Natural Fiber	10
2.2.1 Components of Natural Fiber	12
2.2.2 Oil Palm Fiber	13
2.2.3 Natural Fiber Treatment	14
2.3 Nanomaterials	15
2.4 Classification of Composite	18
2.4.1 Particle Reinforced Composites	19
2.4.2 Natural Fiber Reinforced Composites	19
2.4.3 Polymer Nanocomposites	24
2.5 Ultrasonication	26
2.6 Polymer Degradation	26

2.7	Critical Review	28
2.8	Summary of Literature Review	49
2.9	Research Gap	49
CHAPTER 3 RESEARCH METHODOLOGY		50
3.1	Experimental Methodology	50
3.2	Materials Used	52
3.3	Equipment Used	53
3.4	Experimental Procedure	54
3.4.1	Degassing Process	54
3.4.2	Fiber Preparation / Treatment	56
3.4.3	Fabrication of OPEFB Composites	57
3.4.4	Sonication	58
3.4.5	Fabrication of OPEFB Reinforced Nanocomposites	59
3.5	Testing and Characterization Techniques	62
3.5.1	Mechanical Testing (Tensile Strength)	62
3.5.2	Surface & Fracture Morphology (Macrostructure and Microstructure)	63
3.6	Weibull Analysis	65
3.7	Waste Management	66
CHAPTER 4 RESULTS AND DISCUSSION		67
4.1	Effect of Degassing Process	67
4.1.1	Macrostructure of Degassed E132	67
4.1.2	Microstructure of Degassed E132	73
4.1.3	Tensile Strength of Degassed E132	75
4.2	Effects of OPEFB Fiber	77
4.2.1	Microstructure of OPEFB Fiber	77
4.2.2	Macrostructure of OPEFB Loading	79
4.2.3	Microstructure of OPEFB E132 Composites	80
4.2.4	Tensile Strength of E132 OPEFB Composites	85
4.3	Effect of Sonication (Preliminary Experiments)	89
4.3.1	Immersion Conditions at 20% Amplitude	89
4.3.2	Immersion Conditions at 40% Amplitude	92
4.3.3	Immersion Conditions at 60% Amplitude	94

4.3.4	Water & Ice Bath with Varying Amplitude for Extended Duration	96
4.4	Effects of Nanomaterials	100
4.4.1	Nanofiller (Carbon Nanoplatelets) Loadings	100
4.4.1.1	Surface Fracture of Nanocomposites Loading Variation	100
4.4.1.2	Tensile Strength of Nanocomposites Loading Variation	103
4.4.2	Nanofiller (Carbon Nanotube) Size	105
4.4.2.1	Surface Fracture of Nanofiller Size Variation	105
4.4.2.2	Tensile Strength of Nanofiller (Carbon Nanotube) Size Variation	107
4.4.3	Nanofiller Geometry	109
4.4.3.1	Surface Fracture of Nanofiller Geometry Variation	109
4.4.3.2	Tensile Strength of Nanofiller Geometry Variation	113
4.5	Effects of Matrix Density	116
4.5.1	Surface Morphology of Matrix Variation	116
4.5.2	Tensile Strength of Matrix Variation	124
4.5.3	Weibull Analysis and Modelling	127
4.6	Summary of Results and Discussion	131
CHAPTER 5 CONCLUSION		135
5.1	Conclusion	135
5.2	Recommendations	137
REFERENCES		138
APPENDIX A: SUMMARY OF CRITIAL REVIEW		161
APPENDIX B: SUMMARY OF WEIBULL ANALYSIS		174

LIST OF TABLES

Table 2:1: Main Functions of Matrix and Filler [54]	7
Table 2:2: Mechanical Properties of Common Polymers [63, 64, 65, 66]	9
Table 2:3: Comparison of Fibers Mechanical Properties [41, 77, 78]	13
Table 2:4: Example and Geometry of Nanofillers	17
Table 2:5: Comparison of Natural and Synthetic Fibers Mechanical Properties [41, 77, 78, 103, 113, 114, 115, 116, 117]	20
Table 2:6: Mechanical Properties of Natural Fiber Polymer Composites [38, 39, 118, 119]	21
Table 2:7: Mechanical Properties of Polymer Nanocomposite [66, 136, 137, 138]	24
Table 3:1: List of Materials	52
Table 3:2: List of Equipment and Tools	53
Table 4:1: Macrostructure of Epoxy under Different Degassing Process and Duration	69
Table 4:2: Surface Morphology of Empty Fruit Bunch Fiber	78
Table 4:3: Temperature Recorded under Different Conditions and Durations.	89
Table 4:4: Macrostructure of Epoxy under Different Conditions and Durations at 20%	91
Table 4:5: Temperature Recorded under Different Conditions and Durations.	92
Table 4:6: Macrostructure of Epoxy under Different Conditions and Durations at 40%	93
Table 4:7: Temperature Recorded under Different Conditions and Durations	94
Table 4:8: Macrostructure of Epoxy under Different Conditions and Duration at 60%	95
Table 4:9: Average Temperature Reduction of Water & Ice Bath	96
Table 4:10: Temperature Record under Different Conditions and Durations.	97
Table 4:11: Macrostructure of Epoxy under Different Amplitude with Extended Durations	98
Table 4:12: Summary of Weibull Moduli and Characteristic Strengths	130
Table 4:13: Experimental and Modelled Tensile Strength Values	130

LIST OF FIGURES

Figure 2.1: Matrix and Filler [53]	7
Figure 2.2: Manufacturing Techniques for Polymer Matrix [59]	8
Figure 2.3: Hand Lay-up [68]	10
Figure 2.4: Wet Hand Lay-up Process [67]	10
Figure 2.5: Classification of Natural Fiber [70]	11
Figure 2.6: Structure of a Natural Fiber [72]	12
Figure 2.7: Influence of plant constituents [68]	12
Figure 2.8: Surface Morphology of Fiber [87] (A: Treated Fiber B: Fibrillation of Fiber)	15
Figure 2.9: Morphology with Micro and Nano Fillers	15
Figure 2.10: Classification of Composites [107]	18
Figure 2.11: Failure Mechanisms in NFC [127] (A: Digital B: SEM Micrograph)	22
Figure 2.12: Properties of Polymer Nanocomposite [142]	25
Figure 2.13: Compressive Yield Strength [159]	29
Figure 2.14: Mechanical Properties of D230 & D400 [160] (A: Fracture Toughness, B: Tensile Stress)	30
Figure 2.15: Presence of Bubble using SEM [161]	31
Figure 2.16: TEM Images D400 [141] (a: ED600, b: ED900, c: D400)	32
Figure 2.17: Curvature of the Nanocomposite[162] (A: ML506 ,B: KER 828)	33
Figure 2.18: SEM Image of Silane OPEFB Composite [163]	34
Figure 2.19: Surface Morphology of Fiber Treatment [119] (a: Untreated, b: Hot Water, c: 1 w/v% NaOH, d: 5 w/v% NaOH)	35
Figure 2.20: Tensile Strength Under Varying Conditions [119] (A: Content wt%, B: Treatment)	36
Figure 2.21: Surface Morphology of OPEFB [164] (a: untreated, b:1 w/v%, c: 2 w/v%, d: 3w/v%, e: 4 w/v%, f: 5w/v%)	37

Figure 2.22: Effect of Fiber Loading [39]	38
Figure 2.23: Surface Morphology with 50 wt% of Fiber [38]	39
Figure 2.24: SEM Image of OPEFB Composite [41]	41
Figure 2.25: Qualitative and Quantitative Data of WMCNT Composite [43] (A Tensile Strength:, B: Surface Morphology)	43
Figure 2.26: Stress-Strain Curve of Functionalized Graphene [170]	44
Figure 2.27: Surface Morphology of 0.25 % GNP Composite [140] (a: 30 minutes, b: 1 hour, c: 2 hours, d: 3 hours)	45
Figure 2.28: Tensile Strength of Composites with varying GNP loadings [140] (A: Brittle Epoxy, B: Ductile Epoxy)	45
Figure 2.29: SEM Image of GNP Ductile Epoxy [140] (a: 0.25% GNP, b: 1% GNP, c: 2 % GNP)	46
Figure 2.30: Tensile Properties [171]	47
Figure 2.31: Fracture Surface Morphology [171] (C: NE, D: P-GrNP, E: G-GrNP ,F: E-GrNP)	47
Figure 2.32: GNF Enhancement on Tensile Strength.	48
Figure 3.1: Experimental Flow Chart	51
Figure 3.2: IKA C – MAG HS 7 hot plate	55
Figure 3.3: Cole Parmer Ultrasonic Cleaner	55
Figure 3.4: BVV vacuum chamber	55
Figure 3.5: Fiber Treatment Process	56
Figure 3.6: Composite Fabrication Process	57
Figure 3.7: LSP – 500 Ultrasonic Processor	58
Figure 3.8: Setup of Ice and Water Bath	58
Figure 3.9: Fillers and Epoxy Resin (A: Before Mixing, B: After Mixing)	59
Figure 3.10: (A) Physical Conditions of 0.175g Nanotubes (B) Liquid Phase of OPEFB Nanotube Composite Mixtures (Left: <10 nm, Middle: < 30nm, Right: < 90nm)	60
Figure 3.11: (A) Physical Conditions of 0.175g Nanofiller (B) Liquid Phase of OPEFB Nanofiller Composite Mixtures (Left: Nanoplatelets, Middle: Nanopowder, Right: Nanotube < 30nm)	61

Figure 3.12: Liquid Phase of OPEFB Nanopowder Composite Mixtures (A: Tarbender, B: EpoxAmite 102, C: E132)	61
Figure 3.13: Dimension [173]	62
Figure 3.14: Olympus BX53M Optical Microscope	63
Figure 3.15: Thermo Scientific Quattro S	63
Figure 3.16: Area of Surface Morphology [174]	63
Figure 3.17: Fracture Morphology Specimen Preparation	64
Figure 4.1A – C: Surface Morphologies Under Varying Degassing Methods (A: Hot Water, B: Ultrasonic Bath, C: Vacuum)	74
Figure 4.2: Tensile Strength of Neat E132 Epoxy Under Different Degassing Process	76
Figure 4.3: OPEFB Filler Loading by Weight Percentage	79
Figure 4.4A – G: Surface Morphologies of E132 OPEFB Composites (A: 0 wt% OPEFB, B: 0.3125 wt% OPEFB, C: 0.625 wt% OPEFB D: 1.25 wt% OPEFB, E: 2.5 wt% OPEFB, F: 5 wt% OPEFB, G: 10 wt% OPEFB)	81
Figure 4.5A – G: Surface Fracture of E132 OPEFB Composites (A: 0 wt% OPEFB, B: 0.3125 wt% OPEFB, C: 0.625 wt% OPEFB D: 1.25 wt% OPEFB, E: 2.5 wt% OPEFB, F: 5 wt% OPEFB, G: 10wt% OPEFB)	84
Figure 4.6: Tensile Strength of E132 OPEFB Composites	86
Figure 4.7: Physical Condition of 10 wt% OPEFB Composite After Test	87
Figure 4.8: Stress-Strain Curve of Neat Epoxy	88
Figure 4.9A – C: Surface Fracture of E132 Composite with 0.25 wt% Nanofiller (A: 0.3125 wt% OPEFB, B: 0.625 wt% OPEFB, C: 1 wt% OPEFB)	102
Figure 4.10: Tensile Strength of E132 OPEFB Nanocomposites (Filler Loading Variation) (Graphene Nanoplatelets)	104
Figure 4.11A – C: Surface Fracture of E132 OPEFB Nanocomposite (Nanotube Size Variation: A:<10nm, B:<30 nm, C: < 90nm)	106
Figure 4.12: Tensile Strength of E132 OPEFB Nanocomposites (Nanotube Size Variation)	108
Figure 4.13A – C: Surface Fracture of E132 OPEFB Nanocomposite (Nanofiller Geometry Variation: A: Tube, B: Platelets, C: Spherical)	110

Figure 4.14A – C: SEM Micrographs of E132 OPEFB Nanocomposite (Nanofiller Geometry Variation: A: Tube, B: Platelets, C: Spherical)	112
Figure 4.15: Tensile Strength of E132 OPEFB Nanocomposites (Filler Geometry Variation)	115
Figure 4.16A – C: Surface Fracture of OPEFB Nanocomposite (Matrix Density Variation: A: Tarbender, B: EpoxAmite 102, C: E132)	117
Figure 4.17A – C: SEM micrographs of OPEFB Nanocomposite (Matrix Density Variation: A: Tarbender, B: EpoxAmite 102, C: E132)	119
Figure 4.18A – C: SEM Micrographs of OPEFB Nanocomposite (Matrix Density Variation: A: Tarbender, B: EpoxAmite 102, C: E132)	121
Figure 4.19A – C: SEM Micrographs of OPEFB Nanocomposite (Matrix Density Variation: A: Tarbender, B: EpoxAmite 102, C: E132)	123
Figure 4.20: Tensile Strength of OPEFB Carbon Nanocomposites (Matrix Density Variation)	125
Figure 4.21: Stress-Strain Graph of OPEFB Carbon Nanocomposites (Matrix Density Variation)	126
Figure 4.22A – C: Weibull Plot of OPEFB Nanocomposite (Matrix Variation)	129
Figure 4.23: Summary of the Morphological and Tensile Behavior of Nanocomposites Under the Influence of Varying Matrix Density	134

NOMENCLATURE

Abbreviation / Symbol	Description
ASTM	American Society for Testing and Materials
DGEBA	Diglycidyl Ether of Bisphenol A
DGEBF	Diglycidyl Ether of Bisphenol F
DGEBM	Diglycidyl Ether of Bisphenol M
DMF	Dimethylformamide
GNP	Graphene Nanoplatelets
HE	Hexafluoropropylene
M_c	Molecular Weight Between Crosslink
MWCNT	Multiwalled Carbon Nanotube
NaOH	Sodium Hydroxide
NFC	Natural Fiber Composite
OPEFB	Oil Palm Empty Fruit Bunch
PC	Polycarbonate
PCL	Polycaprolactone
PLA	Poly (L-lactic acid)
PMMA	Polymethylmethacrylate
PNC	Polymer nanocomposites
PP	Polypropylene
PRC	Particle Reinforced Composite
PVDF	Polyvinylidene Fluoride
SCB	Sugarcane Bagasse
SEM	Scanning Electron Microscope
SWCNT	Single Walled Carbon Nanotube
w/v%	Percentage Weight / Volume
wt%	Weight Percent

PUBLICATIONS

D. Wong, M. Anwar, S. Debnath, A. H. Abdullah, S. Izman, and A. Pramanik, "Degassing Process Influence on Tensile Strength of Neat E132 Epoxy Polymeric Materials," *Materials Science Forum*, vol. 1026, pp. 129-135, 2021.

D. Wong, M. Anwar, S. Debnath, A. Hamid, and S. Izman, "A Review: Recent Development of Natural Fiber-Reinforced Polymer Nanocomposites," *JOM*, vol. 73, no. 8, pp. 2504-2515, 2021.

D. Wong, M. Anwar, S. Debnath, A. Hamid, S. Izman, A. K. Basak, and A. Pramani, "Tensile Strength and Morphological Behavior of Treated Oil Pam Empty Fruit Bunch Particle Reinforced Polymeric Composite," *Materials Science Forum*, vol. 1064, pp. 27-37, 2022

D. Wong, M. Anwar, S. Debnath, A. Hamid, and S. Izman, "The Influence Matrix Density on The Weibull Modulus of Natural Fiber Reinforced Nanocomposites," paper presented at the *International Conference on Applied Engineering, Materials and Mechanics*, 7th ICAEMM 2022, In Press.

D. Wong, M. Anwar, S. Debnath, A. Hamid, and S. Izman, "Composite Matrix Density Influence on The Morphological and Tensile Behavior of Natural Fiber Reinforced Nanocomposites," *JOM*, Submitted.

CHAPTER 1

INTRODUCTION

1.1 Background

Currently, polymer-based materials enjoy wide usage across various applications, ranging from household and industrial products to aerodynamics, biomedical, military hardware and even in the development of spacecraft [1, 2, 3, 4, 5, 6]. Polymer composites shine among other materials due to their high strength-to-weight ratio [7, 8]. They are highly sought-after due to their low maintenance requirements, low cost, lightweight, corrosion and impact-resistant properties [9, 10, 11].

Over the years, polymer nanocomposites have gained significant interest from researchers as it has been shown to improve their mechanical performances [12, 13]. The ideal application of a polymer depends on its composition, molecular weight and its monomer unit. Polymeric composites are reinforced with the addition of filler particles into the polymer matrix, resulting in a material with superior properties compared to the parent material. This also has the benefit of reducing the cost of production [2] as costly materials can be substituted with more economical alternatives. Interestingly, polymer nanocomposites have also been developed to bring other functions such as antimicrobial, sensing and detection for advanced food packaging [14].

In the study of composite materials, the matrix is the component that binds the filler particles to form the new material. Reinforcing materials are a form of fillers, they are added into the matrix of the parent material to enhance its mechanical properties. They are categorized into primary and secondary reinforcing materials, wherein the former fibers are commonly used to reinforce a certain material; in the latter, the properties of

the composite are further enhanced [3]. Researchers have been incorporating other materials into polymers as it has been shown to improve miscibility; mechanical properties such as tensile strength and electrical conductivity; additional unique qualities such as flame retardation, and anti-corrosion [4, 5, 15, 16]. These and other unique properties and performance improvements can be imparted due to the interactions between the polymer matrix and filler particles [17, 18]. As such, polymeric composite materials have been a competitive alternative to typical metallic and alloy materials such as aluminium and steel [19].

The high demand for environmentally friendly and sustainable materials has encouraged researchers to make use of natural materials [20]. The high demand for sustainable and environmental materials has allowed natural fiber polymer composites to emerge as a key research area [21, 22]. Natural fibers are more readily available, cheaper, simpler to manufacture and are more likely to create environmentally friendly biocomposites [23, 24, 25]. Meanwhile, synthetic fibers incur a higher cost, require more power for production, impose higher wear on equipment and in some cases, are more difficult to process [26, 27]. Natural fibers can be employed to reinforce polymers to reduce negative environmental impacts associated with non-renewable materials [28, 29, 30]. Recent studies have attempted to fabricate wind turbine blades with the use of natural fiber composites as the conventional materials will result in a 43-million-ton waste by the year 2050 [31].

Malaysia, known to be the second-largest exporter of palm oil in the world, disposes of one ton of empty fruit bunch for every ton of oil produced [32, 33]. This unutilized by-product poses negative impacts on the environment as it is a form of solid waste [34]; the unused agricultural waste would destabilize the aquatic environment, pollute the air and contaminate the soil [35]. Studies have found that oil palm empty fruit bunch (OPEFB) fiber epoxy composites exhibited various mechanical improvements such as tensile strength, impact toughness, longitudinal flexural strength, yield strength and modulus [36, 37, 38, 39, 40, 41]. However, like all other natural fibers, it is susceptible to high moisture absorption due to the presence of hemicellulose which could lead to dimensional instability and decomposition without sufficient treatment [42].

Various studies have concluded that small amounts of nanoparticles as fillers in a polymer matrix such as multiwalled nanotubes, silica nanoparticles and nano clay can improve composite reliability and properties such as tensile strength, elastic modulus, elongation at break and impact strength [43, 44, 45]. Polymer nanocomposites often have substantially better mechanical, thermal, and multifunctional characteristics than traditional polymer composites made with microfillers [46]. With the ongoing research on nanomaterials, it would help researchers better develop polymeric composites that can be highly customized to the requirements of the products based on their application and reduce the environmental impacts. Producing OPEFB reinforced epoxy nanocomposites is a potential way to improve the mechanical performances of the polymer composites and address the environmental issue by utilizing this type of fiber. However, the dispersion of nanofillers remains one of the main obstacles in the production of nanocomposites [47, 48, 49].

1.2 Researched Problem Statement

One of the major challenging issues identified in the production of nanocomposite is the dispersion of fillers. Poor dispersion leads to morphological instability and the formation of weak zones that result in the deterioration of the composites' mechanical performances. Proper dispersion is required in the production of competent composites for its effective performances as its interfacial bonding between the fillers and matrices improves. From literature, factors such as sonication duration, sonication amplitude, filler size, loading and shapes have been reported to influence the dispersion of fillers and the formation of voids within the composite. The presence of a void serves as a potential site for crack propagation and will negatively impact the performance of the composite. Matrix characteristics such as viscosity and molecular weight of the polymer have been reported to influence the dispersion of fillers and their mechanical performances to which lower values have better interfacial bonding and dispersion. To this date, limited research has been conducted to study the influence of matrix density on the degree of filler dispersion in polymer nanocomposites. In response to that, this research project aims to evaluate the

density influence of epoxy alongside the effect of the degassing process, and filler parameters (geometry, size, and loadings) on the degree of dispersion with mechanical performance in mind. The novelty of this research is to study the influence of epoxy density on oil palm fiber polymer nanocomposite.

1.3 Research Questions

- I. Which degassing process and OPEFB filler content provides the most effective tensile strength of the resultant composite?
- II. How do the sonication parameters and nanofiller property affect the matrix/composite?
- III. Does the matrix density of epoxy influence the filler dispersion and the tensile strength of a composite?

1.4 Objectives

The objectives of this research are:

- I. To identify an effective degassing process and OPEFB filler loading on the tensile strength of the resultant composite.
- II. To identify the effective sonication parameter (Duration & Amplitude) and effects of nanofiller properties (Geometry, Size and Loading) on the degree of dispersion and tensile strength.
- III. To evaluate the density influence of epoxy resin on the filler nanoparticle which affects the filler dispersion and tensile strength and to develop an effective model based on epoxy density behaviour.

1.5 Scope

The scope of this study covers the following:

- This research is limited to the fabrication of composites between epoxy polymers, OPEFB fibers and carbon nanoparticles (SWCNT, MWCNT, nanoplatelets and nanoparticle).
- This research is limited to the mechanical testing (tensile strength) of the fabricated composite in accordance with ASTM D638 at room temperature, drawn at a rate of 5mm/ minute.
- This research is limited to the characterization of the samples through optical microscopy and SEM.

CHAPTER 2

LITERATURE REVIEW

This chapter constitutes of review of the literature and evaluation of the researchers that are related to this research topic. Furthermore, the background of some topics, which are necessary for understanding the key features of this research will be discussed. The critical reviews and research gaps of this research project are also addressed.

2.1 Composite

Composite material is a combination of two or more materials with the main objective to attain superior properties and has been long used to solve technological problems. These materials can be designed and manufactured to replace materials such as steel and aluminium in various applications [19]. Its high strength-to-weight ratio and flexibility in design offer great usage in the field of engineering [50]. Composites can lower the coefficient of thermal expansion, increase mechanical strength, higher dimensional stability and wear resistance. However, it is difficult to fabricate and reproduce.

Composite materials are categorised into three distinct phases and their properties are directly influenced by the interaction between them. The matrix phase is continuous, the reinforcing phase is discontinuous (surrounded by a matrix) and the interface phase is, a combination of the filler/reinforcement phase [51]. The reinforcement material is also commonly termed filler. Figure 2.1 illustrates the matrix and filler in 3D.

The matrix is treated as a homogenous and isotropic material, that should account for more than 50% of the composites volume fraction; Likewise, the filler, bounded by the matrix should account for lesser than 50% [52]. The optimal combination of matrix

and filler varies between materials and is still a topic being currently being researched. This is because the properties of a composite are dependent on multiple factors that include the characteristics of the phases (matrix and filler), dimension of filler, morphology and interfacial interactions. Table 2.1 list the main functions of the matrix and filler.

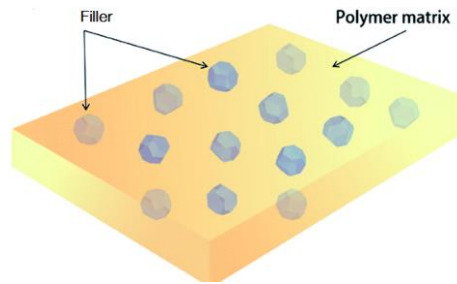


Figure 2.1: Matrix and Filler [53]

Table 2.1: Main Functions of Matrix and Filler [54]

Main Function	
Matrix	Filler
Provide Shape	Provide Strength and Structural Properties
Protect Filler from Chemical and Mechanical Damage	Impart Unique Properties
Bind and Transfer Applied Load to the Filler	Reduce Thermal Expansion

2.1.1 Matrix (Polymer)

The use of polymer as a matrix can also be classified into two distinct types, thermosetting and thermoplastics. The most widely used matrix in polymer composite is epoxy resin (thermosetting) as it presents low shrinkage, low toxicity, has high industrial applications and possesses good adhesion [55]. An effective matrix of a composite should not only provide proper stress diffusion and redistribution of the applied load but also provide good adhesion. Strong adhesion between the matrix and filler will increase the integrity of the composite [52].

Based on the type of polymers, different techniques are used to manufacture composites as depicted in Figure 2.2. Hand layup is considered to be the most basic and labour-intensive method that involves the manual application of matrix and filler [56]. Other methods such as injection moulding, compression moulding and resin transfer moulding where machines are used and are more suited for high-volume applications [57]. The methods presented in Figure 2.2 are classified as primary manufacturing as the final shape of the product is achieved directly. In contrast, secondary manufacturing methods require further operations through machining, such as drilling and milling [58].

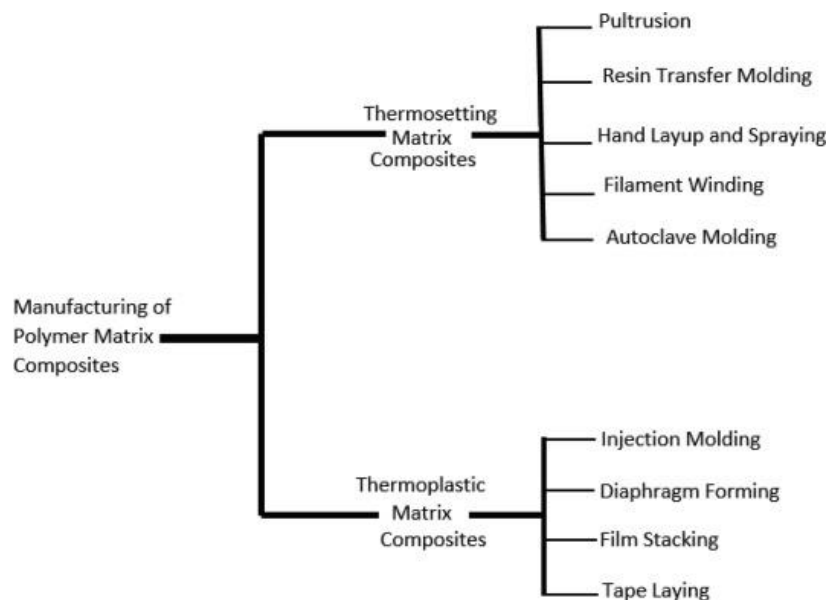


Figure 2.2: Manufacturing Techniques for Polymer Matrix [59]

When considering the use of polymer, several factors such as molecular weight and its viscosity must be taken into consideration; they can affect its mechanical properties and workability. Mechanical performance and processing are linked to polymer molecular weight [60]; Higher molecular weight polymer results in improved toughness and rigidity at the cost of increased viscosity [61]. The viscosity of the polymer in the molten state increases as the molecular weight increases. This is due to the rise in chain entanglement within the polymer [62]. Thus, making the processing of polymer more challenging. When selecting the type of matrix, the liquid matrix should have low viscosity to allow the matrix to penetrate between the filler, and to allow good wettability between the filler and matrix [52]. Table 2.2 presents the mechanical properties of common polymers.

Table 2.2: Mechanical Properties of Common Polymers [63, 64, 65, 66]

Material	Tensile Strength (MPa)	Elastic Modulus (GPa)
Polycaprolactone (PCL)	4 - 785	0.21 – 0.44
Polyester	20.5 – 34.94	0.19 – 0.43
Polycarbonate (PC)	55 – 75	2 – 2.4
Poly (L-lactic acid) (PLLA)	60 – 70	2 - 4
Polymethylmethacrylate (PMMA)	≈ 33	≈ 1.8

2.1.2 Hand Lay-up

The hand layup technique is an open-forming method used to produce composite materials. It is a four-step process, starting with mould preparation, gel coating, lay-up and ending with curing [67]. The surface of the mould is treated with an antiadhesive agent to prevent sticking. The fiber is then manually placed onto the mould, followed by the application of resin using a brush. A hand roller is then used to roll the wet composite

to enhance the interaction between the fiber and the matrix, removing trapped air bubbles [68]. In addition, this process promotes a uniform distribution of the resin and achieves the required thickness. Lastly, the composite is left to cure under atmospheric conditions. These processes are highly dependent on the skill of the operator [69]. Figure 2.3 depicts the schematic of the method.

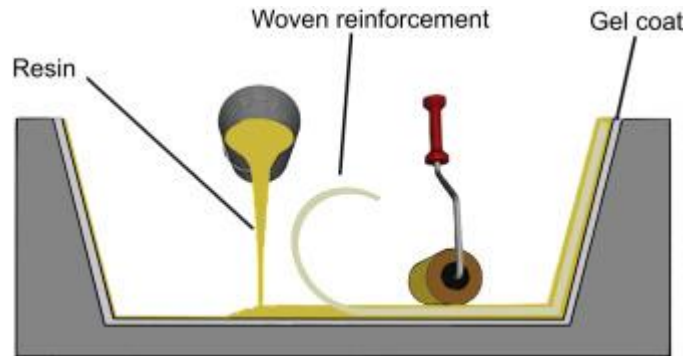


Figure 2.3: Hand Lay-up [68]

Wet hand lay-up is a variation of the hand layup technique, to which a roller is not used. Instead, fillers are gradually added to the resin and stirred until a uniform distribution is achieved. The curing agent is then added to the resin. The composite mixture is then poured into the mould. Similarly, it is then allowed to cure at room temperature. Figure 2.4 presents the flow of this variation of composite fabrication.

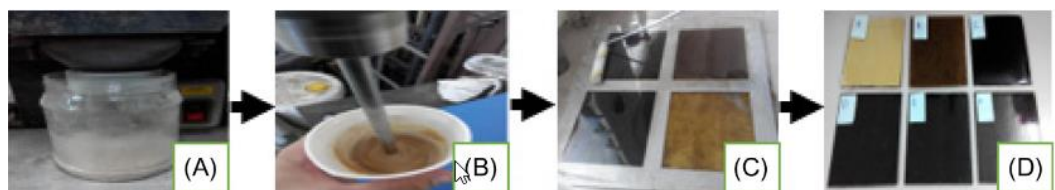


Figure 2.4: Wet Hand Lay-up Process [67]

2.2 Natural Fiber

Natural fibers are easily obtainable with the benefit of being abundantly available. They are classified based on their point of origin (plant, animal and mineral). The most widespread natural fiber and most natural form are yielded from plant fibers. Plant fibers

can be further categorized based on parts of the plants such as bast, leaf, fruits and seed) [70]. Figure 2.5 illustrates the classification of natural fiber.

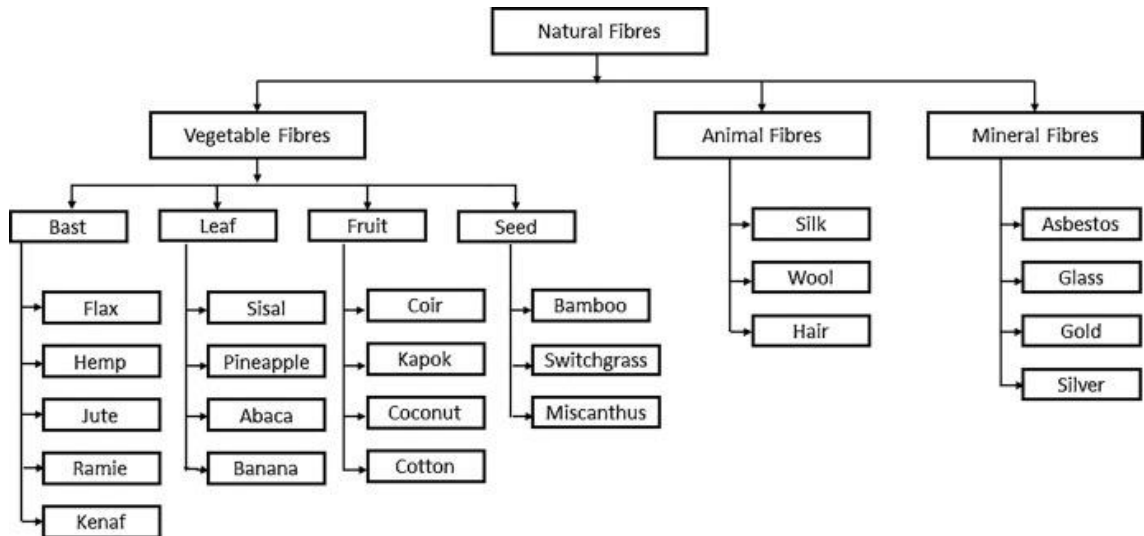


Figure 2.5: Classification of Natural Fiber [70]

2.2.1 Components of Natural Fiber

Natural fibers are a complex natural composite made of cellulose, hemicellulose, lignin, pectin and waxy substances as shown in Figure 2.6 [71, 72]. Cellulose is the most important structural component of the natural fiber, its crystallinity regulates its physical properties (strength and stability) and is known to have poor thermal resistance [72, 73]. Hemicellulose while associated with cellulose microfibrils, it embeds cellulose into a matrix. It is by nature very hydrophilic and contributes to the swelling tendency of the fiber [74]. Lignin not only imparts rigidity to the plant but also acts as a chemical adhesive within the fibers. On the other hand, pectin imparts flexibility and its degradation results in a reduction in mechanical strength [73]. These components play various roles within the fiber. Figure 2.7 presents its influence based on its properties [75].

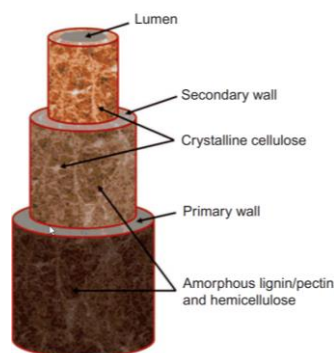


Figure 2.6: Structure of a Natural Fiber [72]

Strength	Lignin → Hemicellulose + Lignin → Non-crystalline Cellulose → Crystalline
Thermal Degradation	Lignin → Cellulose → Hemicellulose
Biological Degradation	Lignin → Crystalline Cellulose → Non-crystalline Cellulose
Moisture Absorption	Crystalline Cellulose → Lignin → Non-crystalline Cellulose → Hemicellulose
UV Degradation	Crystalline Cellulose → Non-crystalline Cellulose → Hemicellulose → Lignin

Figure 2.7: Influence of plant constituents [68]

2.2.2 Oil Palm Fiber

Oil palm fiber is a lignocellulosic fiber, where the cellulose and hemicellulose are bonded in a lignin matrix; [42]. It consist of 50.4 % cellulose, 21.9 % hemicellulose, 10 % lignin and 17.7 % ash [76]. Oil palm fibers have significantly lower densities compared to other natural and synthetic fibers as presented in the table below. Table 2.3 compares the mechanical properties of fibers. Furthermore, it has displayed greater toughness compared to other natural fibers such as coir, hemp and sisal [36].

Table 2:3: Comparison of Fibers Mechanical Properties [41, 77, 78]

Fiber	Density (g/cm ³)	Tensile Strength (MPa)	Young's Modulus (GPa)	Elongation at break (%)
Oil Palm	0.7 – 1.6	60 – 81	1 – 9	8 – 18
Coir	1.2 – 1.5	105 – 175	4 – 6	17 – 47
Hemp	1.5	690	27.6	1.6
Carbon	1.8	1550 – 6960	159 – 965	2.5 – 5.17
Glass	2.5 – 2.7	1034 – 3792	72	1.5 – 3.5
Steel	7.8	200 – 2760	200	0.5 – 35

Oil palm empty fruit bunch (OPEFB) is a fibrous by-product of crude palm oil extraction. It is estimated that 0.2 – 0.3 tons of OPEFB are produced from one ton of fresh fruit bunch [79]. Due to its abundance, low cost and mechanical properties, it has gained the attention of researchers to have high potential in the production of bioproducts [80]. It can be alternative material to be used in the manufacturing industry and composite production. Such availability is prominent in countries such as Indonesia and Malaysia, which are the top two largest palm oil producers in the world [81]. However, like all other natural fibers, it is susceptible to high moisture absorption due to the presence of hemicellulose which could lead to dimensional instability and decomposition without sufficient treatment.

2.2.3 Natural Fiber Treatment

The main drawback of natural fibers as a filler is the result of poor interfacial interaction between the fiber and the matrix; This is attributed to the hydrophilic property of the natural fiber. Therefore, chemical treatments and surface treatments have been employed to improve its compatibility and mechanical performance [82]. Among the various types of natural fiber treatments, physical treatments are less preferred over chemicals as the former results in mechanical damage to the fiber, thus resulting in poorer mechanical properties [36].

Chemical treatments have been shown to remove non-cellulosic contents found on the surface of the fibers which has a direct influence on the properties of the composites [83]. The removal of impurities provides a rougher surface of the fiber, increasing the number of sites for the fiber and polymer to react [84]. This would allow for greater interfacial bonding between the fiber of the matrix. Furthermore, it can also improve the fibers wettability, surface morphology and tensile strength [82].

Treating natural fiber with the use of chemical solutions involves two processes - soaking and drying. Depending on the researcher, various steps could be added such as prewashing and the use of ultrasound. The process of using an alkaline solution to treat the fiber is known as alkalization. This form of treatment has been reported to better reinforce the composite by increasing its hydrophobicity while being an easy, effective and economical process [85]. Furthermore, it has been reported that alkalization of natural fibers breaks the bundle into smaller bundles, it is a process known as fibrillation [86]. Thus, improving the interfacial bonding, and helping to distribute the applied load. The drying process is an important step in the prevention of mould formation and may alter its properties. Figure 2.8A shows the surface morphology of treated natural fiber and Figure 2.8B presents the fibrillation of the fiber.

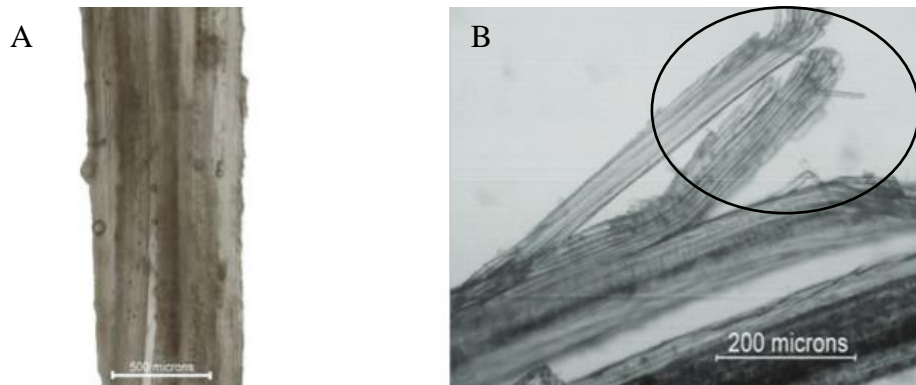


Figure 2.8: Surface Morphology of Fiber [87]
 (A: Treated Fiber B: Fibrillation of Fiber)

2.3 Nanomaterials

Nanotechnology and advancements in manufacturing have led to the fabrication of nanomaterials. Materials with structural units, grains, particles, fibers or other parts in at least one dimension smaller than 100 nm are classified as nanomaterials [88]. They have a myriad of applications in industries such as power generation, engineering, medical and the list continues to grow as more uses for nanomaterials are being developed [89]. Figure 2.9 represents a scheme of the morphology of composites with micro and nanofillers.

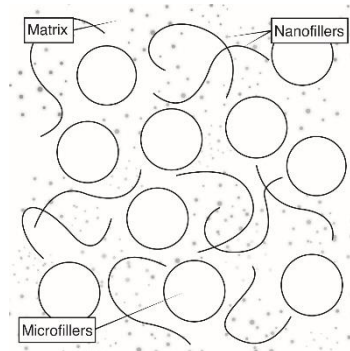


Figure 2.9: Morphology with Micro and Nano Fillers

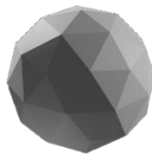
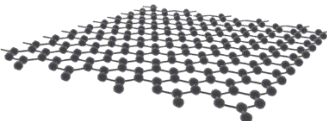
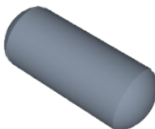
Nanomaterial used as a filler is termed as nanofiller, Nanofillers are categorized based on shapes such as sheet, spherical and fibrous (rod-like) [90, 91]. A study conducted by Zhang et al. [92] explained that the structure (shape and size) of fillers affect the number and mobility of interfacial beads which form the polymer-filler network. The diffusion coefficient of beads and stress contribution are also affected, which influences the strength of the network. For any shapes, a larger filler size increases the void content while simultaneously decreasing its stress contribution, interfacial beads number and mobility. Rod shape filler displays a minimal decrease in stress contribution while decreasing its diffusion coefficient; thus, enhancing its network. It was concluded that rod-shaped fillers are best in reinforcing the matrix followed by spherical and sheet shapes. Table 2.4 illustrates the three different shaped nanofillers.

Nanofillers with all three dimensions less than 100nm are 0D fillers and are usually spherical or cubical shaped [93]. These nanofillers offer novel properties such as optical stability, chemical inertness, cellular permeability and biocompatibility. Therefore, it has great biomedical application, utilizing it in nanomedicine, bioelectronics and biosensors [94].

1D fillers have one of their dimensions less than 100nm and are usually in the shape of sheets or plates [93, 95]. Due to their excellent electrical, magnetic and optical properties, it is widely used in applications such as microelectronics, biosensors, and coatings [96, 97].

Nanofillers with two dimensions less than 100nm are classified as 2D fillers with the shape of a tube, fiber or filament [93, 95]. These types of filler have shown to be useful in a variety of applications such as energy, sensors, photocatalysts, electronics and optoelectronics. In addition, it has been found to impart better flame retardant property compared to 1D and 3D fillers [93]. Furthermore, 2D fillers have also been found to provide a higher degree of reinforcement compared to 3D fillers due to their higher aspect ratio [98].

Table 2:4: Example and Geometry of Nanofillers

Name	Examples	Structure
Spherical	Silica Nanoparticle Fullerene	
Sheet	Graphene Nanosheet	
Fiber / Rod	Cellulose Nanocrystals Carbon Nanotubes	

The diameter of SWCNT ($1 < d < 2$ nm) is inherently smaller than WMCNT ($d > 5$ nm), thus effectively changing its aspect ratio and its properties [99]. A higher aspect ratio of the nanotube has been reported to display better conductivity and mechanical properties. The improvement in mechanical properties such as tensile strength, elasticity and toughness is attributed to a greater load transfer between the filler and the matrix [100]; this mechanics depends on its interface bonding where a smaller diameter provides a stronger interface, improving its performance [101, 102].

Although the use of nanomaterials can impart significant improvements to the polymer composites, it does have its downsides. The high surface area of nanomaterials causes morphological instability that results in the aggregation and agglomeration of the particles [103]. Aggregation and agglomeration are the formations of clusters that could increase their size above the nano level. The main difference between them is aggregations are loosely coherent whereas agglomerations are rigid [104]. Aggregation occurs due to interfacial chemical reactions and its particle transport mechanism [105] while agglomeration is attributed to the strong Van der Waals forces between the particles [106].

2.4 Classification of Composite

Composite materials are classified according to the characteristics of their filler. The three main classifications are particle-reinforced, fiber-reinforced and structural as depicted in Figure 2.10. Each type of composite offers different improvements; Particle Reinforced Composite (PRC) can improve machinability and increase wear and abrasion resistance while fiber reinforced offers greater improvement in mechanical strength. On the other hand, structural composite provides greater performance that is orientation-dependent [107].

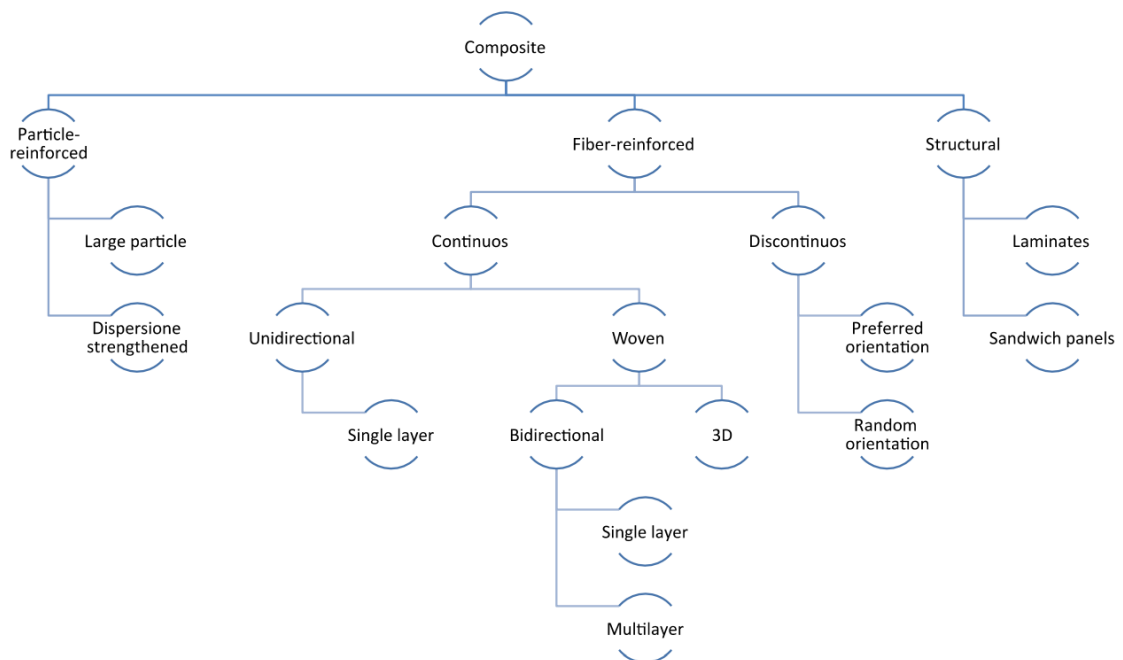


Figure 2.10: Classification of Composites [107]

2.4.1 Particle Reinforced Composites

The effective behaviours of the PRC have been an active research area for many years, specifically on its mechanical properties and microstructure [108]. PRC has recently gained attraction due to its cost-effectiveness, isotropic properties and high degree of wear resistance [109].

Large particle and dispersion-strengthened composites are the two subclassifications of PRC which are dependent on the filler particle; When particle-matrix interaction is not treated at the atomic/molecular level it is classified as a large particle, whereas dispersion-strengthened does, containing particles with the size of 10 – 100nm [110].

In PMC, the matrix bears the main portion of the applied load while the dispersed particle hinders the motion of dislocation, limiting its plastic deformation [107, 110]. Hence, improving the mechanical properties of composites such as hardness, yield strength and tensile strength.

2.4.2 Natural Fiber Reinforced Composites

The combination of plant-derived fibers and the polymeric matrix is termed a natural fiber composite (NFC). Compared to bulk matrices, fibers have better mechanical properties as their reduced dimension leads to fewer imperfections [17]. These materials have seen significant development over the years due to their lower density, high specific strength, and renewable nature. The following factors have been reported to affect the performance of NFC [111]:

- I. Orientation of fiber
- II. Strength of fiber
- III. Physical properties of fiber
- IV. Interfacial adhesion property of fiber

In addition, NFC provides benefits such as producing less pollution during fabrication, lower fuel consumption, reduced gas emission during transport and significant reduction of disposal and energy-consuming disposal efforts [112]. Natural fibers are more readily available, cheaper, simpler to manufacture and are more likely to create environmentally friendly biocomposites [23, 24, 25]. Meanwhile, synthetic fibers incur a higher cost, require more power for production, impose higher wear on equipment and in some cases, are more difficult to process [26, 27]. Therefore, many researchers are in favour of natural fibers over their synthetic counterparts. Table 2.5 compares the mechanical properties of natural and synthetic fibers while Table 2.6 presents the mechanical properties of recently published natural fiber composites.

Table 2:5: Comparison of Natural and Synthetic Fibers Mechanical Properties [41, 77, 78, 103, 113, 114, 115, 116, 117]

Material	Density (g/cm ³)	Tensile Strength (MPa)	Elastic Modulus (GPa)
Oil Palm Fiber	0.7 – 1.6	60 – 81	1 – 9
Kevlar TM	1.1	3500	124 – 130
Coir Fiber	1.2 – 1.5	105 – 175	4 – 6
Hemp Fiber	1.5	690	27.6
Carbon Fiber	1.8	1550 – 6960	159 – 965
Glass Fiber	2.5 – 2.7	1034 – 3792	72
Steel Fiber	7.8	200 – 2760	200

Table 2:6: Mechanical Properties of Natural Fiber Polymer Composites [38, 39, 118, 119]

Material	Tensile Strength (MPa)	Elastic Modulus (GPa)
PCL + OPEFB	9.8 – 48.4	N/A
Polyester + Coir Fiber	17.6 – 24.5	830.9 – 1328.5
Wheat Gluten Bioplastic + OPEFB	≈ 6 – 10.4	N/A
Urea Formaldehyde + Oil Palm Frond	2.8 – 3.9	N/A

However, various drawbacks can be introduced such as increased moisture absorption, lower operating temperature, possible incompatibility and difficulties in predicting mechanical properties [120]. It should also be noted that the condition of the soil, surrounding weather, and processing methods are factors that can influence the characteristic of the natural fiber [121].

The failure mechanism in NFC mainly consists of 3 different forms of defects, fiber pull-out, poor dispersion, and presence of the void. These defects are illustrated in Figure 2.11A and Figure 2.11B. The effect of fiber pull-out has been reported for many years [122, 123]. This originates from the weak interfacial adhesion when subject to tension as the adhesion is insufficient to transfer the stress from the polymer to the fiber until it fractures [17]. Moving on, voids are the presence of unfilled regions within the polymer [124]. It is one of the most common and significant types of manufacturing-induced defect, which negatively impacts the properties such as the tensile strength of the composites [125, 126]. It is believed that mechanical air entrapment is the main cause of void formations. However, other factors such as geometry, mould complexity, resin properties and flow rate can affect its size and location. For every 1 % of void content found in the composite, its mechanical properties can be reduced by up to 20 % [125]. Smaller voids in composites can be combined to form larger voids, introducing further defects [92]. Ramlee et al. [41] have also reported that the lower density fiber contained fewer void content when compared to a higher density fiber counterpart.

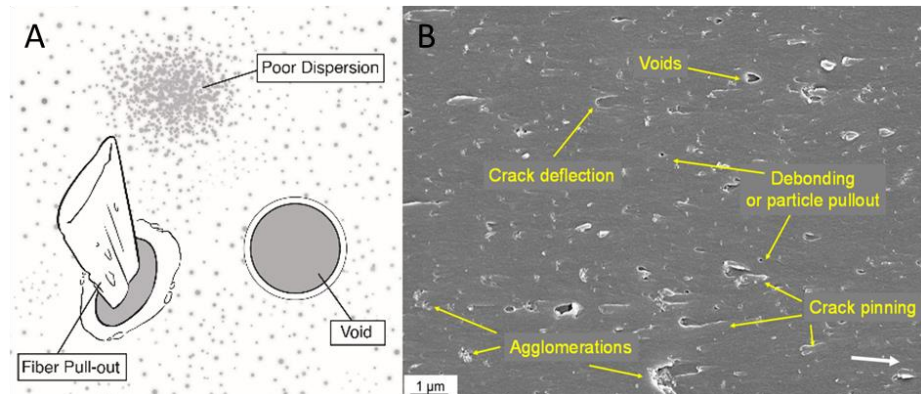


Figure 2.11: Failure Mechanisms in NFC [127]
 (A: Digital B: SEM Micrograph)

Various studies have concluded that the inclusion of natural fibers can improve the mechanical properties of the composite due to the interfacial bonding (hydrogen and covalent bonds) between fiber and hydroxyl groups present in the polymer [36, 37]. The increase of fiber loading has been shown to enhance properties such as stiffness, hardness, tensile strength, yield strength and sound absorption of the composites but at the cost of their resilience, toughness and thermal stability [39, 40].

Automotive companies such as BMW, Volkswagen, Mercedes, Ford and Proton have adopted the use of NFCs in their vehicles [111]. They are highly sought-after due to their low maintenance requirements, low cost, lightweight, corrosion and impact-resistant properties [9, 10]. The lightweight property of NFCs can be used to fabricate interior components, where a 25 % reduction in vehicular weight could reduce the fuel consumption by \$220 billion in energy cost while significantly reducing harmful emissions [128, 129]. Boland et al. indicated that the substitution of synthetic fiber for natural fiber would reduce the energy demand by up to 9.2 % and greenhouse gas emissions up to 18.6 % [130].

As exciting as the potential uses of NFCs, some drawbacks and challenges need to be overcome. These drawbacks of using natural fiber as fillers include [72]:

1. Inconsistent fiber quality from batch to batch
2. High Flammability.
3. Limited performance (Tensile, impact, thermal resistance).
4. Susceptible to moisture absorption.
5. Odour and Fogging

The use of natural fibers alone may also present several issues under varying environmental conditions, where its mechanical properties, flammability and other variations are negatively affected [131, 132]; For example, NFCs tensile and flexural strength will decrease with the increase of moisture content when subjected to humid conditions. In addition, NFCs will not be useful at elevated temperatures, as their properties will alter above 230 °C due to thermal degradation [131, 133].

2.4.3 Polymer Nanocomposites

Polymer nanocomposites (PNC) are the combination of polymer matrix and the use of nanomaterial as fillers. PNC exhibits various advantages in properties such as mechanical, electrical, thermal stability and flame retardancy [134, 135]. Table 2.7 presents the published mechanical properties of polymer nanocomposites. In addition, the formation of suitable PNC can generate new properties for the material presented in Figure 2.12.

Table 2:7: Mechanical Properties of Polymer Nanocomposite [66, 136, 137, 138]

Material	Tensile Strength (MPa)	Elastic Modulus (GPa)
PCL – Poly (lactic acid) – Montmorillonite	38.6	1.18
Polyester – Hydroxyapatite Nanowire	15.0 – 68.0	≈ 0.73 – 1.47
PC – Boron Nitride Nanotubes	34.7 – 62.0	2.32 – 2.80
PMMA – Reduced Graphene Oxide – Hematite Nanoparticles	≈ 36.0 – 73.9	≈ 2.0 – 4.4

Research has found that the size, shape, volume fraction and state of dispersion of the nanofiller will have a direct effect on the properties of the composite [93]. The combination of improved properties with weight reduction, and lower product cost provides important commercial application in the transport sector. Their distinctive enhancement of the composite performance still attracts the interest of researchers even after decades of study. This development resulted in their increase in usage for a variety of applications that can include fields such as aeronautics, automotive, electronics, medical equipment and consumer goods [134, 139].

There are a few known challenges in the fabrication of PNC, the manufacturing industries currently lack the methods for large-scale production [134]. However, one of the major challenging issues identified is the poor dispersion of nanoparticles during the fabrication process [47, 48], preventing the formation of agglomerates and aggregates. Several methods have been explored to mitigate this issue. For example, a research study found that after one hour of ultrasonication where the particles in the solution were agitated, no significant clusters were observed in the mixture [140]. In another research, it was reported that with a higher molecular weight of curing agents, the dispersion of nanoparticles can be improved [141]. However, the effects of sonication parameters on the polymer matrix and matrix density have been scarcely reported.

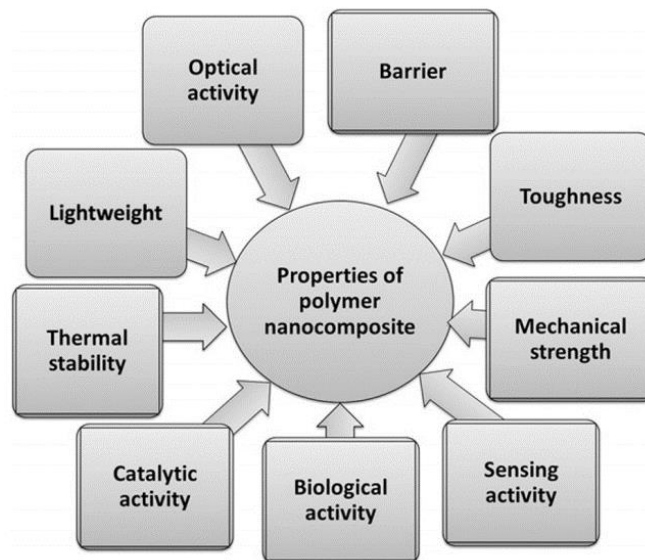


Figure 2.12: Properties of Polymer Nanocomposite [142]

2.5 Ultrasonication

The application of acoustic vibrations to a sample is known as sonication, and frequencies above the 20 kHz range are classified as ultrasonication. When the vibrations are transmitted through a liquid medium, cavitation occurs [143]. The collapse of small bubbles creates high pressure and speed liquid jets that result in strong hydrodynamic shear forces [144]. Ultrasonication has been a common technique used to disperse nanomaterials as its de-cluster the nanoparticles and is an alternative to conventional mixers such as high-speed mixers [145, 146]. This homogenization method requires no mechanical forces, easy to perform and is overall a clean process [144].

While the application of ultrasonic can improve the dispersion of filler materials, it has been reported to degrade the polymer. The cavitation effects generated in the polymer solution have been identified to be the cause of degradation in polymer solutions [147]. As ultrasonic waves pass through the polymer solution, the localized shear gradient produces tears of molecules leading to chain scission and the decreases in molecular weight [148].

2.6 Polymer Degradation

The degradation of polymers can affect changes both in their chemical structures and their physical properties. Heat, light, chemicals and any externally applied force on the polymer can alter its colour, and shape and lead to a reduction in tensile strength and molecular weight due to changes in its polymer chain [149]. The alteration in the colour of the polymer can be termed yellowing/browning.

Thermal degradation can be defined as the loss of physical, mechanical, or electrical qualities caused by the effect of heat or elevated temperature on the material, product or assembly [150]. A polymer degrades at a point of temperature that causes higher vibrational energy, resulting in a bond rupture [151]. Furthermore, the presence of oxygen has modest effects on the initial decomposition temperature in most cases,

therefore bond ruptures are mostly related to thermal processes rather than oxidative processes [151]. The addition of heat also alters the co-planar configuration of the polymer, thus changing its conjugation length, and affecting the absorption of chromatic wavelength. Thus, exhibiting chromatic alterations of the polymer [152]. Thermal degradation of polymers is separated into two distinct reactions, the random chain scission and chain-end scission of C – C bonds, resulting in the reduction of molecular weight and generating volatile products respectively [148, 150]. For the random chain scission mechanism, the backbone of the polymer is broken down randomly and forms free radicals; this causes the polymer to separate into smaller molecules, resulting in the rapid reduction in molecular weight and mechanical strength of the polymer [150, 153]. For chain-end scission mechanism, also known as depolymerization. It is an unstoppable process, beginning from the chained end of the polymer and then successively releasing the monomers. The molecular weight of the polymer gradually decreases, and a considerable quantity will be discharged at the same time [150, 153].

Thermal oxidation is a process that involves the consumption of oxygen as well as a radical chain process, triggered by the decomposition of hydroperoxide [154, 155]. However, it is not clear whether the kinetic parameters of the reaction are common to all epoxy resin [155]. The influence of the thermal oxidation degradation mechanism depends on the chemical structure of the polymer and the majority of the polymers are susceptible to it [156]. Krauklis et al. [157] investigation has revealed that the yellowing of epoxy is due to the thermal oxidative carbonyl formation.

Mechanochemical degradation is defined as the progressive changes in the structure and properties of a material under the effects of an external mechanical field (ultrasound, vibratory milling, etc) [158]; These changes involve the deformation of chains, the rupture of the chemical bonds in the main valance, and the reorganization of super molecular structure. The degradation effects not only rely on the nature and duration of the externally applied action but also on the properties of the material itself.

2.7 Critical Review

In 2020, Reyes et al. [159] studied the effect of varying structural features of the epoxy system by varying the resin and its hardener; focusing on its mechanical and thermal properties. The experiment was performed using three different epoxy resins such as Diglyceryl Ether of Bisphenol A (DGEBA), Diglyceryl Ether of Bisphenol F (DGEBF) and Diglyceryl Ether of Bisphenol M (DGEBM) alongside four different amine hardeners. The resins were first degassed at 100°C under a vacuum for 1 hour and then mixed with its hardener at a ratio of 1:1. The mixture was then poured into its moulds and underwent multiple curing treatments; at 150°C for 2 hours, followed by 177°C for 4 hours and lastly at 205°C for 2 hours. It was found that DGEBF resin showed the lowest yield strength followed by DGEBA then DGEBM; This can be attributed to the resin's epoxy equivalent weight where higher force is required to initiate motion in the crosslinked network. In addition, the effect of amines has been shown to reduce its strength in the order of BisPA ~ BisMA > TPE-R > MDA. It was concluded that isopropyl linkages present in BisPA and BisMA better improve stiffness and reduce molecular mobility / segmental motion compared to methylene linkages in MDA. On the other hand, ether linkages in TPE-R reduce its mechanical performance due to the increase in flexibility, allowing greater molecular rearrangement. Figure 2.13 presents the compressive yield strength of the epoxies.

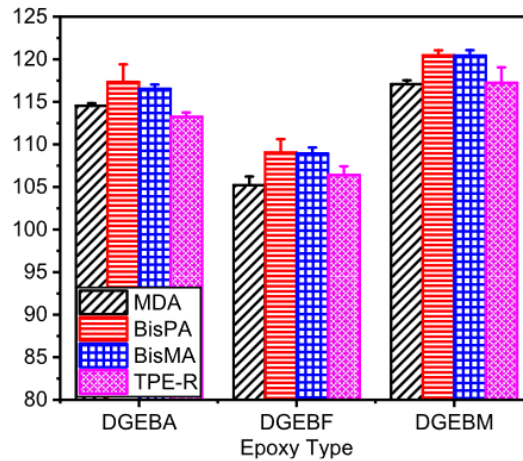


Figure 2.13: Compressive Yield Strength [159]

In 2020, Patterson et al. [160] investigated the performance of glass fiber reinforced epoxy resin systems with different molecular weights between crosslinks (M_c). Vacuum-assisted resin transfer moulding method was used to fabricate the composites; where the resins were initially preheated to 60°C and then degassed for 10 – 20 minutes under vacuum. The composite was cured at 80°C for 2 hours followed by 150°C for 8 hours. The specimens were later then cut using a water jet with an abrasive. It was reported that the short beam strength of D2000 and D400 were 56% and 27% higher than D230 at -60°C respectively; to which higher M_c polymer resulted in a tougher composite. Furthermore, it was found that higher M_c polymer resulted in greater fracture toughness at room temperature. However, D230 and D400 samples demonstrated similar ultimate tensile strength; Figure 2.14 presents the mechanical properties of D230 and D400 samples. It can be concluded that the increase in M_c improves the toughness of the polymer. The authors stated that due to the elastomeric properties of D2000 sample, the tensile test and fracture toughness could not be conducted at room temperature. It could be suggested that these two tests be conducted at sub glass transition temperature as the short beam test has indicated a significant difference in performance.

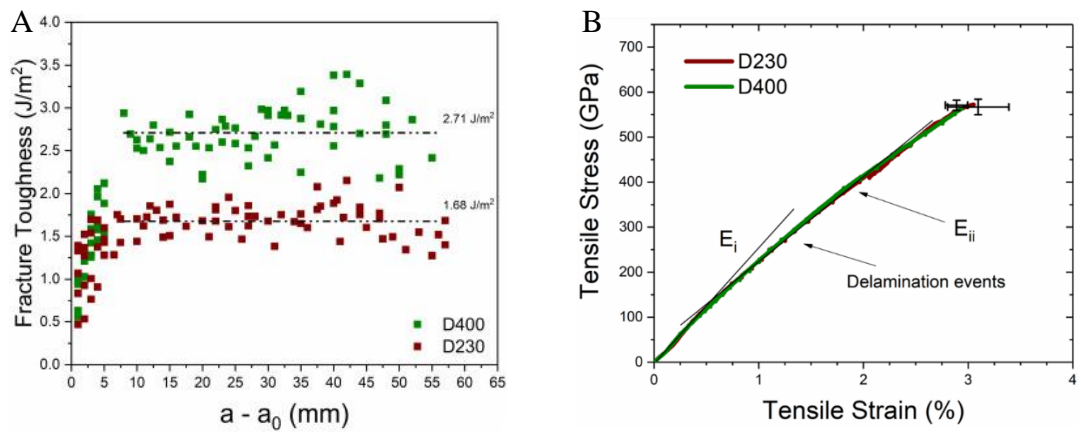


Figure 2.14: Mechanical Properties of D230 & D400 [160]
(A: Fracture Toughness, B: Tensile Stress)

The use of different polymer matrices of varying densities to fabricate OPEFB composites was undertaken by Cheng et al. [37]. The matrix used consisted of Polypropylene (PP), epoxy and Poly (lactic acid) (PLA) with the densities of 0.9gcm^{-3} , 1.16gcm^{-3} and 1.24gcm^{-3} respectively. Both PP and PLA composites were processed using compression moulding while epoxy composite was fabricated using vacuum-assisted resin infusion. The epoxy was cured at room temperature for 24 hours and underwent a post-curing at 80°C for 16 hours. It was found that the incorporation of OPEFB in epoxy matrix resulted in the most effective enhancement in longitudinal flexural strength, attributing to the hydrogen and covalent bonding between the hydroxyl group of OPEFB fiber and epoxy matrix. In addition, the epoxy composite was given the highest efficiency factor (ratio of longitudinal strength over calculated value following the rule of mixture) at 0.87; This was followed by PLA composite at 0.72 and PP composite at 0.62. The low performance of PP composite is a result of poor interfacial adhesion and poor wetting on OPEFB. In conclusion, OPEFB was only an effective filler when accompanied by PLA and epoxy. In addition, the viscosity of the matrix can also affect the compatibility between the fiber and matrix. One of the main concerns identified in this research paper is the use of different fiber volume percentages; where epoxy composite had 30%, PP had 39.72% and PLA had 39.55%; This could have posed significant changes to the performance of the composite.

Wang et al. [161] fabricated composites with the use of different epoxy systems; Three different epoxies (Araldite 2020, DP460 and DP490) of varying viscosities were used to produce piezoelectric fiber composites. The piezoelectric fiber was filled with the resin to form the composite layer, undergoing a cure at 80°C for 2 hours. The composite was then thinned to 200µm with a lapping machine. In the encapsulation process, the sample was heated to 80°C and kept for 0.5 hours using a self-made packaging platform. It was reported that the high viscosity of DP490 made it difficult to uniformly fill the fiber even after being subjected to a vacuum environment as shown in Figure 2.15; the presence of a bubble results in the lowest polarization and driving performance. It can be concluded that the fluidity of an epoxy resin can affect the drive performance of piezoelectric composite due to the presence of air.

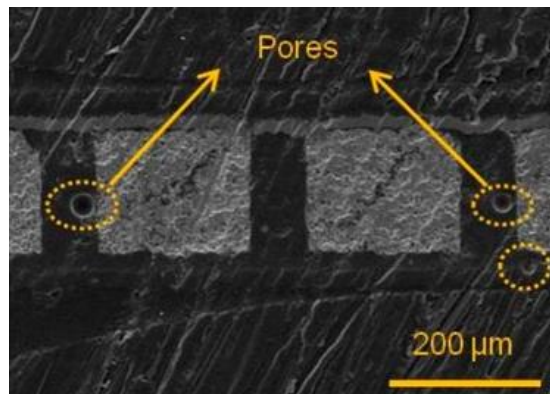


Figure 2.15: Presence of Bubble using SEM [161]

In the previous works that have been presented, resin matrix has been the main variation source of variation. Siddheshwar et al. [141] took a different approach by varying the epoxies curing agent; manipulating their molecular weight to study its morphological properties. LY 556 epoxy resin was used alongside different curing agents (D400, ED600 and ED900) with a molecular weight of 400g/mol, 600g/mol and 900g/mol respectively. The nanocomposite was prepared by mixing 3 wt% modified clay in acetone and epoxy resin. The mixture was sonicated for 20 minutes using a probe sonicator and degassed for 10 minutes. It was found that composite with a higher molecular weight curing agent displayed better dispersion with better platelet separation

as shown in Figure 2.16. In addition, the use of ED600 and ED900 was reported to significantly improve its elongation at break; However, it comes at the cost of significantly reducing its tensile strength and modulus. In conclusion, higher molecular weight curing agent results in better dispersion and elongation of a break.

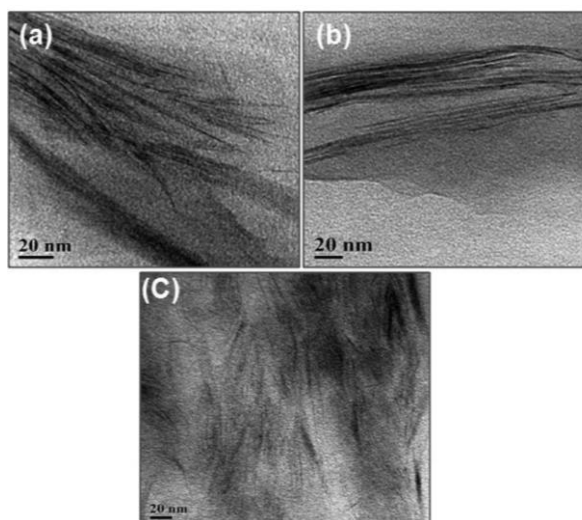


Figure 2.16: TEM Images D400 [141]
(a: ED600, b: ED900, c: D400)

In 2019, Tabatabaeian et al. [162] investigated the types of epoxy resin and the influence of carbon nanotube on the cured shape of nanocomposites. Two different epoxy resins (ML 506 and KER 828) were used and were reinforced by unidirectional E glass fiber alongside a multi-walled carbon nanotube. The composites were fabricated using the hand lay-up method. The addition of MWCNT was shown to reduce the curvature of the laminate with the epoxy system of lower density and viscosity as shown in Figure 2.17A and Figure 2.17B. It was concluded that each epoxy system has distinctive properties and curing reactions and further investigation is required. In addition, the presence of nanoparticles was shown to reduce the weight loss percentage of the nanocomposite after being subjected to thermal cycle fatigue conditions; This is due to the degradation of the matrix and evaporation of moisture present in the resin. It should be noted that different concentrations of MWCNT were used for both epoxy systems; 0% ~ 0.5% were used for ML 506 system while 0% and 1% were used for KER 828. Hence,

a proper comparison between the use of the epoxy system cannot be obtained. On another note, the method to disperse nanoparticles in the matrix and the dispersion behaviours of the composite were not reported; This is a key area which can influence the properties of the composites.

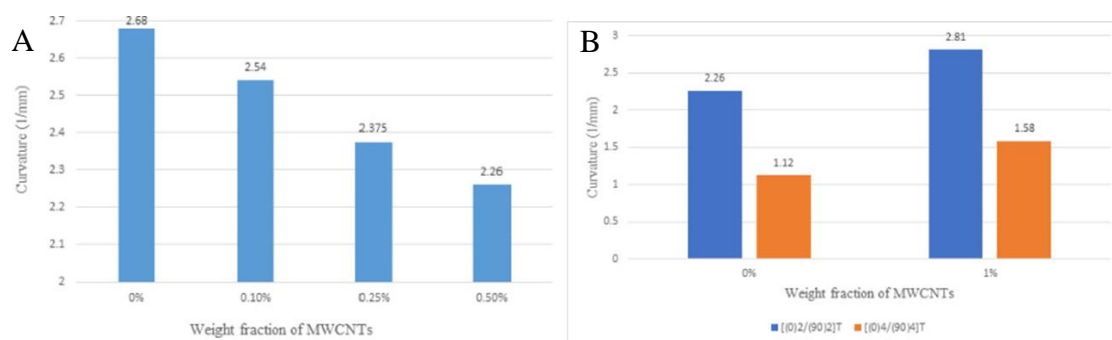


Figure 2.17: Curvature of the Nanocomposite[162]
(A: ML506 ,B: KER 828)

In 2021 Ramlee et al. [163], investigated the effects of silane and hydrogen peroxide treatment on OPEFB and sugarcane bagasse (SCB) fiber reinforced phenolic hybrid composites. The fibers are treated using 2% v/v silane and 4% v/v hydrogen peroxide, it is then repeatedly washed with water until a pH value of 7 is achieved. The fibers were then kept in distilled water for 24 hours before being dried at 100°C. The composites were fabricated using the hand lay-up method and compressed using a hot press moulding machine. It was reported that silane-treated composites displayed better tensile strength compared to hydrogen peroxide-treated composites; Silane treated OPEFB composite displayed a tensile strength of 8.35MPa while hydrogen peroxide-treated OPEFB composite displayed 6.13MPa, an improvement of 36.22%. This is a result of good interfacial bonding between fiber and matrix. Figure 2.18 shows the SEM image of the silane-treated OPEFB fracture tensile sample, where the void, fiber pull out and fiber breakage is indicated. In addition, it was also reported that silane-treated composites displayed lower void content as compared to hydrogen peroxide treated where it was reported to have 9.18% and 9.72% respectively. Furthermore, SCB displayed lower

void content compared to OPEFB with 6.05% and 9.18% respectively. This might be due to the incompatibility between the OPEFB fiber and the matrix.

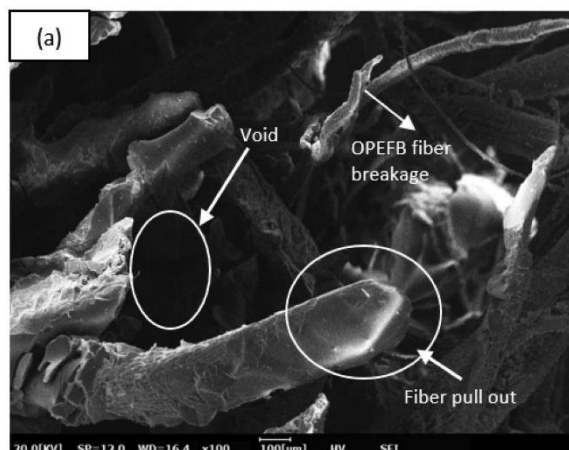


Figure 2.18: SEM Image of Silane OPEFB Composite [163]

Chaiwong et al. [119] investigated the effects of treating OPEFB using hot water and different concentration of sodium hydroxide (NaOH) on the mechanical properties of wheat gluten-based bioplastic. The raw palm fiber was first washed thoroughly and then soaked in 90°C water for 90 minutes to remove residual surface materials such as waxes and hemicellulose. The hot water-treated fibers were then soaked in sodium hydroxide solution (1 w/v% and 5 w/v%) at room temperature for 2 hours followed by a wash with distilled water. All treated fibers were then dried in a hot oven at 105 °C for 24 hours. Finally, these fibers were cut and passed through a 250um sieve. It was found that the use of alkali treatment eliminates hemicellulose and waxes as the wavenumber at 1744cm⁻¹ is absent in the FTIR spectra. In addition, using SEM, fiber treated with 5 w/v% NaOH solution presented a rougher surface compared to 1 w/v% NaOH solution, presented in Figure 2.19. The rougher surface of the fiber improved the wetting ability with the matrix and allowed the effect of mechanical interlocking to take place. It was concluded that 5 w/v% NaOH better improves the interfacial adhesion between the fiber and matrix.

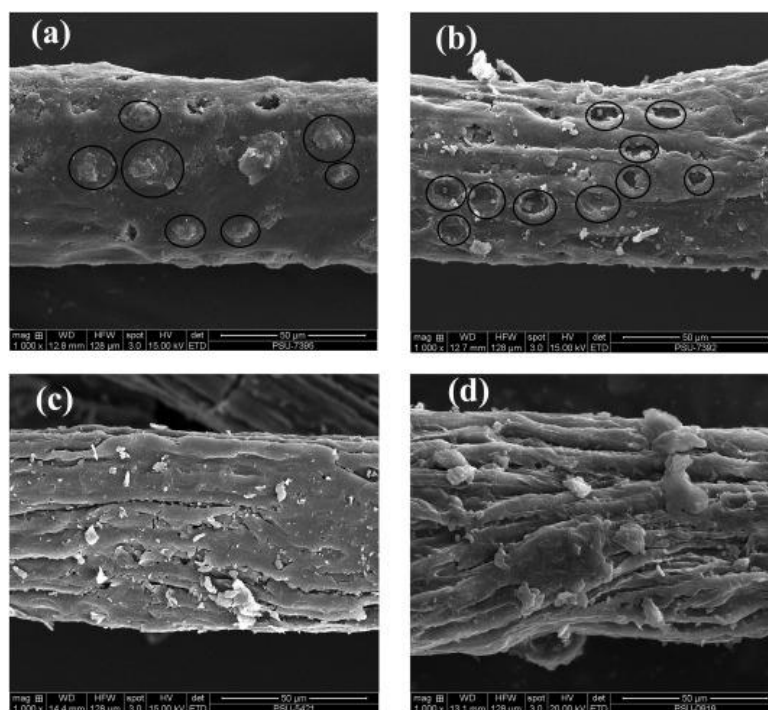


Figure 2.19: Surface Morphology of Fiber Treatment [119]
(a: Untreated, b: Hot Water, c: 1 w/v% NaOH, d: 5 w/v% NaOH)

In the same study by Chaiwong et al. [119], the effects of fiber treatment and fiber loading on the mechanical properties of the composite were explored. The composites were prepared at various filler contents (0 %, 5 %, 10 %, 15 % and 20 %) and under different treatment conditions (untreated, hot water, 1% NaOH and 5% NaOH). Wheat - gluten bioplastic and fillers were mixed for 3 minutes in a two-roll mill at room temperature. The mixtures were then heated for 3 minutes at 140°C and then compressed for 7 minutes using a compression moulding machine with 300 Pa of pressure at 140°C. The tensile strength of composite under varying contents and treatments is presented in Figure 2.20A. It was presented that 15% of untreated fiber loading exhibited the highest tensile strength at 10.41 MPa. At low fiber content, each fiber-matrix detachment formed a stress concentration zone resulting in crack initiation. Therefore, resulting in reduced strength. However, above 15%, dispersion of fiber became a challenge, leading to agglomerations and resulting in poorer fiber-matrix adhesion. Looking at Figure 2.20B, fibers treated with 5% NaOH resulted in the highest tensile strength at 13.75 MPa. The

increase in tensile strength is attributed to the removal of impurities. Thus, allowing greater adhesion characteristics.

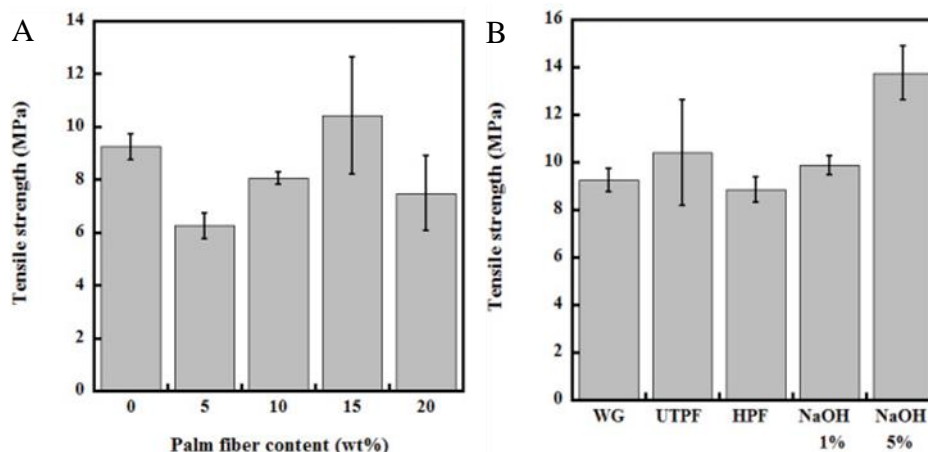


Figure 2.20: Tensile Strength Under Varying Conditions [119]
(A: Content wt%, B: Treatment)

In 2020, Radzi et al. [164] similarly studied the effects of treating OPEFB using a varying concentration of NaOH (1 w/v% to 5 w/v% at 1% increment). The fibers were soaked in NaOH solution for 99 minutes and underwent an ultrasonic bath at 80°C. It was then washed with deionized water and dried at 70 °C for 8 hours. Lastly, the fibers were then sieved to the length of 2 – 5mm. It was found that using 1 to 3 w/v% NaOH, a large sum of silica remains present in the fibers. Increasing the concentration to 4 and 5 w/v% NaOH, silica components were found to be completely removed. At 5 w/v% NaOH, a rougher fiber surface of OPEFB was observed; This is a result of a huge amount of hemicellulose components being removed. Figure 2.21 presents the surface morphology of OPEFB by SEM. By undergoing alkaline treatment, hemicellulose and silica in the fiber were found to be effectively removed, where the most significant effect was seen with the use of 5 w/v% concentration.

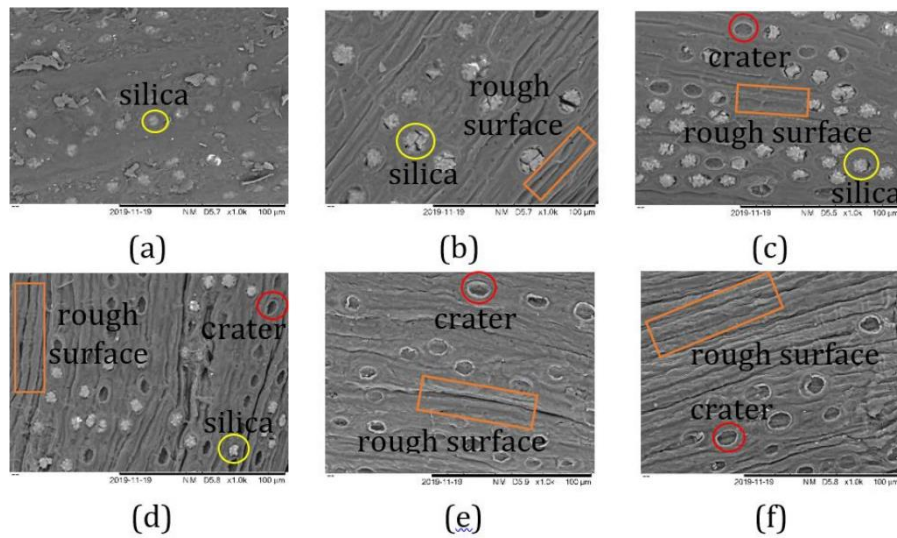


Figure 2.21: Surface Morphology of OPEFB [164]
 (a: untreated, b: 1 w/v%, c: 2 w/v%, d: 3w/v%, e: 4 w/v%, f: 5w/v%)

Ahmad et al. [39] successfully fabricated polycaprolactone composite with the use of untreated OPEFB fiber with varying filler loadings (12.2 %, 23.8 %, 34.7 %, 45 %, 54.7 % and 63.8 %). The fibers were washed with distilled water for 24 hours and then dried in an oven at 80°C. The dried fibers are crushed and then sieved through a 250 μm laboratory test sieve. The matrix and filler were mixed for 20 minutes using a blending machine and then preheated for 10 minutes at a temperature of 80°C. The composites were then allowed a breathing time for 10s to release bubbles before being pressured for 10 minutes under 100kg/cm² and allowed to cool at room temperature. The highest elongation and tensile strength were achieved with a filler loading of 12.2 % at 105.2mm and 48.4 MPa respectively. Further increase in filler loading was shown to reduce the tensile strength and elongation of composites, which was attributed to the weak interfacial interactions. The decrease in performance was caused by the fiber-fiber interaction, which led to the formation of voids which serves as sites for crack propagation. The tensile modulus of the composite on the other hand has been shown to improve with the increase of filler loading, up to 63.8 % at 250 MPa. Figure 2.22 presents the effect of fiber loading. It was explained tensile modulus has lower sensitivity to the variations in interfacial adhesions compared to tensile strength and the high tensile moduli of the fiber itself

helped increased the modulus of the composite. The study also revealed that the dielectric absorption property of the composite was found to increase with higher filler loading.

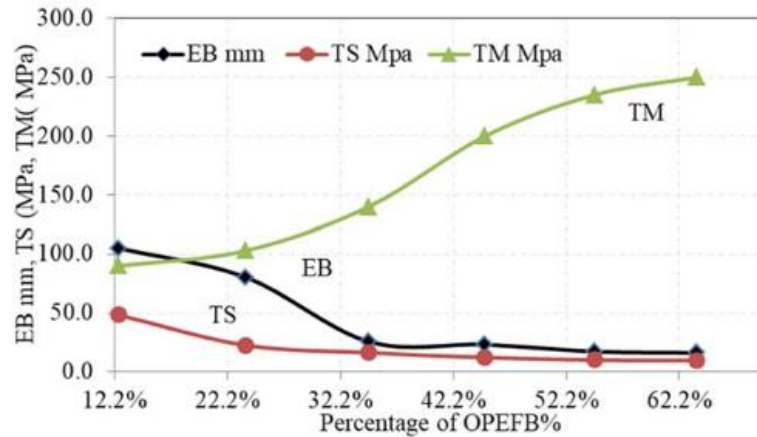


Figure 2.22: Effect of Fiber Loading [39]

Richard et al.'s [38] use of an additional 10.0 wt% untreated oil palm frond into its urea-formaldehyde composite has been reported to increase its tensile strength and flexural strength by 40.0 % and 2.5% respectively. The fibers and polymer matrix were mechanically stirred until homogenous. The mixture was then poured into a mould followed by undergoing a hot press process at 5 MPa. The composites were hot-pressed for 1200 seconds at 175 °C and then cold-pressed for 1200s at 28 °C. Similar to the previous research, the increase of filler loading increases the composites' tensile modulus; where was found to have a 95% increase with the additional content. The stiffness of the fibers contributed to the improvements in the mechanical strength of the composites. Factors such as fibers dispersion, heating/cooling time, and applied pressure were also reported to influence the mechanical performance of the composite. The authors indicated that the use of untreated fibers and poor dispersion may have contributed to the low mechanical properties of the composite as fiber breakage / pull-out; Voids were observed under SEM and shown in Figure 2.23.

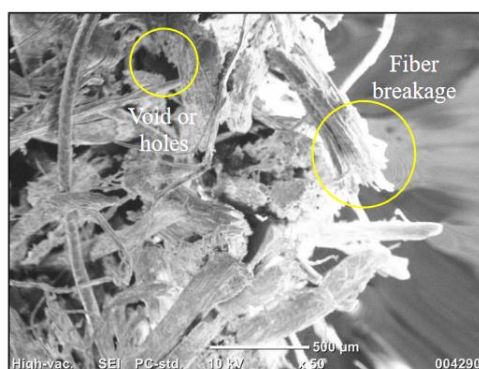


Figure 2.23: Surface Morphology with 50 wt% of Fiber [38]

Suoware et al. [165] developed polyester composites with the use of NaOH-treated oil palm fiber alongside different flame retardants. The fibers were first washed using hot water and then soaked in n-Hexane for 12 hours. The fibers were then treated with a 5% NaOH solution for 2 hours and washed with distilled water before being dried under the sun for 3 days. The composites were fabricated using hand layup compression molding. It was reported that the inclusion of 10.0 wt% fiber loading has been shown to increase the composites' impact strength by 22.3 % and reduce their flame propagation by 10.5 %. The incorporation of oil palm fiber allows the transfer of load from the matrix to the fiber, increasing the resistance to fiber-matrix debonding; allowing the composite to dissipate energy along with the interface [166]. The fiber treatment further improves the interfacial interaction between the fiber and matrix by creating a large volume of reaction sites, thus resulting in improved strength. In addition, the oil palm fiber helps reduce the composites' flammability as their lignocellulosic nature forms into char upon combustion, acting as a barrier to the transfer of heat and interferes with the combustible gases. Furthermore, it was found to reduce toxic emissions by 18.3 % and total smoke release by 35.2 %. However, the use of oil palm fiber reduces the time of ignition by 42.5 %. The addition of aluminium tri-hydroxide into the composite has also shown to lower its impact strength while ammonium phosphate and gum arabic did not. The combination of aluminium tri-hydroxide and ammonium phosphate and gum arabic in the oil palm composite resulted in the weakest flame energy for flame propagation, reducing

its flammability. Thus, the use of oil palm fiber alongside a suitable flame retardant can bring great benefits to the construction and furnishing industries.

A study on the fabrication of hybrid phenolic composite consisting of untreated OPEFB and SCB fiber by Ramlee et al. [41], has been shown to improve the performance of the composite. OPEFB fiber was first dried in the oven at 40 °C for 24 hours. On the other hand, SCB was immersed in tap water for 24 hours then rinsed with hot water. SCB fiber was then dried in the oven at 60 °C for 48 hours before being crushed to a size of ~13mm. Fiber and fillers were mixed manually for 15 minutes before being spread into the mold. The composites were then compressed for 10 minutes at 150 °C with a pressure of 40 tons. It was later then cold-pressed for 5 minutes before being cut. Pure OPEFB fiber composite was shown to have displayed better tensile strength and tensile modulus compared to pure SCB fiber composite. However, OPEFB fiber composite showed higher water absorption, resulting in greater thickness swelling. A factor leading to water absorption is the presence of voids in which pure OPEFB fiber composite was found to have greater content at 10.95 %. The incorporation of SCB fiber in OPEFB fiber phenolic composite was shown to increase the composites' tensile strength by up to 12.4 % and reduce their water absorption by 6.9 %. The addition of SCB fiber into OPEFB composite has also led to better fibers distribution and reduced fiber pull-out. The authors have also reported that the use of untreated fiber results in weak dispersion and adhesion as impurities on the surface of the fiber present a difficulty for the resin to cover it. Figure 2.24 illustrates the fracture surface morphology of OPEFB composite by SEM. Hence, further research should be conducted to evaluate the influence of fiber treatment alongside the hybridizing of fibers to better develop biocomposites with greater physical properties and lower water absorption.

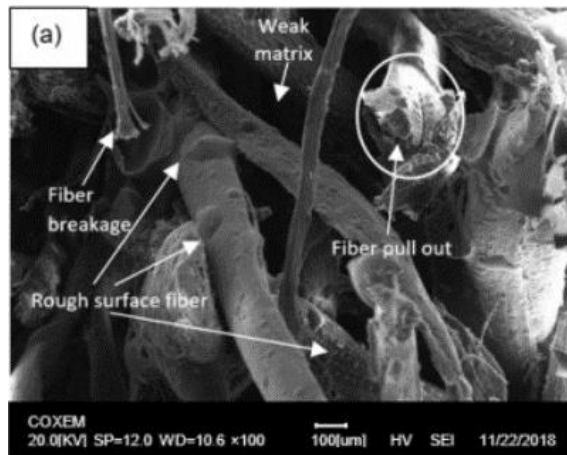


Figure 2.24: SEM Image of OPEFB Composite [41]

Experiments have also been conducted to study the performance of the natural fiber composites with the use of nanomaterials. The first research in this sub-topic by Saba et al. [167] has shown that the dynamic mechanical properties of cured epoxy resin can be improved by varying the loading of nano OPEFB fiber. The study reported that the addition of 3 % nano OPEFB filler composite was the most effective as it improved the storage modulus and loss modulus by approximately 40% and 48 % respectively; The presence of nano OPEFB filler inhibits the segmental motion of the polymeric chain ensured by better dispersion. Composites with 3 % filler loading were found to have better dispersion, distribution with no void and aggregate filler within its matrix compared to higher loading. The increase of filler content beyond this point promotes stronger particle-particle interaction that results in its reduced performance. The use of nano OPEFB in the composites has also been shown to lower its damping factor as it restricts the polymeric movement; Agglomerations and voids in the composites evident at higher filler loading improve its damping behaviour as it allows the polymer chain to move. The ability of nano OPEFB to improve the dynamic properties of a composite should be further investigated as it is a promising structural material substitution for cement, aggregates, and bricks.

Research has also been conducted on the use of CNT in NFCs. Mahalingam et al. [168] studied the use of CNT filler to improve the rigidity of coir-fiber fly-ash epoxy

composite. CNT was first added with the epoxy and then stirred for 1 hour with the use of a mechanical stirrer. Coir fibers and fly ash were then added to the mixture and stirred again for 1 hour. It was later poured into the mold and cooled at room temperature. It was found that increasing the content of CNT in 1 wt% of coir fiber and fly ash composite, decreases its shear modulus; At 0.5 wt% and 1.0 wt% of CNT, it was reduced by 7.0 % and 13.6 % respectively. A few experiments were conducted with varying the content of fillers (CNT, coir fiber, fly ash) in the range of 0 – 2.0 wt%. It was found that the increase in coir and fly ash results in higher shear modulus while the increase of CNT marginally improves its shear modulus. The composite displayed its highest shear modulus of 1050.8 MPa at 0.25 wt% CNT and 1.5 wt% of coir and fly ash. The use of the multiple linear regression model indicated that it is possible to achieve a 13.3% by incorporating 0.008 wt% of CNT, 1.62 wt% of coir and 1.95 wt% of fly ash. Thus, indicating only a tiny fraction of CNT is required to improve the composites' properties. The study of other shaped nanomaterials and their influence should be a topic for future research.

Amoroso et al. [169]. studied the dispersion of MWCNT with varying loadings (0.01 wt%, 0.1 wt%, 0.3 wt%, 0.5 wt%, 1 wt%, 3 wt%, 5 wt%) in high density polyethylene (HDPE). HDPE pellets were first grounded to a fine powder and dried in a vacuum at 40 °C for 12 hours. The powders were then mixed with MWCNT before being fed to a 16mm co-rating parallel twin-screw extruder; between the temperature of 135 °C to 155 °C at a speed of 100 rpm. The extruded strands were made into pellet form and dried for 8 hours. The standard dumbbell-shaped tensile bars were fabricated using a piston injection mold system at a temperature of 160 °C, the pressure of 450 bar and mold temperature of 50 °C. It was found that the addition of MWCNT up to 0.5 wt% resulted in reduced tensile strength, indicating that polymer chains stretched in the direction of the applied load. The addition of 3 wt% MWCNT resulted in the highest tensile strength at ~34.97 MPa, improving its strength by 13.6 % compared to the neat condition. The tensile strengths of the nanocomposites are presented in Figure 2.25A. The presence of the MWCNT - polymer network formed a high resistance for the polymer chain to orientate, stiffening the matrix. From the SEM micrographs presented in Figure 2.25B, no large agglomerations were observed. Furthermore, a thin layer of polymer matrix was shown

to coat the MWCNT as highlighted in a circle. Thus, allowing uniform stress distribution and effective load transfer.

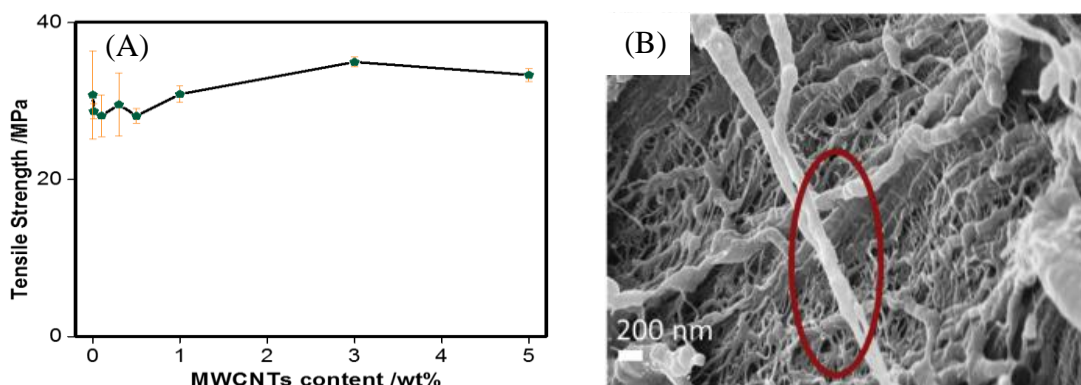


Figure 2.25: Qualitative and Quantitative Data of WMCNT Composite [43]
(A Tensile Strength:, B: Surface Morphology)

Najafi et al. [170] investigated the toughening of graphene-based polymer nanocomposites with the use of chemical functionalization. Graphene samples underwent UV/Ozone treatment for a duration of 0.5 hours up to 5 hours. It is later then exfoliated and then deposited on a silicon wafer with a 300 nm thick oxide layer. The silicon wafer was then spin-coated with PMMA which was later then soaked in NaOH solution to etch the silicon oxide. Figure 2.26 shows the stress-strain curve of the composites under varying degrees of functionalization. Higher maximum stress was observed with functionalized graphene (FG) compared to graphene alone and 20 % showed the highest maximum stress. It was found that a higher functionalization degree leads to an excessively strong interfacial bonding, which induces greater rigidity that ultimately results in higher brittle behaviour. Furthermore, 1 – 2 hours of treatment was reported to result in a higher concentration of hydroxyl groups on the graphene; resulting in the formation of more hydrogen bonds. Thus, causing higher interfacial shear strength and strain. However, a longer duration of treatment imparts the reduction of oxidized graphene, decreasing the presence of hydroxyl groups.

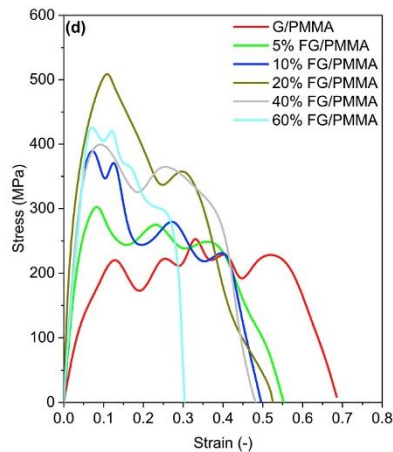


Figure 2.26: Stress-Strain Curve of Functionalized Graphene [170]

Kilic et al. [140] investigated the tensile behaviour of two different epoxy polymer systems reinforced by graphene nanoplatelets (GNPs) and dispersion methods to fabricate the nanocomposites. Two different epoxy systems were used and termed “ductile epoxy” and “brittle epoxy”. The use of ultrasonication and high shear mixing was used for the dispersion of GNPs. The samples were prepared by mixing the 0.25% nanofiller in both epoxy systems using a probe sonicator at 40% amplitude for 30 minutes, 1 hour, 2 hours and 3 hours. The “ductile epoxy” was degassed inside a vacuum oven at 90 C for 20 minutes whereas “brittle” epoxy did not undergo degassing as it resulted in foams. It was found that the increase in sonication time resulted in a decrease in particle size of GNPs. Figure 2.27 shows the dispersion of GNP where agglomerates were still present even after 30 minutes and no significant agglomerates were observed after 1 hour. In addition, it was found that dispersing GNP into the hardener resulted in lower tensile properties. Furthermore, the tensile strength reinforcement with the addition of GNP into the two epoxy systems was also investigated; Figure 2.28 presents their tensile strength under different loading and mixing parameters. It was reported that only 0.25 % GNP in “brittle epoxy” increased the tensile strength and the longer sonication duration of 2 hours only improved it by 0.9 MPa. On the other hand, the tensile strength of ductile epoxy composite increased with increasing GNP content up to 1% loading and higher loading decrease its strength. This is attributed to the increased size of agglomerates present in the composite as shown in Figure 2.29. In contrast to the brittle epoxy, higher tensile

strength was achieved with the shorter sonication duration at 1% GNP. The largest increase of 41% was achieved by undergoing 30 minutes of sonication followed by 60 minutes of high shear mixing.

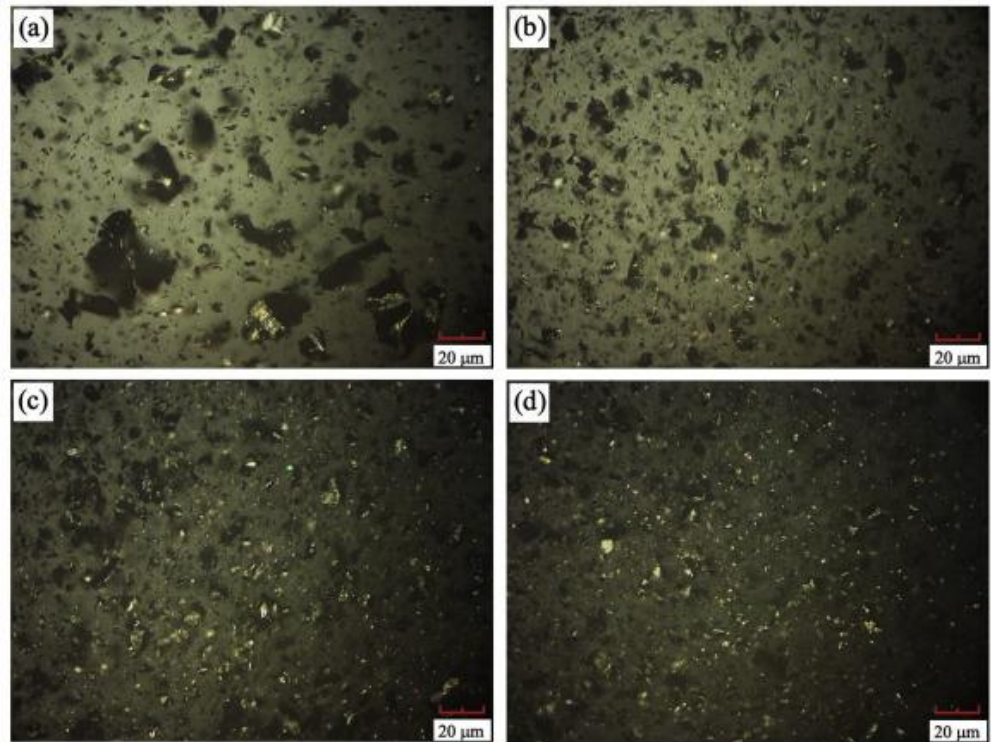


Figure 2.27: Surface Morphology of 0.25 % GNP Composite [140]
(a: 30 minutes, b: 1 hour, c: 2 hours, d: 3 hours)

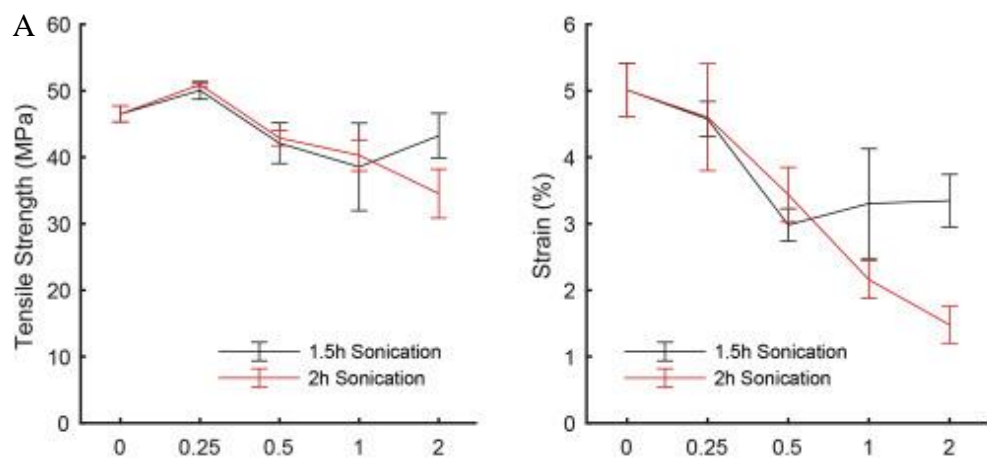


Figure 2.28: Tensile Strength of Composites with varying GNP loadings [140]
(A: Brittle Epoxy, B: Ductile Epoxy)

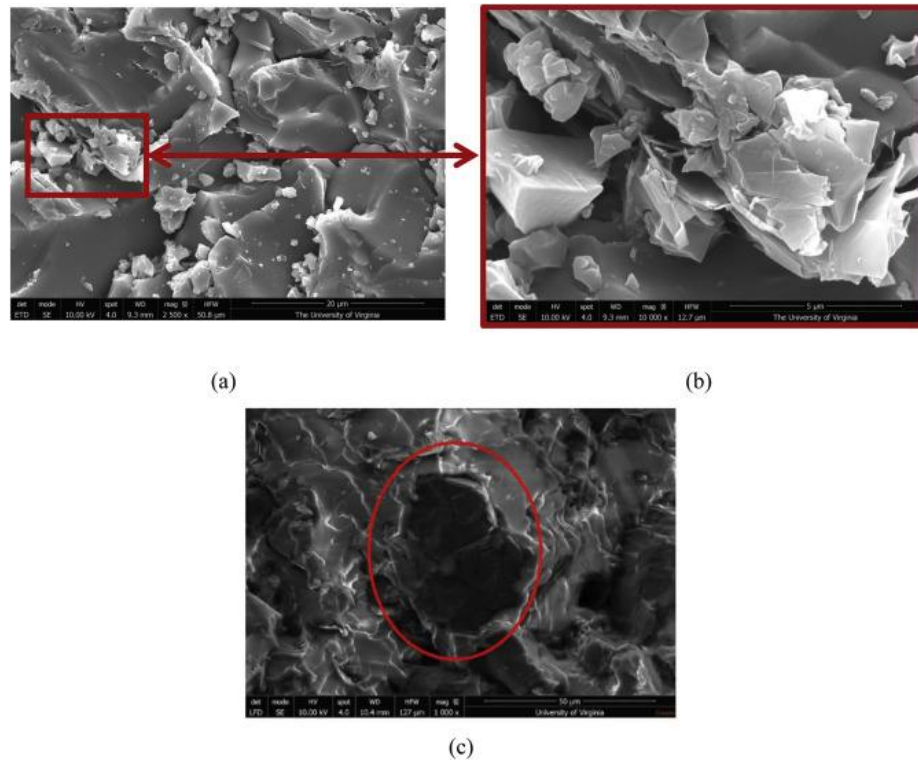


Figure 2.29: SEM Image of GNP Ductile Epoxy [140]
(a: 0.25% GNP, b: 1% GNP, c: 2 % GNP)

Khan et al. [171] investigated the effects of functionalizing graphitic nanoparticles on epoxy polymer composites. Graphitic nanoparticles (GrNP) at 0.5 wt% of epoxy resin were blended with the curing agent via a 1500 rpm high-speed mechanical agitator for 15 minutes, followed by then sonication at 60% amplitude for 1 hour. The resin and accelerator were later then added to the mixture and blended once more for 15 minutes. The end mixture was then degassed and poured into a silicone mold. Precuring and post-curing were carried in an oven at 120°C for 2 hours and 160°C for 8 hours respectively. It has been found that the addition of graphene increased the tensile strengths of composites as compared to neat epoxy (NE) as presented in Figure 2.30; the addition of pristine (P) GrNP improved the tensile strength by ~13%, followed by epichlorohydrin (E) GrNP improved the tensile strength by ~30% while 3-glycidoxypropyltrimethoxy silane (G) GrNP improved the tensile strength the highest by ~36%. These improvements in strength are attributed to better interaction between filler and matrix as the fillers

restrict the crack propagation along the crack path. Furthermore, surface functionalization of the GrNP instilled stronger interfacial adhesion between the filler matrix and the dispersion of fillers. Thus, improving the loading transferability, resulting in superior strength. Figure 2.31 presents fracture surface morphology under a high-resolution field emission scanning electron microscope; Figure C presented a mirror-polished surface indicating brittle failure. Figure D shows debonded region and evidence of aggregated fillers due to weak Van der Waals. Figure E presents a fine river-like structure, suggesting improved fracture roughness in accordance with the plastic deformation of the matrix. Lastly, Figure F indicates shear-yielding zones and agglomerated fillers.

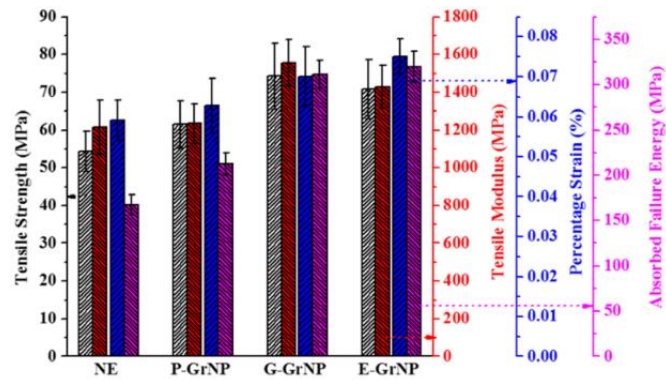


Figure 2.30: Tensile Properties [171]

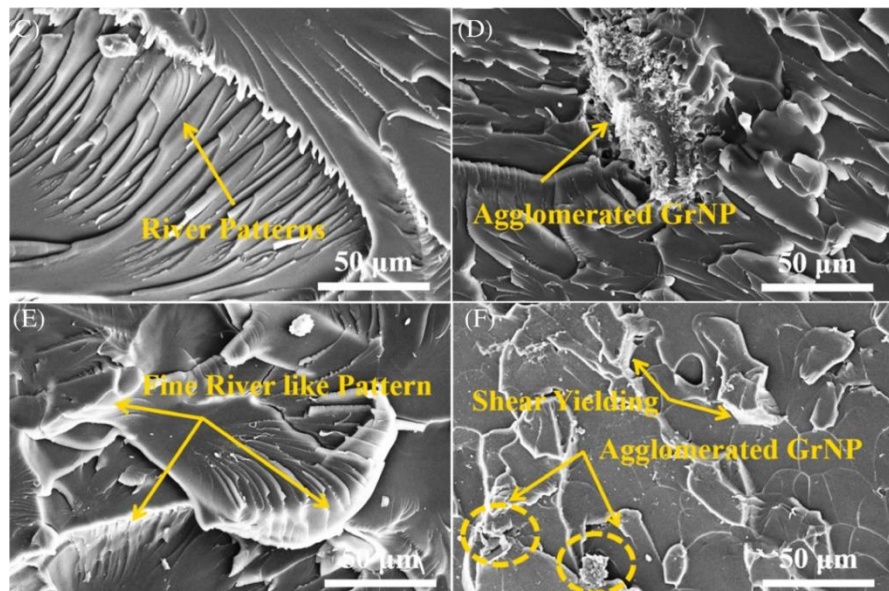


Figure 2.31: Fracture Surface Morphology [171]
(C: NE, D: P-GrNP, E: G-GrNP, F: E-GrNP)

A similar research with the use of graphene nanoparticles was conducted by Tarhini et al. [172]. The author reported an easy and scalable fabrication process to develop polymer composite films with enhanced mechanical properties. The graphene nanoflakes (GNF) / Polyvinylidene Fluoride (PVDF) – Hexafluoropropylene (HE) composite films were fabricated using a simple film formation process. The matrix was first dissolved in hot dimethylformamide (DMF) while GNF were dispersed in DMF with varying content (0 %, 6.5 % 9.9 % and 20 %) via sonication at 35 °C for 35 minutes. The solution was mixed using a magnetic stirrer until the exact volume of graphene was obtained; every 5 minutes 2 ml of GNP dispersion was added to 25ml of PVDF – HE. The whole solution was stirred for an additional 10 – 15 minutes before being poured into a silicone mold. It was later then placed in an oven at 90 °C for 24 hours. It was found that increasing the concentration of GNF in the composite improves its tensile strength as illustrated in Figure 2.32. GNF resists the segmental movement of the matrix chain and increment is attributed to the proper dispersion of filler in the matrix. Thus, allowing stronger interfacial adhesion between them.

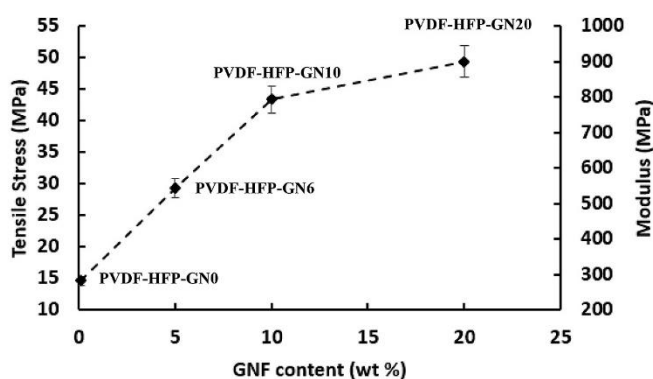


Figure 2.32: GNF Enhancement on Tensile Strength.

2.8 Summary of Literature Review

In a nutshell, various researchers have studied the use of different polymer matrices by varying their epoxy equivalent weight, and molecular weight between crosslink and viscosity. However, the influence of polymer matrix density has yet to be established. In addition, it has been accepted, that the addition of microfillers and nanofillers can improve the mechanical performance of composites. However, limited studies have incorporated the use of OPEFB and carbon nanomaterials together. Furthermore, treating the natural fiber, has been shown to improve the adhesion between the polymer matrices. Lastly, various studies have shown that the use of sonication can improve filler dispersion. However, the effects of sonicating the polymer matrix with respect to duration and amplitude remain unknown.

A summary of the critical review presented in Chapter 2 Section 7, with the focus on presenting the use of materials, methodologies, and outcomes can be found in Appendix A.

2.9 Research Gap

Researchers have experimented on a wide range of natural fiber composites and nanocomposites with varying degrees of success. Literature has shown that by incorporating oil palm fibers and carbon nanoparticles as fillers, the tensile performance of the composites can be improved. However, limited research has been conducted to study the influence of matrix characteristics, specifically the density of the matrix. As such, this research project aims to investigate the influence of polymer matrix density alongside the effects of degassing processes, filler parameters (geometry, size, and loadings), with regards to its tensile strength and dispersions of fillers.

CHAPTER 3

RESEARCH METHODOLOGY

This chapter reviews the methodology and the experimental design of this research project. It contains detailed information on the experimental methodologies, materials, and apparatus.

3.1 Experimental Methodology

This research project was designed with the intention to achieve the objectives outlined in Chapter 1. The first objective contained two components – identifying the most effective degassing parameters on epoxy resin and the effective loading of treated micro OPEFB fillers. Surface morphologies (macrostructure and microstructure) and tensile tests of the samples were conducted. The identified effective parameters will then be used in the fabrication process of OPEFB polymer nanocomposites.

In the second objective, there are also two components – identifying the most effective sonication process (qualitatively) on epoxy resin and the effects on dispersion and tensile strength by incorporating varying nanofiller properties into the epoxy resin.

In the final objective, the influence of epoxy resin density with the incorporation of micro and nanofiller was studied via surface morphologies analysis and tensile test. In addition, a model was developed based on the obtained experimental data. The experimental flow chart of this research is illustrated in Figure 3.1.

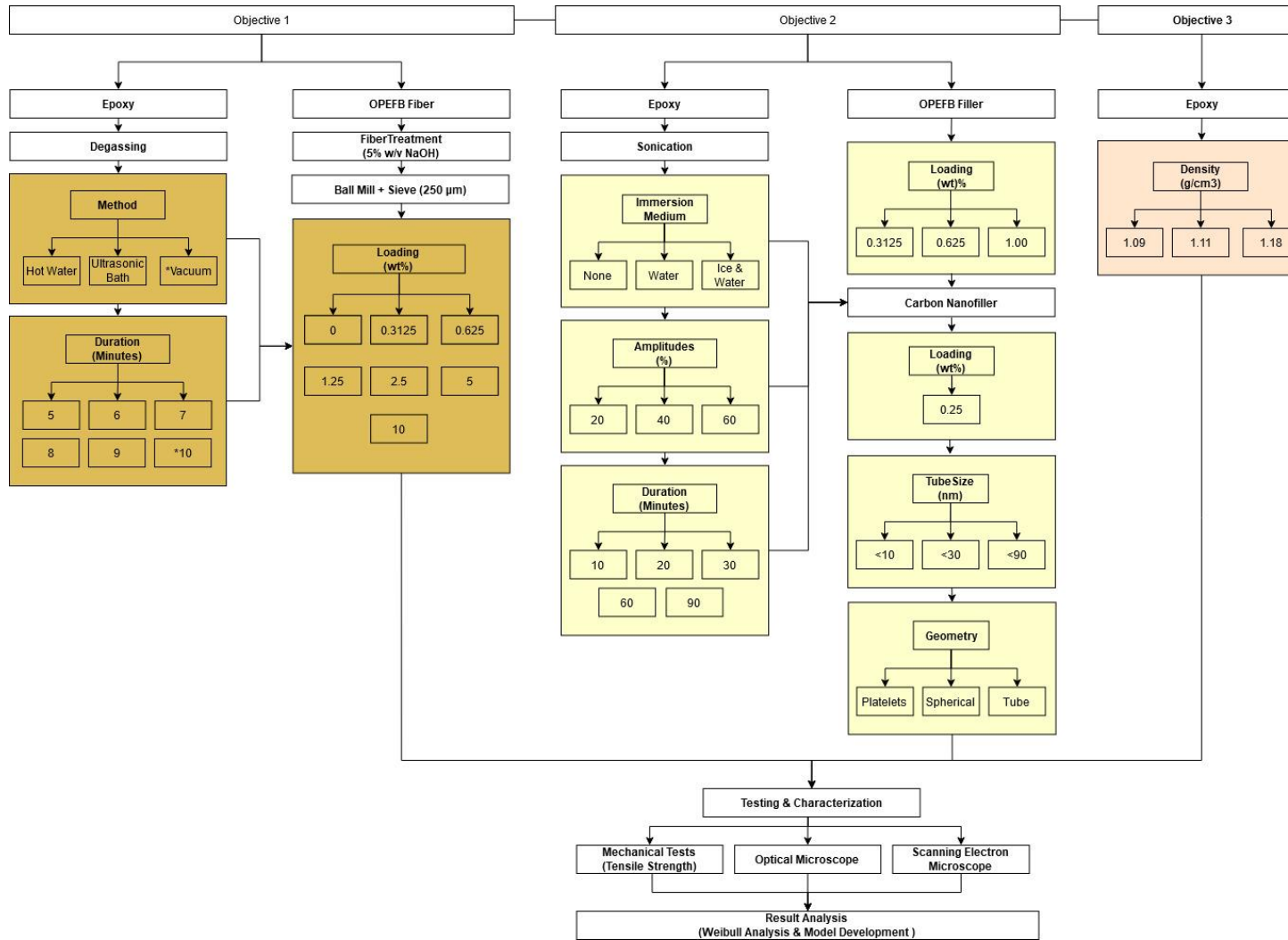


Figure 3.1: Experimental Flow Chart

3.2 Materials Used

Table 3.1 presents the list of materials used in this research project. Based on the density of the epoxies (Item 1 – 3) provided by the manufacturer; it is classified into Tarbender is classified as low density at 1.09 gcm^{-3} , EpoxAmite 102 as medium density at 1.11 gcm^{-3} , and E132 as high density at 1.18 gcm^{-3} .

Furthermore, different types of nanofillers (Item 6 – 9) were introduced in this research study; these fillers are classified into 3 different geometries (Platelets, Tubes and Spherical). Additionally, the nanotubes are then classified into 3 different sizes ($< 10\text{nm}$, $<30\text{nm}$, and $<90\text{nm}$).

Table 3:1: List of Materials

No.	Material	Function	Source
1.	E – 132 Epoxy Resin & H - Hardener	Matrix	Fong Yong Chemical
2.	Tarbender	Matrix	Smooth-On
3.	EpoxAmite 102	Matrix	Smooth-On
4.	Oil Palm Fiber	Microfiller	Sarawak Oil Palm
5.	NaOH Solution	Fiber Treatment	Bendosen
6.	Graphene Nanoplatelets	Nanofiller	Merck (Sigma Aldrich)
7.	Single Walled Carbon Nanotube	Nanofiller	Merck (Sigma Aldrich)
8.	Multi Walled Carbon Nanotube	Nanofiller	Merck (Sigma Aldrich)
9.	Multi Walled Carbon Nanotube	Nanofiller	Merck (Sigma Aldrich)
10.	Carbon Nanopowder	Nanofiller	Merck (Sigma Aldrich)

3.3 Equipment Used

Table 3.2 presents the list of equipment and tools used in this research project.

Table 3.2: List of Equipment and Tools

No.	Equipment	Function
1.	Binder Oven	Used to dry the fibers and post-curing of samples.
2.	Ball Mill	Used to grind fibers into powder form.
3.	Weight Balance	Used to measure the mass of the materials.
4.	Hot Plate	Used to heat water and treat fibers.
5.	Ultrasonic Cleaner	Used to degas fabricated samples.
6.	Ultrasonic Processor	Used to promote filler dispersion,
7.	Disposable Cups	Used to contain matrix components and fillers.
8.	Popsicle Sticks	Used to stir matrix components and fillers.
9.	Vacuum Pump	Used to degas polymer matrix/composites.
10.	Universal Testing Machine	Used to conduct the tensile tests on fabricated samples.
11.	Optical Microscope	Used for surface morphological study.
12.	SEM	Used for surface morphological study.
13.	Sieve and Shaking Machine	Used to separate filler powders into the respective particle size.

3.4 Experimental Procedure

3.4.1 Degassing Process

E132 epoxy resin and H – 9 hardener (mixed with a ratio of 2:1 by weight) were used in this study. The resin was stirred for 2 minutes and then immediately subjected to degassing process as described below (hot water, ultrasonic bath, and vacuum chamber). The mixture was then left to cure for 24 hours in a dry and shady area under atmospheric conditions. The hardened samples were then later subjected to post-cure treatment at 90°C for 2 hours in an oven.

Hot water. The plastic container containing the epoxy resin was immersed in a beaker containing water at 60°C. Constant heat was supplied using an IKA C – MAG HS 7 hot plate (Figure 3.6) and a thermometer were used to measure the temperature of the water for a duration of 5 to 9 minutes.

Ultrasonic Bath. The plastic container containing the epoxy resin was immersed in Cole Parmer Ultrasonic Cleaner (Figure 3.7) and filled with room temperature water. The resin was then subjected to the degas setting, working for 6 seconds and stopping for 2 seconds. It was turned on for a duration of 5 to 9 minutes.

Vacuum. The plastic container containing the epoxy resin was degassed in a BVV vacuum chamber (Figure 3.8) with a dual-stage 3CFM vacuum pump. It was turned on for a duration of 5 to 10 minutes.



Figure 3.2: IKA C – MAG HS 7
Hot Plate



Figure 3.3: Cole Parmer Ultrasonic
Cleaner



Figure 3.4: BVV Vacuum Chamber

3.4.2 Fiber Preparation / Treatment

Raw OPEFB fiber (obtained from Sarawak Oil Palms Berhad) was first washed and then soaked in water at 90°C for 90 minutes. It was later then immersed in 5% W/V NaOH solution at room temperature for 2 hours. Once both soaking treatments have taken place, it was then rinsed with distilled water to remove its remaining impurities. The treated fiber was later then dried in an oven at 105°C for 24 hours in accordance with ASTM D2495 - 07. The dried fibers were then processed into powder form using a CAPCO Ball Mill Model 3, which rotated vertically at 250rpm at room temperature; 3 different diameters of the stainless ball (12 mm, 18mm and 25mm) were used. The fine powders were then passed through a 250µm sieve and stored in airtight containers for further use. A summary of the process is displayed in Figure 3.9.

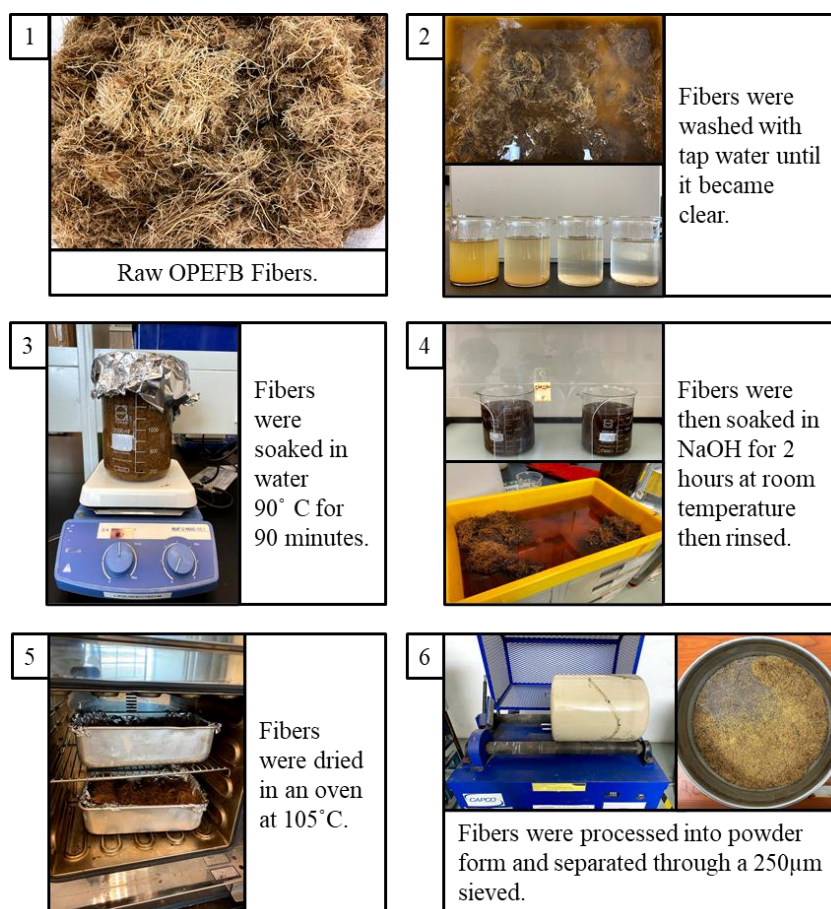


Figure 3.5: Fiber Treatment Process

3.4.3 Fabrication of OPEFB Composites

Epoxy composites used in this research project were fabricated via the wet hand lay-up method as described in Chapter 2 Section 1.2. The respective weight of E 132 epoxy resin, H – 9 hardener and oil palm filler were measured independently using an electronic weight balance. Oil Palm fillers were contained in disposable plastic containers. The oil palm fillers were poured into the epoxy resin and mixed for a duration of 3 minutes to promote dispersion. The hardener was later then poured into the resin-filler mixture and then mixed for an additional 2 minutes; Scaping while stirring technique at an approximate rotation of 120 rpm was employed in both mixing procedures. The combined mixtures were then placed inside the BVV vacuum chamber only and subjected to and degassed for 10 minutes. The mixtures were then left to cure for 24 hours in a dry and shady area under atmospheric conditions. The hardened samples were then later subjected to post-cure treatment at 90°C for 2 hours in an oven. Lastly, samples were then removed from the mould and allowed to cure at room temperature for 2 hours before being kept in an airtight container. For each batch, 6 samples were made, where 5 were subjected to tensile tests and 1 for characterization. A summary of the process is displayed in Figure 3.10.

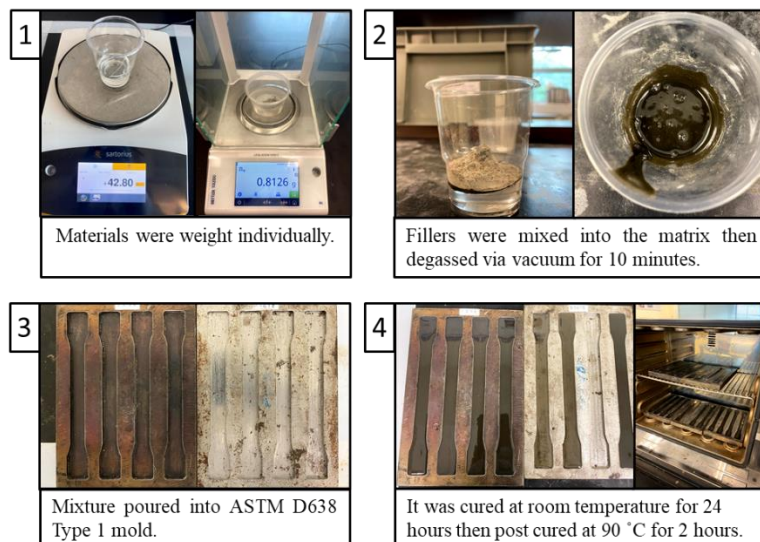


Figure 3.6: Composite Fabrication Process

3.4.4 Sonication

Tarbender epoxy resin was weighed and then poured into plastic containers. The resin was subjected to three different immersion conditions (no medium, water bath and ice & water bath). The resin was later then subjected to ultrasonication with varying amplitudes (20%, 40% and 60%) and durations (10 minutes, 20 minutes, 30 minutes) using LSP – 500 Ultrasonic Processor as shown in Figure 3.11. Based on the effective immersion condition, this part of the experiment was repeated for an extended duration of up to 90 minutes with a 30-minute interval; while at the same time being subjected to the same varying sonication amplitudes. For every 30 minutes of processing, 15 minutes break is given to prevent the ultrasonic processor from overheating. Figure 3.12 presents the immersion of resin under ice and water bath.



Figure 3.7: LSP – 500 Ultrasonic Processor

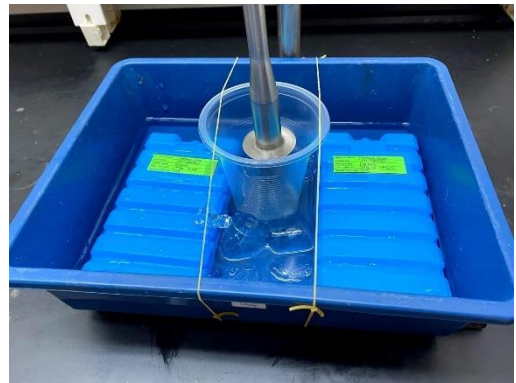


Figure 3.8: Setup of Ice and Water Bath

3.4.5 Fabrication of OPEFB Reinforced Nanocomposites

The epoxy nanocomposite fabrication processes are very similar to the process described in Chapter 3 Section 3.4.3. The respective weight of epoxy resins, hardeners, oil palm fillers and carbon nanofillers were measured using an electronic weight balance. Oil palm and carbon fillers were contained in separate disposable plastic containers as shown in Figure 3.13. Both oil palm and carbon fillers were carefully poured into the epoxy resin and then mixed as before without the hardener. The mixtures were then placed inside an ice and water bath (as presented in Fig 5 minutes before the sonication process. Prior to sonication, the horn was submerged into a similar type of epoxy dip and sonicated for 3 minutes to reduce contamination. It was then sonicated with an amplitude of 20 % for 10 minutes to promote filler dispersion whilst limiting the degradation of the mixture. The hardener was later then poured into the resin-filler mixture and then mixed for an additional 2 minutes. The mixtures were then finally poured into the tensile moulds and underwent similar curing treatments. This procedure was repeated using different types of CNT particles size, different type of nanofiller and different types of epoxies.

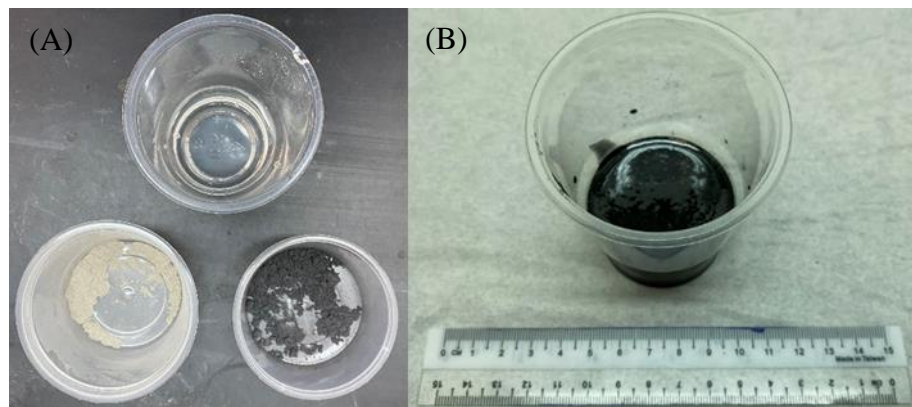


Figure 3.9: Fillers and Epoxy Resin
(A: Before Mixing, B: After Mixing)

Figure 3.14 and Figure 3.15 present the physical conditions of the varying nanofillers at a weight of 0.175 g alongside their excess composite mixtures. Figure 3.16 on the other hand depicts the physical condition of the OPEFB nanocomposite mixture with the use of varying epoxy matrix density.

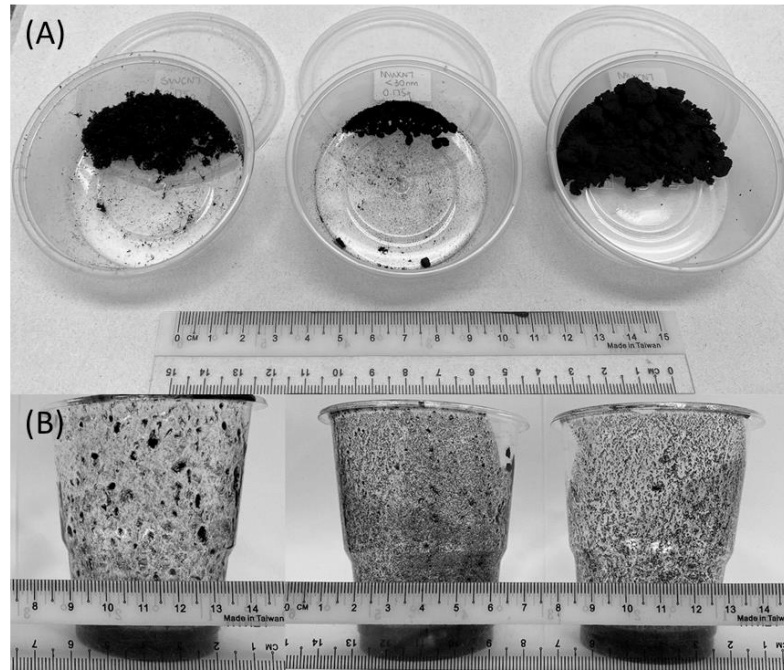


Figure 3.10: (A) Physical Conditions of 0.175g Nanotubes
(B) Liquid Phase of OPEFB Nanotube Composite Mixtures
(Left: <10 nm, Middle: < 30nm, Right: < 90nm)



Figure 3.11: (A) Physical Conditions of 0.175g Nanofiller
 (B) Liquid Phase of OPEFB Nanofiller Composite Mixtures
 (Left: Nanoplatelets, Middle: Nanopowder, Right: Nanotube < 30nm)

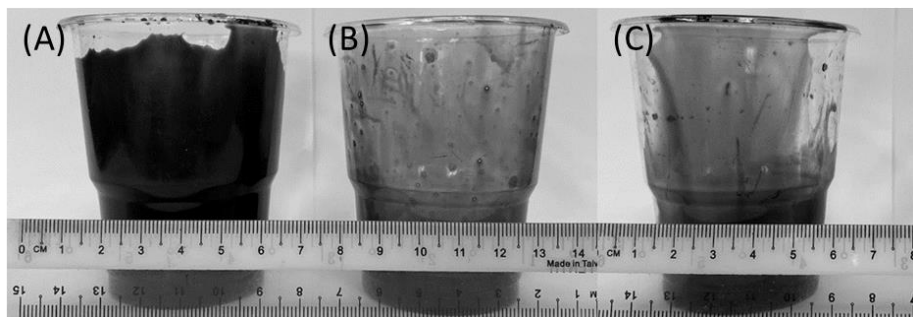


Figure 3.12: Liquid Phase of OPEFB Nanopowder Composite Mixtures
 (A: Tarbender, B: EpoxAmite 102, C: E132)

3.5 Testing and Characterization Techniques

3.5.1 Mechanical Testing (Tensile Strength)

Tensile tests were conducted in accordance with ASTM D638 - 14 standards with 5 fabricated specimens. ASTM Standard D638 type -I was used as a reference; dimensions are presented in Figure 3.2; having an overall length (LO) of 165mm, the distance between gap (D) 115mm, length of the narrow section (L) 57mm, gauge length (G) 50mm, the radius of filler (R) 76mm, the width of a narrow section (W) 13mm, width of a narrow section (W) 13mm, overall width (WO) 19mm and thickness (T) 3.2mm [173]. It is later then drawn at a rate of 5 mm/minute using Lloyd LR10K Universal Testing Machine. The UTM used has a load range of 10.0kN, with an accuracy of $\pm 0.5\%$ load cell used.

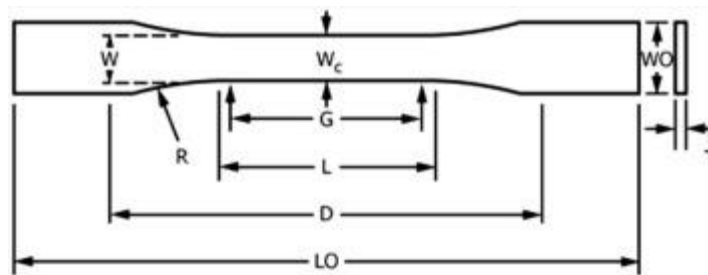


Figure 3.13: Dimension [173]

As required by ASTM D638 – 14 standards, the tensile strength has to be calculated by dividing the maximum load experienced over the average original cross-sectional area of the sample. It is then reported to three significant figures.

Tensile Strength (MPa)

$$= \frac{\text{Maximum Load (N)}}{\text{Average Original Cross Sectional Area (mm}^2\text{)}} \text{ Equation (3.1)}$$

3.5.2 Surface & Fracture Morphology (Macrostructure and Microstructure)

The surface morphologies of the oil palm fibers and samples fabricated were examined at 2 different scales (macro and micro); wherein the former, images were taken with the use of a camera and in the latter, micrographs were obtained via Olympus BX53M optical microscope is shown in Figure 3.3. Samples were not coated with conductive layer. Additionally, SEM micrographs were taken with the use of Thermo Scientific Quattro S as shown in Figure 3.4. This device poses accelerating voltage range of 200V – 30kV.



Figure 3.14:Olympus BX53M Optical Microscope

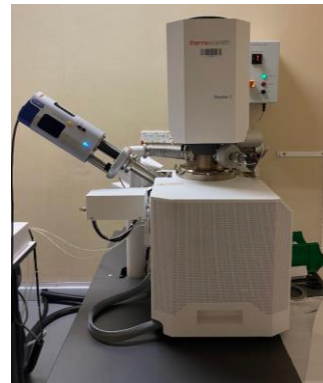


Figure 3.15: Thermo Scientific Quattro S

The surface morphology of the samples using the optical microscope was analysed based on the upper surface of the sample. Figure 3.5 illustrates the location of the area where images of the samples were taken (marked in red).

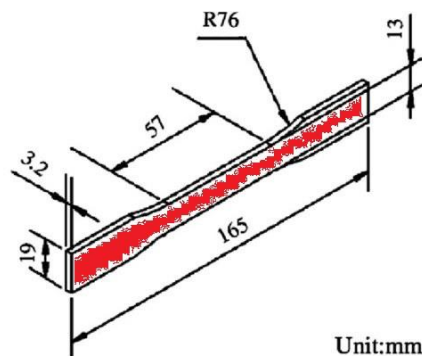


Figure 3.16: Area of Surface Morphology [174]

After conducting the tensile tests, the specimens producing the closest tensile strength to their average value were selected to undergo fracture morphology analysis. The fractured specimens were carefully cut using a drumel tool, approximately 1cm away from the point of fracture. These specimens were then filed using a metal file for plastic to ensure a flat surface for stable analysis while ensuring the point of fracture was left untouched. The surface fracture specimens were then placed inside an airtight plastic container for morphological studies. Figure 3.17 presents the tools used to prepare the tiny specimens and the specimens under an optical microscope.

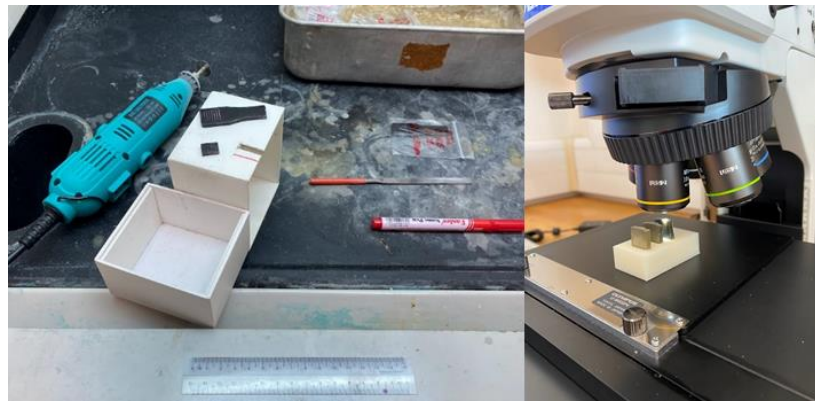


Figure 3.17: Fracture Morphology Specimen Preparation

3.6 Weibull Analysis

The weakest link theory suggests that longer fibers are weaker compared to their shorter variant. Weibull distribution is one of the few statistical distributions to verify this theory and has been widely used to represent the strength of materials and reliability evaluation as the parameters for this model can be adjusted to take various forms [175, 176]. The Weibull model is expressed in Equation 3.2.

$$P_f(\sigma) = 1 - e^{\left(\frac{-\sigma - \sigma_t}{\sigma_0}\right)^m} \quad \text{Equation (3.2)}$$

$P_f(\sigma)$ represents the probability of failure with the range 0 to 1. Stress or other parameters are denoted as σ while σ_0 is a scaling constant/characteristic strength and σ_t is the threshold stress where no failure occurs in the material. σ_t usually taken as 0. Weibull modulus, m , reflects the reliability of the material, a larger value indicates higher reliability [177]. Equation 3.2 can be rearranged to form a linear equation. It is expressed in Equation 3.3.

$$\ln \left[\ln \left[\frac{1}{1 - P_f(\sigma)} \right] \right] = m \ln[\sigma] - m \ln[\sigma_0] \quad \text{Equation (3.3)}$$

Materials with higher m values such fiber reinforced composites require 5 or more sample sizes as the N value [178]. The sample results are sorted from least to greatest based on σ and then assigned a probability occurrence, P , where I is the numbered of the sample expressed in Equation 3.4.

$$P = \frac{i - 0.5}{N} \quad \text{Equation (3.4)}$$

The Weibull analysis can be approached by plotting $\ln \left[\ln \left[\frac{1}{1 - P_f(\sigma)} \right] \right]$ against $\ln[\sigma]$ and obtaining the best fit line. The slope of the line would represent the material's reliability [178]. The parameter of the Weibull distribution can calculate by applying the linear regression method [176]. Lifetime distribution and life cycle analysis are not applicable in this study due to a limited number of test specimens.

3.7 Waste Management

Waste management is very important in this research project as it contains nanoparticles and chemicals that are harmful and toxic. These materials are required to be disposed of in a manner which will not pose any significant threat to the environment.

After the completion of each experiment, the equipment placed inside the fume hood is shut with the exhausted system turned on to ensure fumes and particles are removed. The equipment is then wiped down with dampened tissues, which are then enclosed inside a plastic bag along with the contaminated gloves and coveralls. The plastic bag and waste are then disposed of inside the laboratory's respective contaminated waste bin. In addition, all the used solutions and chemicals are also disposed of inside the laboratory chemical waste containers. Unused nanoparticles and chemicals are containerised and then placed back into their respective storage space in accordance with the safety and handling data sheet for safekeeping.

CHAPTER 4

RESULTS AND DISCUSSION

This chapter reviews the results obtained from the experiments conducted in this research project. The effects of degassing neat E - 132 epoxy, treatment of OPEFB, OPEFB filler loading rate, sonication parameters (immersion medium, amplitude, and duration), nanofiller parameters (loading, size, geometry), matrix density variation and model development are presented and discussed.

4.1 Effect of Degassing Process

4.1.1 Macrostructure of Degassed E132

The physical condition and macrostructure of E132 epoxy resins subjected to different degassing processes and durations are presented in Table 4.1. Interestingly, after 5 minutes of process, a reduction in macro bubbles within the mixture was observed in all processes; It was observed that the vacuum process showed the highest reduction of bubbles followed by hot water and then ultrasonic bath. The hot water treated mixture presented a smaller and greater number of bubbles when compared to the ultrasonic bath treated which has larger bubbles and lower numbers.

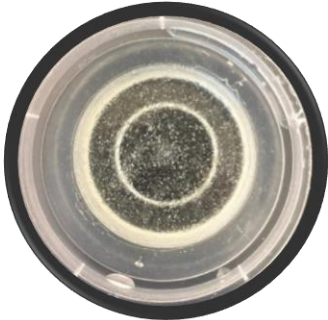
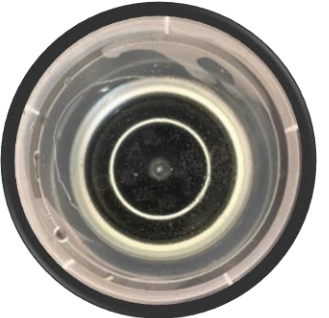
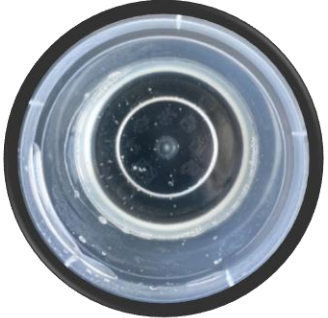
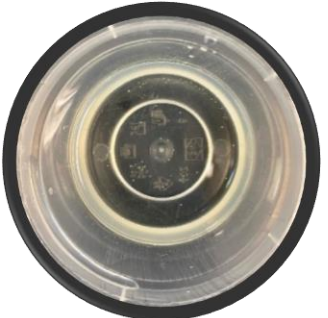
After 6 minutes of process, lesser bubbles in the mixture can be observed across all processes. The most significant changes observed with the additional 1 minute can be seen with the ultrasonic bath process, as bubbles on the surface of the mixture were absent.

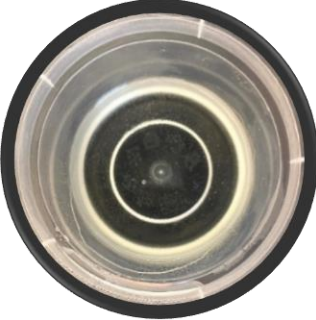
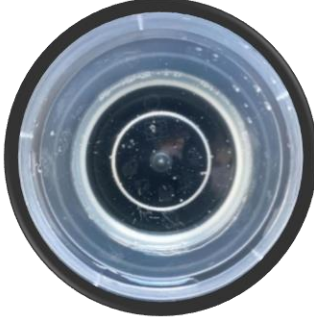
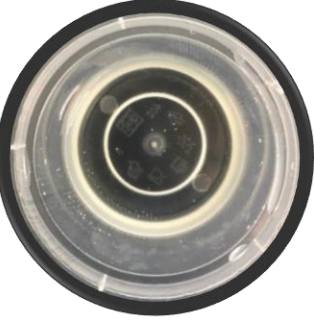
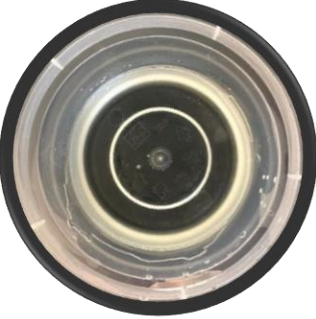
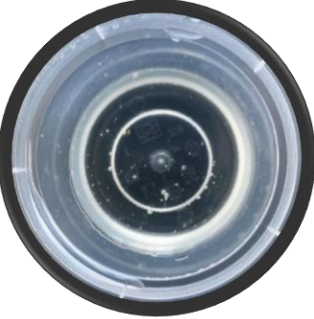
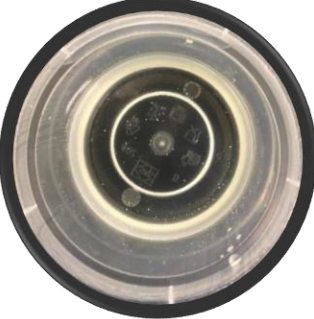
After 7 minutes of process, the most notable observation was found to be with hot water treated as the smaller bubbles dissipated from the mixture. In addition, vacuum treated mixture showed a minimal reduction in bubble whereas ultrasonic bath treated showed negligibility improvement.





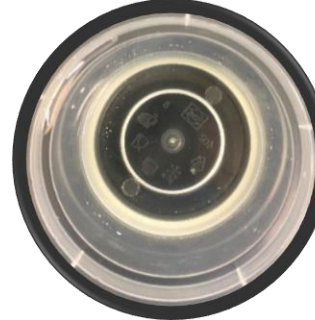
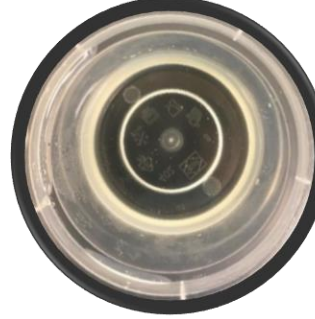
After 8 minutes of process, vacuum treated mixture showed a similar reduction in bubble whereas no reductions were observed in hot water treated and ultrasonic bath treated mixtures. It should be noted that both hot water processed, and ultrasonic bath processed mixtures resulted in reduced workability as they quickly became gel liked after being removed from the water, indicating the curing/hardening of the epoxy mixture.

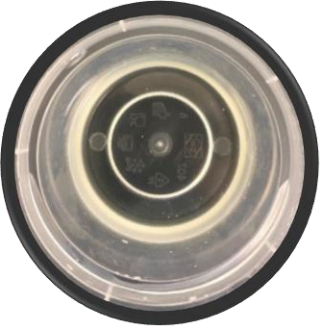
After 9 minutes of process, both hot water processed, and ultrasonic bath processed mixtures hardened in their container and a longer duration of process was not warranted. On the other hand, the vacuum-treated mixture showed a further slight reduction in bubbles. After 10 minutes of the vacuum process, fewer bubbles were observed within its mixture.

Table 4:1: Macrostructure of Epoxy under Different Degassing Process and Duration

Process/ Duration	Hot Water	Ultrasonic Bath	Vacuum
0 Minutes	 <div data-bbox="1588 687 1863 745" style="border: 1px solid black; padding: 2px; display: inline-block;">5x Magnification</div>		
5 Minutes			

Process/ Duration	Hot Water	Ultrasonic Bath	Vacuum
6 Minutes			
7 Minutes			

Process/ Duration	Hot Water	Ultrasonic Bath	Vacuum
8 Minutes	 A top-down view of a circular container with a dark center. The inner surface is mostly clear with a thin, yellowish ring of residue.		
9 Minutes	 A top-down view of a circular container. The inner surface is heavily covered with a thick, yellowish, porous-looking residue.		
8 Minutes	 A top-down view of a circular container. The inner surface is mostly clear with a thin, blueish ring of residue.		
9 Minutes	 A top-down view of a circular container. The inner surface is heavily covered with a thick, blueish, porous-looking residue.		
8 Minutes	 A top-down view of a circular container with a dark center. The inner surface is mostly clear with a thin, yellowish ring of residue.		
9 Minutes	 A top-down view of a circular container with a dark center. The inner surface is mostly clear with a thin, yellowish ring of residue.		

Process/ Duration	Hot Water	Ultrasonic Bath	Vacuum
10 Minutes	N/A	N/A	

4.1.2 Microstructure of Degassed E132

The surface morphologies, microstructure under x50 magnification of E132 epoxy resin based on its effective duration of each degassing process are presented in Figure 4.1 A-C, for hot water, ultrasonic bath, and vacuum, respectively. Based on Figure 4.1A it is revealed that the hot water process produces microvoids that are concentrated linearly (marked in a continuous circle) and occasionally isolated (marked in a dotted circle). Figure 4.1B shows that large amounts of microvoids are presented despite undergoing degas process. Figure 4.1C shows a comparatively cleaner surface with minimal presence of microvoids that are isolated (marked in a continuous circle). Undergoing different degassing processes has shown to result in different micro void behaviour; the vacuum process has proven to be an effective method of removing microvoids whereas, on the other hand, the ultrasonic bath remains ineffective.

A possible explanation for these observations lies within their respective degassing process. In the case of hot water, a part of the heat energy was absorbed by the entrapped air. Thus, allowing the air/void to rise due to the convection current [179]; where hot air rises. For ultrasonic baths, the high-frequency ultrasonic sound waves are responsible for the cavitation process which aids the removal of entrapped air [180]. However, it is believed that during the experiment, cavitations did not occur near the surface of the matrix. Hence, showing the large amounts of microvoids on its surface. Lastly, in the case of vacuum degassing, the presence of a negative pressure environment allows the internally pressured air to be released from the matrix to achieve a pressure equalized environment. Therefore, this process resulted in the lowest presence of microvoids.

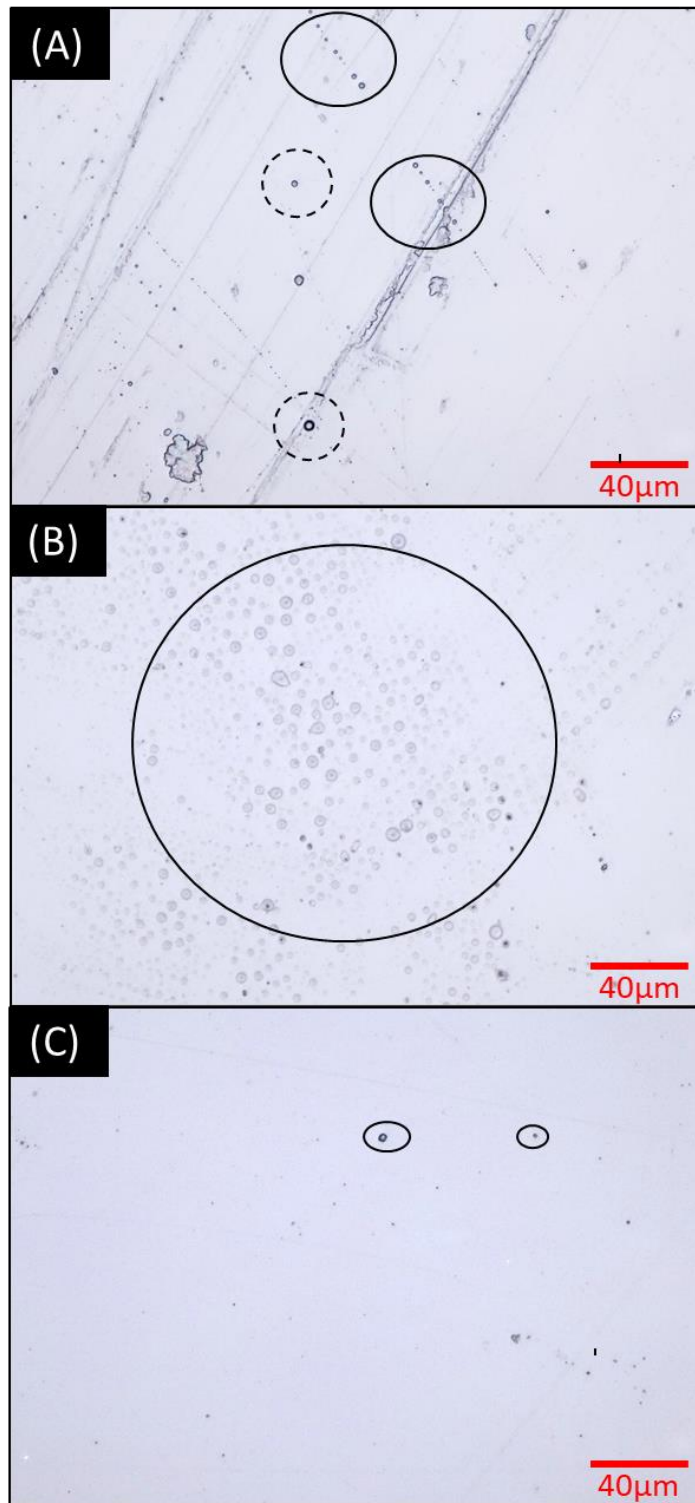


Figure 4.1A – C: Surface Morphologies Under Varying Degassing Methods
(A: Hot Water, B: Ultrasonic Bath, C: Vacuum)

4.1.3 Tensile Strength of Degassed E132

Figure 4.2 shows the average tensile strength of neat E132 epoxy resin under different degassing processes. The graph indicates that the vacuum process results in the highest average tensile strength at, 48.8 MPa compared to the ultrasonic bath and hot water process; with an increase of 12.2 % and 16.8 % respectively. It should be noted that both ultrasonic bath and hot water processes resulted in higher variability in terms of their tensile performance, producing an inconsistent behaviour.

Looking further into the matter, both these processes (ultrasonic bath & hot water) share similar traits such as the introduction of heat and the use of water. It was reported by Gu et al [181], that lower temperature should be used during processing to minimize the void defect. On the other hand, inferior mechanical performance and durability can be observed when excess water reacts with neat epoxy [182]. Thus, explaining the observed variation. When comparing these two processes, the ultrasonic bath process has a higher average higher tensile strength compared to the hot water process despite displaying higher microvoids on its surface. This could suggest that E132 epoxy resin is more sensitive toward heat energy (hot water processed) compared to mechanical forces (ultrasonic bath). However, both these have shown significant variation, possibly a sign of artifact. Therefore, further investigation will be required.

Based on the collected data, the use of vacuum degassing method produced higher tensile strengths with lower variation. This is result of reduced defects within its matrix in the form of microvoids as shown in Figure 4.1C, allowing greater load transfer. With reduced flaws size and number of defects, the material will also be able to perform more consistently.

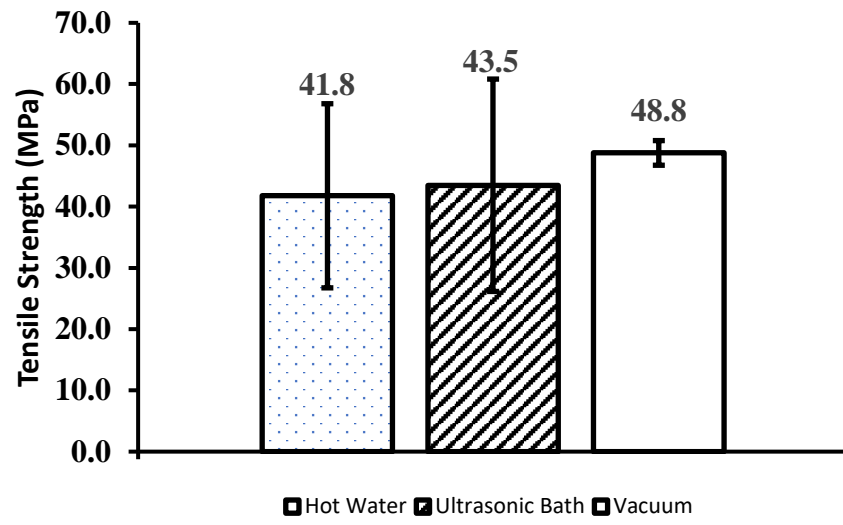


Figure 4.2: Tensile Strength of Neat E132 Epoxy Under Different Degassing Process

4.2 Effects of OPEFB Fiber


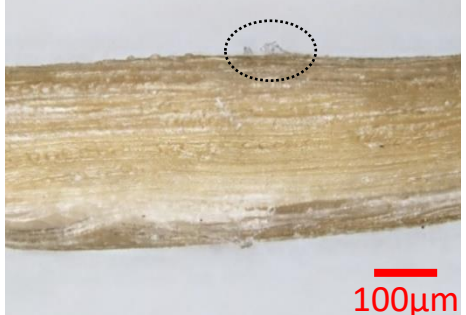

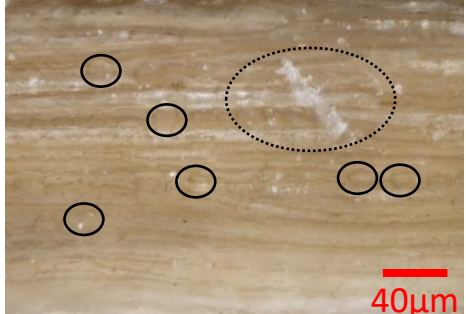
4.2.1 Microstructure of OPEFB Fiber

From the research conducted, it was found that the use of sodium hydroxide to treat OPEFB can improve the interfacial adhesion between the fiber and matrix effectively [86, 119, 164]. To that end, the fiber treatment process used in this experiment was adopted from Chaiwong et al. [119] where 5% W/V NaOH solution was used as it was reported to be the most effective.

The surface morphology (microstructure) of untreated and treated OPEFB is presented in Table 4.2. It can be observed that the surface of the untreated fiber is uneven and contained a variety of impurities, presenting materials in the form of different structures and pigmentations. Based on the literature, these impurities exist in the form of a thick layer encompassing the fiber, it consists of hemicellulose, waxes, pectin, and silica bodies [119, 164].

After treatment, the surface of fiber presented a consistent and cleaner outlook. Furthermore, small rigids are observed. Thus, producing a rougher surface appearance. Upon higher magnification, many small holes (marked in continuous circles) can be observed on the surface of the fiber. This observation is attributed to the removal of covering materials such as wax, pectin and silica bodies via the hot water treatment [119, 183]. In addition, the roughness of the fiber is the result of hemicellulose removal via NaOH treatment [119, 184]. Similar morphologies were reported in the works of Chaiwong et al.[119] , Faizi et al.[86] and Radzi et al.[164]. Furthermore, fibrillation of the fiber was observed (marked in dotted circles) which is the result of alkalization [86, 87].

Table 4:2: Surface Morphology of Empty Fruit Bunch Fiber

Magnification	Untreated	Treated
x20		
x50		

4.2.2 Macrostructure of OPEFB Loading

The physical condition, the macrostructure of E132 OPEFB composite was subjected to different loadings of OPEFB filler (0 wt%, 0.3125 wt%, 0.625 wt%, 1.25 wt%, 2.5 wt%, 5 wt% and 10 wt%), are presented in Figure 4.3. It was observed that with the increasing content of OPEFB filler, the composites became darker and less translucent. These physical changes in terms of colour and translucency are the results of light scattered by the small filler particles present within the composite samples [185]. Between the filler loadings of 0 wt% and 2.5 wt%, significant differences can be observed. This behaviour has also been reported by Lee [186]; where the amount of filler quantity in translucent matrix increases, its translucency can be observed to decrease almost linearly. However, no significant difference can be distinguished via the naked eye with loadings of 2.5 wt% and higher.

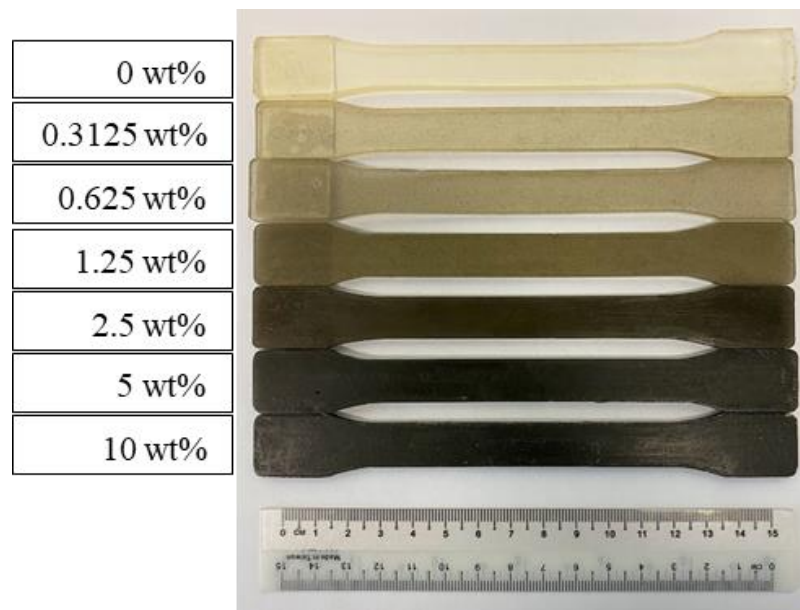


Figure 4.3: OPEFB Filler Loading by Weight Percentage

4.2.3 Microstructure of OPEFB E132 Composites

The surface morphologies, the microstructure of E132 epoxy composites with ascending filler loadings of OPEFB (0 wt%, 0.3125 wt%, 0.625 wt%, 1.25 wt%, 2.5 wt%, 5 wt%, and 10 wt%) under x50 magnification are presented in Figure 4.4A – G. Based on the figures presented below, the presences of the microvoids are marked in continuous circles.

The presence of microvoids is marked in a solid lined circle. The surface of the sample with 0 wt% in Figure 4.4A presented an overall cleaner surface compared to the other samples. With the introduction of filler contents, the presence of white particles was observed (marked in dotted lined circles) as indicated in Figure 4.4 B to G. The presence of these particles are also observed to increase in quantity with increased filler loading, indicating successful impregnation of OPEFB fillers within the polymer matrix. Good dispersion of fillers can be observed with filler loadings of 0.3125 wt%, 0.625 wt% and 1.25 wt%, as presented in Figure 4.4B to D. However, the presence of agglomerations (marked in a solid lined rectangle) can be observed in Figure 4.4 E to G. The epoxy resin E132 with 10 wt% filler in Figure 4.4G was observed to have a significant difference in the dispersion and distribution of fillers (marked in dotted and dashed lined circle).

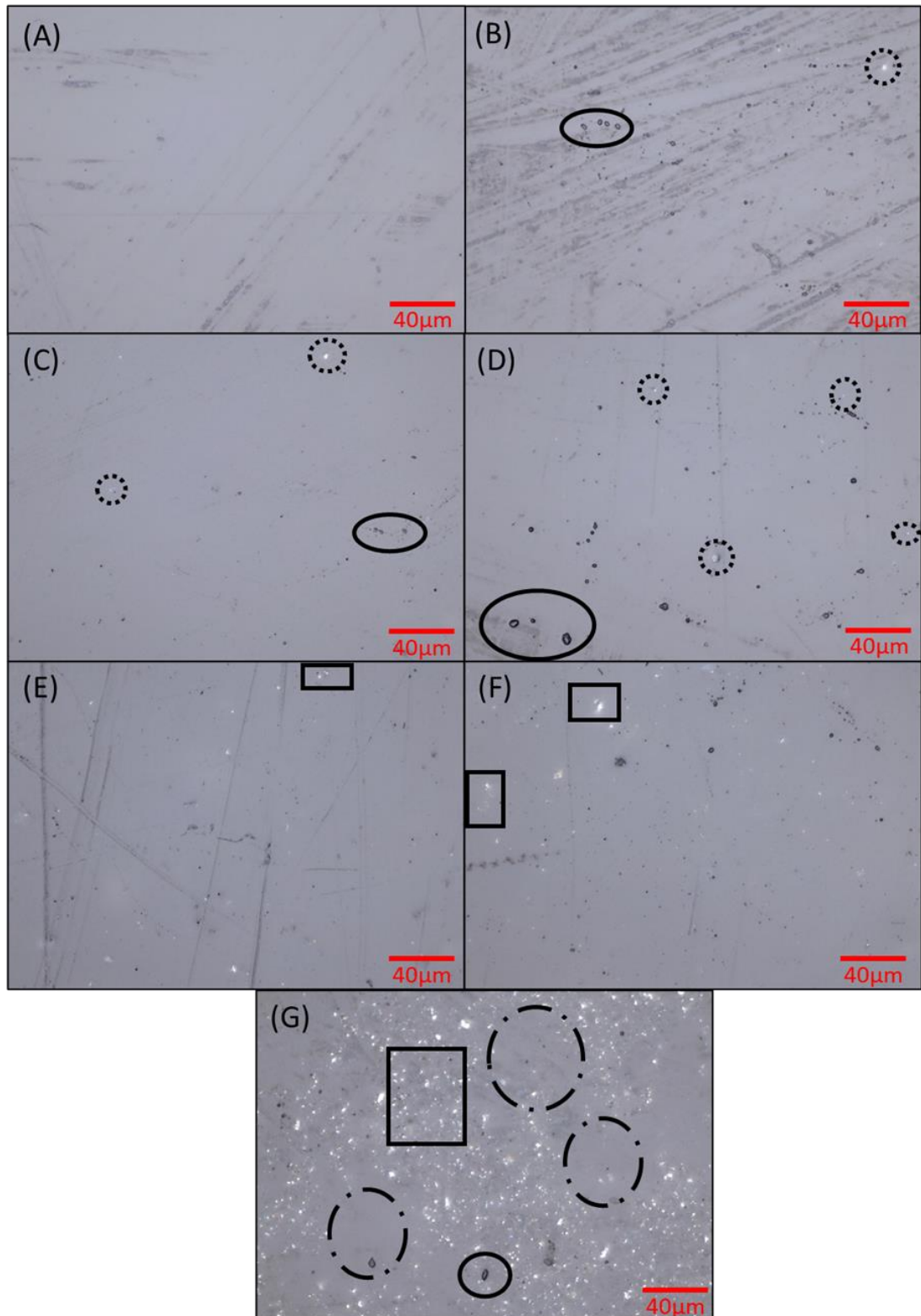


Figure 4.4A – G: Surface Morphologies of E132 OPEFB Composites
 (A: 0 wt% OPEFB, B: 0.3125 wt% OPEFB , C: 0.625 wt% OPEFB
 D: 1.25 wt% OPEFB , E: 2.5 wt% OPEFB , F: 5 wt% OPEFB, G: 10 wt% OPEFB)

The surface fracture of E132 epoxy composites with ascending filler loadings of OPEFB (0 wt%, 0.3125 wt%, 0.625 wt%, 1.25 wt%, 2.5 wt%, 5 wt%, and 10 wt%) under x10 magnification are presented in Figure 4.5A – G.

The surface fracture / crossed section of the fabricated samples presented in Figure 4.5A to G were analyzed under x10 magnification. The surface of the sample with 0 wt% in Figure 4.5A presented a largely smooth and glossy surface with few apparent markings. These markings resemble the patterns of river lines and are associated with slow crack propagation [187]. Crack bridging and branching in both directions (indicated by the arrows) were also observed. Crack branches emerge due to the increase in surface area that occurs during crack development, as the release rate of stored energy exceeds the amount of energy released [188]. Furthermore, crazes are also observed around the crack branches (marked in solid rectangle lines).

With the introduction of the OPEFB filler to the polymer matrix, a much rougher surface fracture can be observed due to extensive crack bifurcation and profuse microcracking. This rough appearance occurs as the excess energy could not be dissipated by further accelerating the crack, it has instead created multiple surface fractures, to allow for greater energy dispersion [187]. Upon closer inspection, conical parabolic markings appear on the surface fracture of the composites, featuring granular surface features, as observed in Figure 4.5B. These markings are formed from the interaction of the primary crack, where the initiation of the secondary crack nucleates in front of the primary crack [187, 188, 189]. The presence of this damage zone is believed to shield the primary crack from the applied stress intensity factor, hence enhancing the measured mechanical performance [187]. In that regard, it can be observed that the size and density of these markings behaved differently with the increases with higher filler loadings, this can be seen in Figure 4.5B to G. The higher the filler loading, the smaller the size and the higher the density of the conical parabolic markings became. The size and density of the markings have been reported to be indicators of the local crack velocity to which, the smaller the size and higher the density, the faster the crack propagates [190]. Thus, showing that the increase in filler loading results in faster crack propagation.

Figure 4.5B, 0.3125 wt% OPEFB, presents the fracture region close to the fracture origin. A mirror zone can be observed at the bottom left corner of the figure followed by a mist zone and hackle zone; This figure exhibits a series of well-defined fracture regions. In addition, exposed fractured OPEFB filler was observed (marked in a dotted circle), indicating that there is good adhesion between the filler and the matrix. Figure 4.5C, 0.625 wt% OPEFB, presents a much rougher fracture surface as compared to previous surfaces. Upon further inspection, smaller conical shaped cracks are found within the conical parabolic markings. This feature can also be clearly observed with an increased number of smaller cracks with 1.25 wt% OPEFB, in Figure 4.5D. With the filler loading of 2.5 wt% and higher, the presence of particle pullout has been observed and indicated. With the further increase in its filler loading, at 10 wt%, severe agglomeration and particle pullout have also been observed. This indicates there is poor adhesion between the filler and the matrix alongside poor dispersion and poor distribution of fillers. It should also be noted that the presence of shear bands can be observed in Figure 4.5B to D, less noticeable in Figure 4.5E and absent in Figure 4.5F and Figure 4.5G.

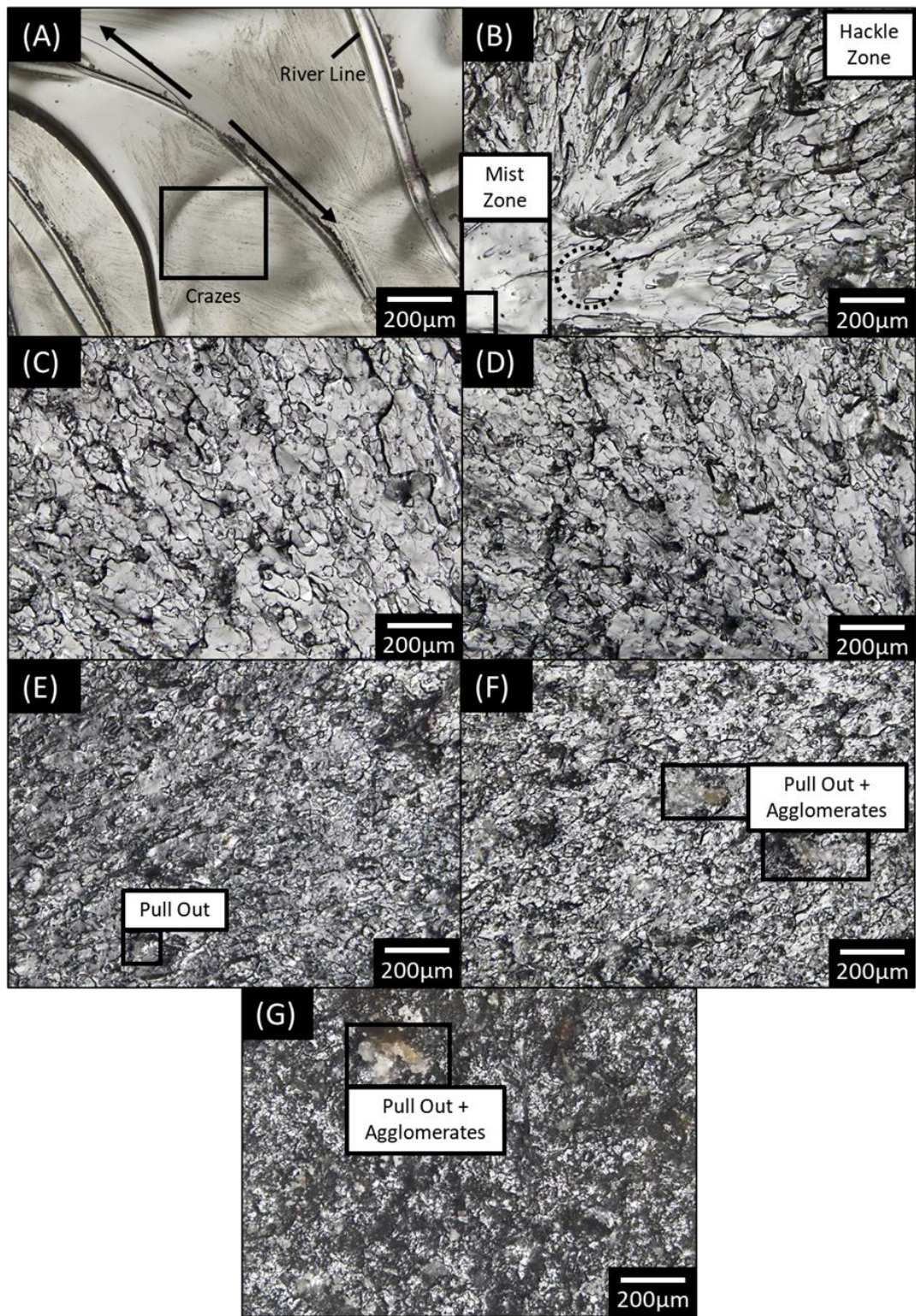


Figure 4.5A – G: Surface Fracture of E132 OPEFB Composites
 (A: 0 wt% OPEFB, B: 0.3125 wt% OPEFB, C: 0.625 wt% OPEFB
 D: 1.25 wt% OPEFB, E: 2.5 wt% OPEFB, F: 5 wt% OPEFB, G: 10wt% OPEFB)

4.2.4 Tensile Strength of E132 OPEFB Composites

Figure 4.6 shows the average tensile strength of E132 epoxy under varying OPEFB filler loadings. The incorporation of OPEFB fillers from 0.3125 wt% to 2.5 wt% was shown to have a reinforcing effect on the fabricated composites. Based on the morphology of the surface fracture in Figure 4.5B to E, it is believed that the presence of the parabolic markings and smaller conical shaped cracks found within the said markings restricts the primary crack [187]. Thus, leading to higher tensile performance. Additionally, it is also believed that the presence of such a shear band helps attenuate the propagating fracture, improving its mechanical performance [187].

Filler loading of 1.25 wt% was shown to achieve the highest average tensile strength of 57.3 MPa, a 17.4 % improvement compared to the neat condition. It is believed that the presence of smaller conical shaped cracks within the conical - parabolic markings in Figure 4.5D further restricts the crack, resulting in improved performance. Mahalingam et al. [168] investigation with the use of coir fiber similarly showed the highest improvement in mechanical performance at 1.5 %. By doubling the filler loading to 2.5 wt%, it was shown to have the least reinforcing effect on the composites, having an average tensile strength of 51.6 MPa, resulting in a 5.7 % improvement compared to the neat condition. This can be an indication that the filler content reached a saturation limit between the loadings of 1.25 wt% and 2.5 wt%.

Further filler content above 2.5 wt% was shown to negatively influence the average tensile strength of the composites. This can be the result of increased difficulty to disperse fillers, and more prone to agglomeration. Thereby reducing the adhesion between matrix and fillers [119, 191]. This can be confirmed in Figure 4.4E, where signs of agglomeration are present and in Figure 4.5E where particle pullout can be observed. These figures indicated weaker interfacial adhesion between the matrix and filler, explaining the reduced performance in tensile strength.

Interestingly, the incorporation of 10 % OPEFB filler, drastically reduces its tensile strength to 11.5 MPa, having a 76.4 % reduction compared to the neat condition. With the decrease in tensile strength, higher elongation of the sample was observed. Using the surface morphology of 10 % OPEFB filler indicated in Figure 4.6G and Figure 4.7G, it is believed that the poor and uneven distribution of fillers is the main cause of the reduction of its tensile strength; Instead of restricting the movement, it elongates under tension. The physical condition of the tested sample is shown in Figure 4.7 supports the above statement.

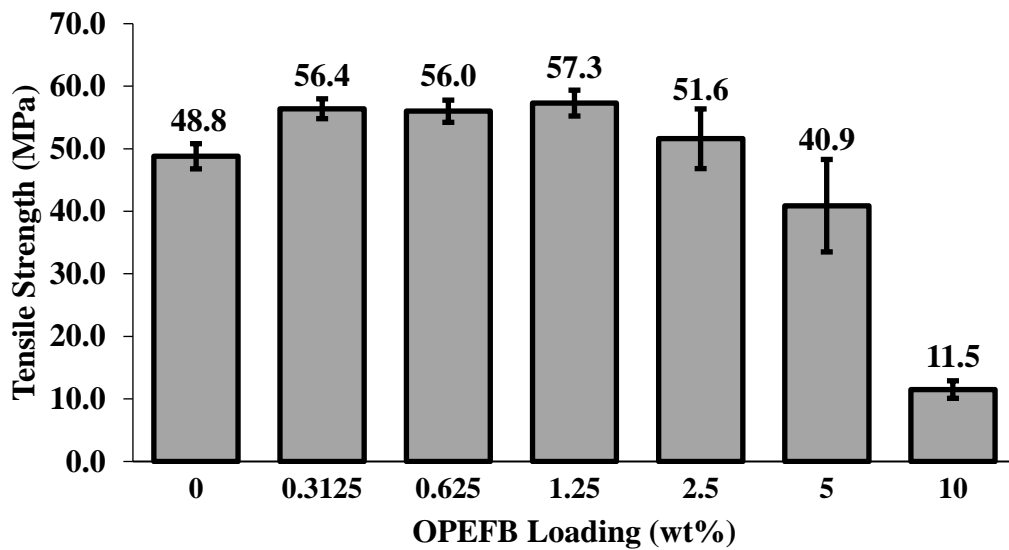


Figure 4.6: Tensile Strength of E132 OPEFB Composites

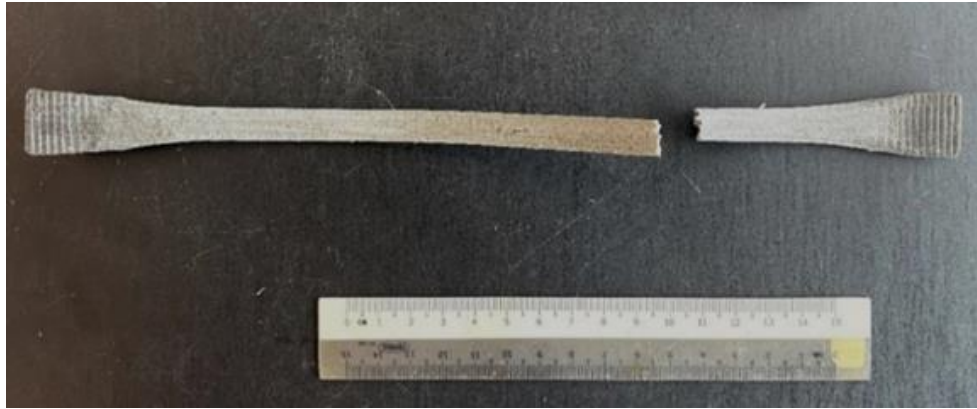


Figure 4.7: Physical Condition of 10 wt% OPEFB Composite After Test

Figure 4.8 presents the stress-strain curve graph of neat / vacuum degassed epoxy. The region shaded in blue indicates the elastic region of the polymer; whereas the region shaded in yellow indicates the plastic region of the polymer. In the elastic region, intermolecular forces are greater than the then applied force. However, once the applied load overcomes the intermolecular forces binding the sample, and exceeds its elastic limit, it then transitions to a plastic region where permanent/plastic deformation occurs. As the applied force continues to increase, it will reach a maximum point; the highest point on the stress axis is known as Ultimate Tensile Strength. As the material is subject to further deformation in terms of strain, it will reach a point where the material breaks apart which has mainly been referred to as the fracture point.

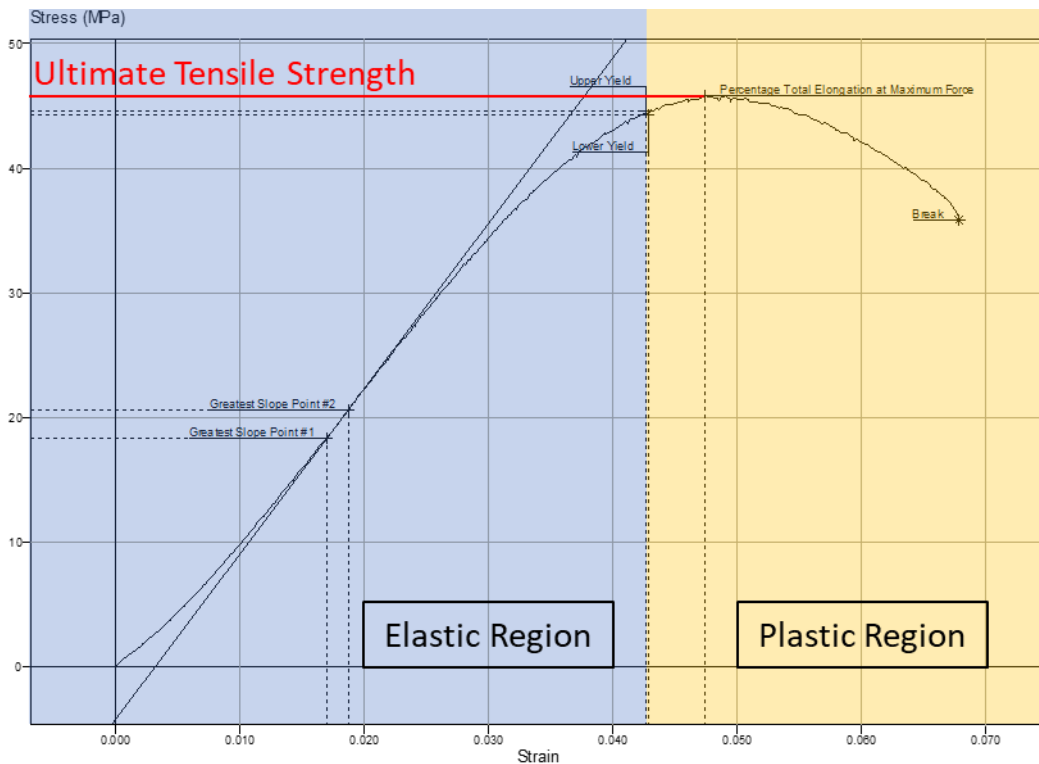


Figure 4.8: Stress-Strain Curve of Neat Epoxy

As per ASTM D 638 – 14, Equation 3.1 must be used to calculate the tensile strength. The maximum load was obtained via the Lloyd LR10K Universal Testing Machine software while the individual sample dimensions were keyed into the software prior to testing. A sample calculation of the shown sample is calculated as below:

$$\begin{aligned}
 \text{Tensile Strength (MPa)} &= \frac{\text{Maximum Load (N)}}{\text{Average Original Cross Sectional Area (mm}^2\text{)}} \\
 &= \frac{2096.5 \text{ N}}{43.2 \text{ mm}^2} \\
 &= 48.5 \text{ MPa (Three Significant Figure)}
 \end{aligned}$$

4.3 Effect of Sonication (Preliminary Experiments)

At the start of the sonication experiments, the temperature of the epoxy resins was recorded under different immersion conditions (no medium, water bath and water & ice bath) and varying amplitude (20%, 40% and 60%) for up to 30 minutes. The container with no medium melted within a second due to the high temperature produced; As a result, accurate temperature readings could not be taken, and experiments proceeded with water bath and water & ice bath conditions only. In the following subchapters, the findings by varying sonication amplitude, duration and immersion conditions are presented.

4.3.1 Immersion Conditions at 20% Amplitude

Table 4.3 presents the recorded temperature of the resin under the two conditions at 20% amplitude. In addition, Table 4.4 presents the macrostructure of Tarbender epoxy resins under different conditions and durations up to 30 minutes.

Table 4:3: Temperature Recorded under Different Conditions and Durations.

Duration / Immersion	Water Bath	Water & Ice Bath
0 minutes	23.0 °C	5.0 °C
10 minutes	56.0 °C	38.0 °C
20 minutes	64.0 °C	54.0 °C
30 minutes	64.0 °C	52.0 °C

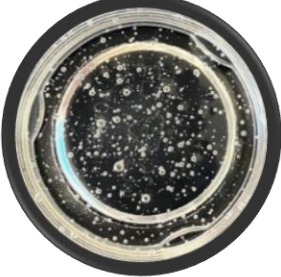






After 10 minutes of sonication, bubbles within the resin rose to the surface. Resin in the water bath was shown to have bubbles larger in size and greater in number as compared to the resin in the water & ice bath. Despite sonication, bubbles can still be

observed within the resin in water & ice bath. It was recorded that the use of ice helped reduced the temperature of the resin by 18 °C.

After 20 minutes of sonication, the presence of bubbles on the surface of the resin for both immersion conditions increased. It should be noted that bubbles within the resin in the water & ice bath were observed to have decreased. In addition, the colour of the resin in the water bath displayed minor changes, becoming slightly yellow whereas no colour changes were observed with resin in the water & ice bath. The additional 10 minutes of sonication further increased the temperature of the resin by 8 °C and 16 °C for water bath and water & ice bath respectively.

After 30 minutes of sonication, the size of bubbles on the resin in the water bath increased and its colour further darkened. Resin in water & ice bath was observed to have increased in number and size of bubbles on its surface alongside minimal discolouration. The further increase in sonication duration resulted in no temperature difference in the water bath and a 2 °C decrease in the water & ice bath. Furthermore, the presence of ice helped reduce the temperature of the resin by 12 °C.

Table 4:4: Macrostructure of Epoxy under Different Conditions and Durations at 20%

Duration / Condition	Water Bath	Water & Ice Bath
0 minutes		
10 minutes		
20 minutes		
30 minutes		

4.3.2 Immersion Conditions at 40% Amplitude

Table 4.5 presents the recorded temperature of the resin under the two conditions at 40% amplitude. In addition, Table 4.6 presents the macrostructure of Tarbender epoxy resins under different conditions and durations up to 30 minutes.

Table 4.5: Temperature Recorded under Different Conditions and Durations.

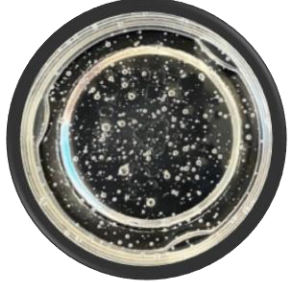






Duration / Immersion	Water Bath	Water & Ice Bath
0 minutes	23.0 °C	5.0 °C
10 minutes	85.0 °C	66.0 °C
20 minutes	96.0 °C	66.0 °C
30 minutes	96.5 °C	66.0 °C

After 10 minutes of sonication, bubbles within the resin rose to the surface. Resin in the water bath was shown to have bubbles larger in size and greater in number as compared to the resin in the water & ice bath. Resins in both conditions displayed minor discolouration, turning slightly yellow. Furthermore, no significant bubbles were observed in the resin under both conditions. It was recorded that the use of ice helped reduced the temperature of the resin by 19 °C.

After 20 minutes of sonication, the presence of bubbles on the surface of the resin for both immersion conditions increased. In addition, the discolouration of the resin in both conditions was observed to have increased. The additional 10 minutes of sonication increased the temperature of the resin in the water bath by 11 °C whereas no temperature change was recorded with resin in the water & ice bath.

After 30 minutes of sonication, the presence of bubbles on the surface of the resin for immersion condition further increased; The surface of resin in the water bath was fully covered by bubbles. In addition, the discolouration of both resins was observed to have further increased as well. The increase in sonication duration resulted in a 0.5 °C increase in the water bath while no temperature difference in the water & ice bath was recorded.

Table 4:6: Macrostructure of Epoxy under Different Conditions and Durations at 40%

Duration / Condition	Water Bath	Water & Ice Bath
0 minutes		
10 minutes		
20 minutes		
30 minutes		

5x Magnification

Bubbles

4.3.3 Immersion Conditions at 60% Amplitude

Table 4.7 presents the recorded temperature of the resin under the two conditions. The macrostructure of Tarbender epoxy resins under different conditions and durations up to 30 minutes are presented in Table 4.8.

Table 4:7: Temperature Recorded under Different Conditions and Durations

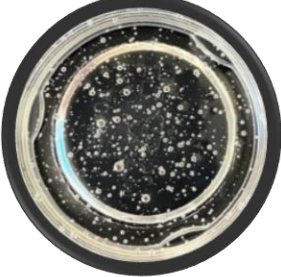






Duration / Immersion	Water Bath	Water & Ice Bath
0 minutes	23.0 °C	5.0 °C
10 minutes	99.5 °C	70.0 °C
20 minutes	100.5 °C	74.0 °C
30 minutes	100.0 °C	76.0 °C

After 10 minutes of sonication, bubbles within the resins rose to the surface. Resins in both conditions displayed discolouration, turning slightly yellow. Furthermore, no significant bubbles were observed in the resin under both conditions. It was recorded that the presence of ice helped reduced the temperature of the resin by 29.5 °C.

After 20 minutes of sonication, the discolouration of the resin under both conditions increased; resin in the water bath presented a darker yellow tone. In addition, more bubbles were found on the surface of the resins in both conditions. This observation is significantly noticeable with resin in a water bath as most of its surface has been fully covered. Furthermore, the increase in duration was recorded to have increased the temperature of the resin by 1 °C and 4 °C for water bath and water & ice bath respectively.

After 30 minutes of sonication, the yellow discolouration of the resin further increased, turning dark yellow-brown. The resin under the water bath had its surface fully covered by bubbles. Whereas the mixture under water & ice bath was observed to have lesser bubbles, but larger in size. In addition, the increase in duration was recorded to have increased the temperature of the mixture under water & ice bath by 2 °C, 24 °C lower compared to water bath condition.

Table 4:8: Macrostructure of Epoxy under Different Conditions and Duration at 60%

Duration / Condition	Water Bath	Water + Ice Bath
0 minutes		
10 minutes		
20 minutes		
30 minutes		

5x Magnification

4.3.4 Water & Ice Bath with Varying Amplitude for Extended Duration

It is revealed that the presence of ice in the sonication process leads to a lower temperature and lower formation of bubbles on the resin. Based on the data collected, Table 4.9 presents the average temperature reduction of water & ice bath compared to water baths under varying sonication amplitude. At higher sonication amplitude, ice has been shown to be more effective at reducing the temperature of the resin; where ice has been calculated to have the least temperature reduction at 20% and the most at 60%. By doubling the amplitude from 20% to 40%, it was shown to decrease the average temperature by 99.3%. Therefore, water & ice baths will be used for future sonication processes. The experiments were continued using a water & ice bath for an extended duration of up to 90 minutes to observe the behaviour of the resin.

Table 4:9: Average Temperature Reduction of Water & Ice Bath

Sonication Amplitude	Average Temperature Reduction of Water & Ice Bath
20%	13.3 °C
40%	26.5 °C
60%	26.7 °C

Table 4.10 presents the recorded temperature of the resin under different sonication amplitudes. The macrostructure of Tarbender epoxy resins under different amplitude and durations up to 90 minutes are presented in Table 4.10.

Table 4:10: Temperature Record under Different Conditions and Durations.










Duration / Amplitude	20%	40%	60%
0 minutes	5.0 °C	5.0 °C	5.0 °C
30 minutes	52.0 °C	66.0 °C	76.0 °C
60 minutes	52.0 °C	66.0 °C	80.0 °C
90 minutes	51.0 °C	64.0 °C	81.0 °C
Average	51.7 °C	65.3 °C	79 °C

After 30 minutes of sonication, discolouration of the resins was observed with all amplitudes. The intensity of yellow tone increases with higher sonication amplitude. In addition, bubbles were also observed on the resin. Bubbles on the resin at 20% amplitude and 40% amplitude were smaller in size compared to 60% amplitude. However, most bubbles were observed at 40% amplitude, followed by 60% amplitude and the least at 20% amplitude. Similar observations were also seen after 60 minutes of sonication.

After 90 minutes of sonication, continued discolouration of the resin was observed with all amplitudes and increases with higher amplitude. Resin with 20% amplitude presented the least discolouration with a darker yellow tone while resin with 60% amplitude turned brown. Furthermore, the number of bubbles was observed to have reduced at 40% and 60% amplitude as compared to the previous duration.

Increasing the sonication amplitude increases the rate at which sonotrode travel. Thus, increasing the volume being displaced, resulting in larger bubble size and number [192]. This can explain most of the observations presented in Table 4.4, Table 4.6, Table 4.8, and Table 4.11. Furthermore, the increase in amplitude also causes cavitations to occur, releasing heat in the process [143]. This also explains the rise in average resin temperature which has been calculated to be 51.7 °C, 65.3 °C, and 79 °C for 20%, 40% and 60% respectively.

Table 4:11: Macrostructure of Epoxy under Different Amplitude with Extended Durations

Duration / Amplitude	20%	40%	60%
30 minutes			
60 minutes			
90 minutes			

The increase in sonication duration and amplitude was also shown to alter its physical appearance, turning yellow in colour as presented in Table 4.4, Table 4.6 and Table 4.8. This can be classified as polymer degradation as its colour changes under the influence of an applied force [149] which in this case results in ultrasonic degradation. Krauklis et al. [157] explain that discolouration is an irreversible ageing mechanism and the yellowing of the polymer is the result of carbonyl group formations in the backbone of the polymer; attributed to the thermal oxidation process. Furthermore, Li et al. [147] have reported that the higher intensity and duration of sonication, the higher degradation can be induced in the polymer. This degradation can lead to performance failure while in service. Therefore, to reduce the degradation while promoting filler dispersion, water & ice bath at 20 % amplitude for 10 minutes will be used for future sonication processes. However, further investigation will be required to study the effects of the sonication parameters to ensure good particle dispersion and prevent/reduce polymer degradation.

4.4 Effects of Nanomaterials

Based on the experimental data collected, OPEFB filler loading of 0.3125 wt% to 1.25 wt% displayed favourable and relatively similar tensile performance. With the interest to develop and fabricate high tensile strength OPEFB nanocomposites, the methodology adopted was to include a total filler loading (OPEFB and nanofiller) no greater than 1.25 wt% as to avoid potential agglomerations. It is shown that a filler loading above 1.25 wt% yielded a lower performance as the filler reached a saturation point. Hence, three distinct loadings of OPEFB (0.3125 wt%, 0.625 wt% and 1.0 wt%) were incorporated alongside 0.25 wt% nanofillers. Several studies have reported that the addition of carbon nanofillers of 0.25 wt% greatly improves the mechanical properties of the nanocomposites [168, 193]. Carbon nanoplatelets were chosen as the initial nanofiller as it is the highest dimension (2D nanomaterial) among the four nanomaterials used in this research.

In the following subsection of this chapter, the size and geometry of the nanoparticle fillers were studied, to which each parameter had three variations. Carbon nanotubes were classified into <10nm, <30nm and < 90nm. While the geometries of the carbon nanofiller were separated into platelet, tube and spherical.

4.4.1 Nanofiller (Carbon Nanoplatelets) Loadings

4.4.1.1 Surface Fracture of Nanocomposites Loading Variation

The surface fractures of the OPEFB E132 composite filled with 0.25 wt% nanofiller under varying OPEFB filler loadings (0.3125 wt%, 0.625 wt% and 1.0 wt%) are presented in Figure 4.9A – C respectively. The nanofillers used are graphene nanoplatelets with a thickness of 6 – 8 nm on average and a particle size of 15 μm .

With the introduction of nanofillers, the surface fracture of the OPEFB nanocomposite appeared to be darker as compared to the OPEFB composite in Figure

4.5B – D. This is potentially contributed by the presence of carbon particle that is naturally black in colour. In addition, the presences of dark spots are more noticeable.

Figure 4.9A, E132 composite with 0.3125 wt% OPEFB 0.25 wt% nanofiller, has been observed to be noticeably rougher as compared to Figure 4.5B. We can observe a significant increase in crack bifurcation and the density of parabolic markings while being smaller in size. Thus, suggesting faster crack propagation [190]. Smaller conical shaped cracks have also been similarly found within the conical - parabolic damage zone.

In the previous discussion, it was established that there is a relationship between the filler loading and the size and density of the conical - parabolic markings; where the higher the filler loading, the smaller the size and the higher the density of the conical – parabolic markings became. By comparing the total weight percentage of fillers, this nanocomposite of 0.5625 wt%, produced more marking in the fractured surface than 0.625 wt% of OPEFB in Figure 4.5C. Thus, indicating that the inclusion of nanoplatelets results in faster crack propagation.

With the introduction of higher OPEFB filler loading, both particle pull-outs and particle agglomerations have been observed and indicated on the fracture surface of the nanocomposites in Figure 4.9B and Figure 4.9C, for E132 composite with 0.625 wt% OPEFB 0.25 wt% nanofiller and 1 wt% OPEFB 0.25 wt% nanofiller respectively. The agglomerations are a result of filler–filler interaction that makes a weak point, that leads to pull out and ultimately reduces its tensile strength [194]. These figures highlight the poor adhesion between the fillers and the matrix alongside poor dispersion and poor distribution of fillers.

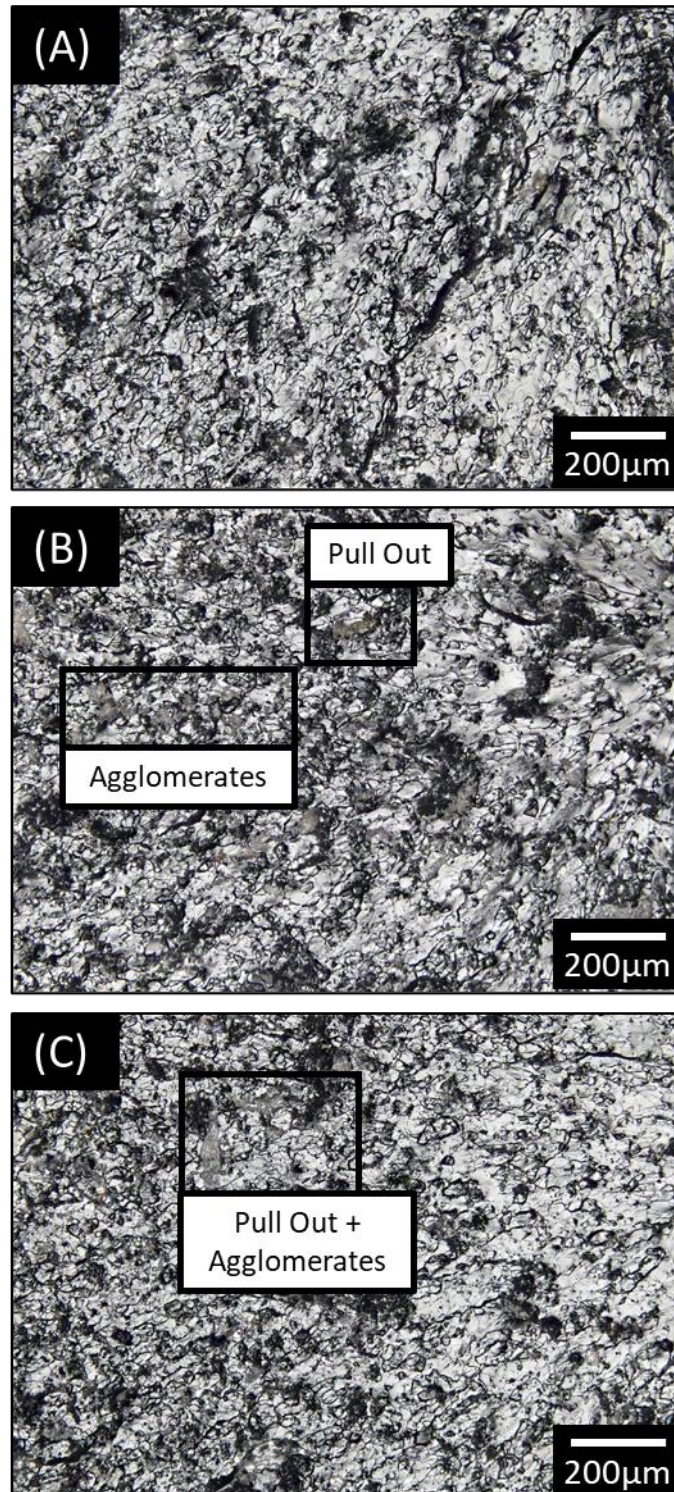


Figure 4.9A – C: Surface Fracture of E132 Composite with 0.25 wt% Nanofiller
(A: 0.3125 wt% OPEFB, B: 0.625 wt% OPEFB, C: 1 wt% OPEFB)

4.4.1.2 Tensile Strength of Nanocomposites Loading Variation

Figure 4.10 presents the average tensile strength of OPEFB Nanoplatelets E132 composite with a constant nanoplatelets loading of 0.25 wt%, under varying OPEFB filler loadings (0.3125 wt%, 0.625 wt% and 1.0 wt%). Based on the results obtained, the combination of 0.3125 wt% OPEFB and 0.25 wt% nanofiller was shown to further increase the tensile strength of the composites by 1.5 MPa, resulting in an additional 2.63 % improvement. Based on the morphology of the surface fracture in Figure 4.9A, it is believed that the presence of the parabolic markings and smaller conical shaped cracks found within the said markings restricts the primary crack [187]. Thus, leading to higher tensile performance. Additionally, it is also believed that the presence of a shear band helps attenuate the propagating fracture, improving its mechanical performance [187].

Additional content of OPEFB fillers (0.625 wt% and 1 wt%) in combination with 0.25 wt% nanofillers did not result in tensile strength reinforcement but instead a minor reduction. Both combinations of composites displayed lower average tensile strength of 0.9 MPa and 0.6 MPa for 0.625 wt% OPEFB and 1 wt% OPEFB respectively when compared to the composite without nanoplatelets; the average reduction in tensile strength is equivalent to 3.06 % and 2.51 % respectively, presenting a minor significance. The concept of solvent and solute can be loosely applied here, to which the solvent is the matrix and solute is the filler that can reach a saturation point. Based on the morphology of the surface fracture in Figure 4.9B – C, particle pull-outs and particle agglomerations have been observed, explaining its reduced tensile strength.

From the collected data, it is found that the combination of 0.3125 wt% OPEFB filler and 0.25 wt% carbon nanoplatelets in the E132 polymer matrix resulted in the most compatible tensile strength, attaining an average of 57.9 MPa, achieving a total improvement of 18.7 %.

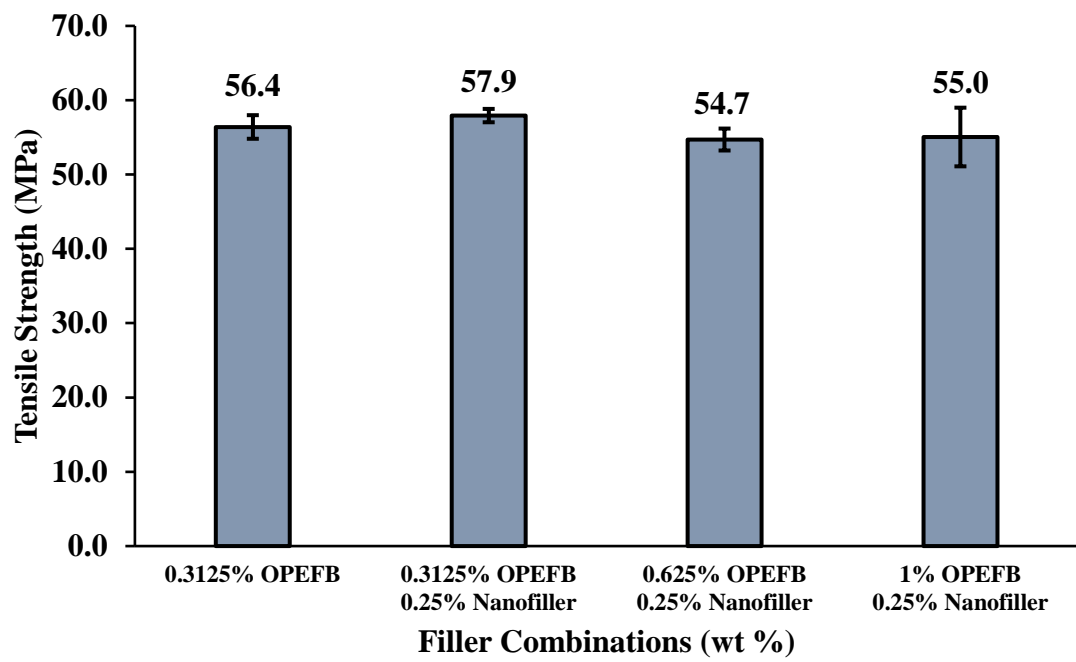


Figure 4.10: Tensile Strength of E132 OPEFB Nanocomposites
(Filler Loading Variation)
(Graphene Nanoplatelets)

4.4.2 Nanofiller (Carbon Nanotube) Size

4.4.2.1 Surface Fracture of Nanofiller Size Variation

The surface fracture of OPEFB E132 composite filled with carbon nanotubes (SWCNT & MWCNT) of different sizes (< 10 nm, < 30 nm and <90 nm) are presented in Figure 4.11A – C respectively. In these figures, the presence of a void cavity, outlined by a circular morphology can be observed in each figure.

Figure 4.11A, E132 composite filled with OPEFB and nanotube <10 nm, presents a smoother surface fracture compared to previous morphology with the incorporation of nanofillers, E132 composite filled with OPEFB and nanotube <10 nm, presents a smoother surface fracture compared to previous morphology with the incorporation of carbon nanofillers. This figure exhibits two different fracture regions, separated by a dashed white line; where the mist zone is on the left, and the hackle zone on the right. Taking a closer look at the micrographs via digital zoom, high density and small-sized conical – parabolic markings were present within the hackle zone. Thus, indicating that there is weak resistance to crack propagation on the left and experienced more resistance on the right.

Figure 4.11B, E132 composite filled with OPEFB and nanotube <30 nm, presents a rougher and more granular surface fracture as compared to Figure 4.11A. This is a result of higher density parabolic markings on its surface. Upon further inspection, the line of the conical – parabolic markings appeared to be not only thicker but also more homogenous. Furthermore, it is believed this composite experienced fast crack propagation, as indicated by the increase in density and smaller sized conical – parabolic markings.

Figure 4.11C, E132 composite filled with OPEFB and nanotube <90 nm, interestingly presents a less granular surface fracture with the signs of crack branching and crack deflections (T – junction). The latter occurs when the secondary crack intersects with the primary crack, where it will change its direction perpendicularly and terminate the crack [188].

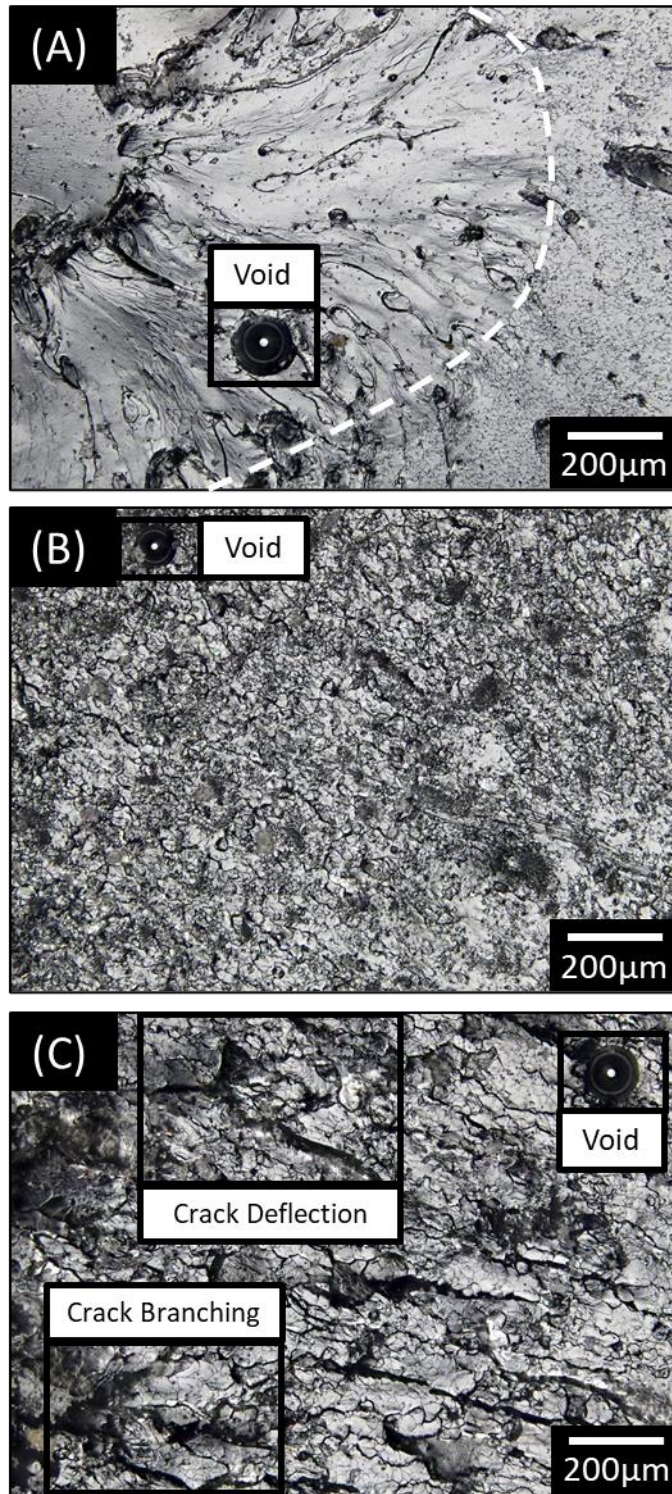


Figure 4.11A – C: Surface Fracture of E132 OPEFB Nanocomposite (Nanotube Size Variation: A:<10nm, B:<30 nm, C: < 90nm)

4.4.2.2 Tensile Strength of Nanofiller (Carbon Nanotube) Size Variation

Figure 4.12 presents the average tensile strength of 0.3125 wt% OPEFB and 0.25 wt% carbon nanofiller E132 composites under varying nanotube sizes. Based on the results obtained, the incorporation of carbon nanotube < 10 nm yielded a significantly lower tensile strength. The surface fracture of this composite, Figure 4.11A, indicated weak resistance to the crack propagation and the presence of a void further contributed to its overall lower tensile performance.

With the use of a larger-sized carbon nanotube (<30 nm and 90 nm), the average tensile strength of the composites displayed negligible differences, whereas composites containing carbon nanotubes < 90 nm were 0.2 MPa lower. Interestingly, the surface fractures of these composites show a different morphology. Composite with the use of carbon nanotube < 30 nm in Figure 4.11B is more granular, featuring higher density and smaller sized conical – parabolic markings. On the other hand, composite with the use of carbon nanotube < 90 nm in Figure 4.11C is less granular with the presence of crack lines in the form of crack branching and “T junctions”. Furthermore, the size of the void in composite with carbon nanotube < 30 nm features a void smaller than the void present in composites with carbon nanotube < 90 nm. This could contribute to its slightly lower tensile strength.

Kritikos and Karatasos [195] explained that the mobility of the nanofiller also plays a role in the enhancement process, where a larger nanofiller size imparts a longer desorption process and slower mobility on the absorbing layer. As a result, this can increase the viscosity of the mixture. The increased viscosity can contribute to the formation of voids within the matrix as more internal pressure is required to release the entrapped air. As shown previously, the presence of a void has been shown to reduce tensile strength. In addition, larger aspect ratio nanofillers have been shown to result in larger carrying capacity. However, this also leads to higher interfacial stress that can cause earlier debonding [196]. This understanding explains the drastic reduction observed with the composite made with carbon nanotube < 10 nm, which possesses the highest aspect ratio among the three nanotubes used in this research.

Based on the average tensile strength results, it is believed that there is a threshold limit of nanofiller size on the effects of tensile strength reinforcement. The increase in nanofiller size higher than 30 nm, resulted in similar tensile strength when compared to nanofiller size less than 30 nm. With that, carbon nanotubes between 10 to 30 nm filler are determined to be the most effective size, as it resulted in composites with a lower variation of tensile strength between samples.

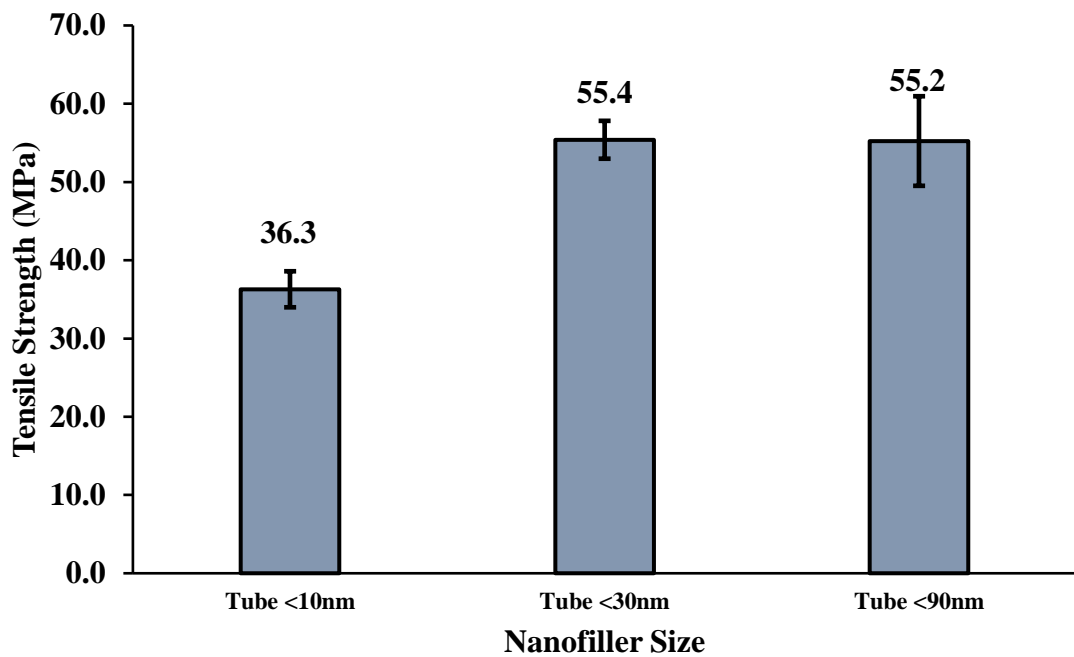


Figure 4.12: Tensile Strength of E132 OPEFB Nanocomposites (Nanotube Size Variation)

4.4.3 Nanofiller Geometry

4.4.3.1 Surface Fracture of Nanofiller Geometry Variation

Figure 4.13A-C presents the surface fracture of OPEFB E132 nanocomposites filled with varying nanofiller geometries (Tube, Platelets and Spherical). Figure 4.11A and Figure 4.10B have been covered in the previous sub-chapter on the influence of filler loading rates and filler sizes respectively.

Based on Figure 4.13, the overall fracture surface of the composites appears to have different morphology; The changes in geometry from tube to platelet and spherical result in a less granular surface fracture. Upon closer inspection, these granules are the conical – parabolic markings. Figure 4.13A, composite filled with nanotubes presents the highest density with the smallest sized marking among the three different nanofiller geometry. Thus, indicating that it experienced the fastest crack propagation because of embrittlement.

Figure 4.13B, composite filled with graphene nanoplatelets presents a surface fracture featuring crack branches alongside smaller conical shaped cracks within the conical – parabolic damage zone. The presence of the crack branches indicates that the composite experienced high stress and released high energy via crack bifurcations as indicated in the figure [188].

Figure 4.13C, composite filled with spherical nanopowder presents a surface fracture that is uniquely different compared to the previous surface fracture; it is comparatively smoother, consisting of fewer conical – parabolic markings that are also larger and accompanied by spherulitic morphology. This morphology is indicative of a crack arrest as the energy release rate is insufficient to bypass the spherulite [190]. With the use of digital zoom, crack pinning can be observed throughout its surface fracture; it is easily identified by the presence of its characteristic tails [197]. Crack pinning is associated with increased toughness as the particle impedes the propagation of the crack by bowing out the crack front between the particles [197]. In addition, the spherulitic morphology indicated in the figure closely resembles a ductile tear, where the eye of it

appears to have a sign of necking. It is believed that the use of spherical shaped nanofiller increases the ductility, as it is an attractor for polymer chain entanglement as reported by Riggleman et al [198].

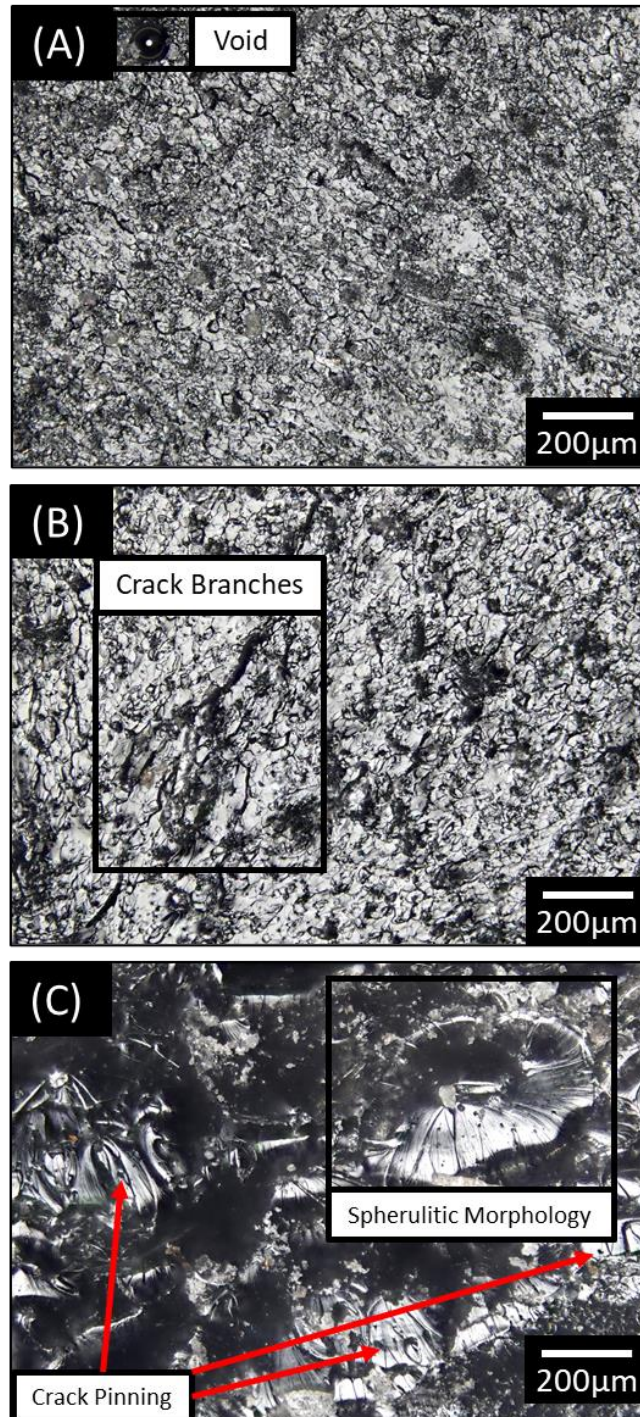


Figure 4.13A – C: Surface Fracture of E132 OPEFB Nanocomposite (Nanofiller Geometry Variation: A: Tube, B: Platelets, C: Spherical)

Figure 4.14A-C presents the SEM micrographs of OPEFB E132 nanocomposites filled with varying nanofiller geometries (Tube, Platelets and Spherical). These micrographs were analysed under varying magnification to verify and depict the incorporation of the respective fillers. The transition from tube to platelets and spherical fillers similar show the reduction in crack bifurcation; thus, presenting a lesser granular surface fracture.

In Figure 4.14A, tube/rod-like structures were present and were caught to be entangled among each other. This indicates that the nanotube fillers were nested together in the form of agglomerates. Furthermore, it is also observed that the nanotubes were poorly distributed. It should also be noted that the fracture can be observed to have multiple layers, where it is lower on the right section and increase in height to the left.

In Figure 4.14B, the presence of platelet-shaped structures can be observed in toward the centre of the micrographs. Upon closer inspection, it can be observed that a portion filler has been left exposed as a result of the fracture. This indicates that good adhesion / interfacial bonding between the filler and matrix was achieved. The fracture of nanoplatelets composite was observed to have a reduced layer of fracture as compared to the composite filled with nanotubes. Furthermore, a smoother and cleaner surface fracture was observed.

In Figure 4.14C, the presence of circular structures can be observed through the micrographs. The fillers are observed to be well dispersed with good distribution and no signs of agglomeration. Among the three different nanofiller geometries used, spherical shaped fillers were shown to produce the smoothest surface fracture with the lowest cracks and layers.

Based on the qualitative data obtained in this research project, it can be concluded that the use of spherical shaped nanofillers achieved better dispersion than tube-shaped nanofillers. This further supports the hypothesis that the dispersion of a filler improves with a more uniform and symmetrical structure.

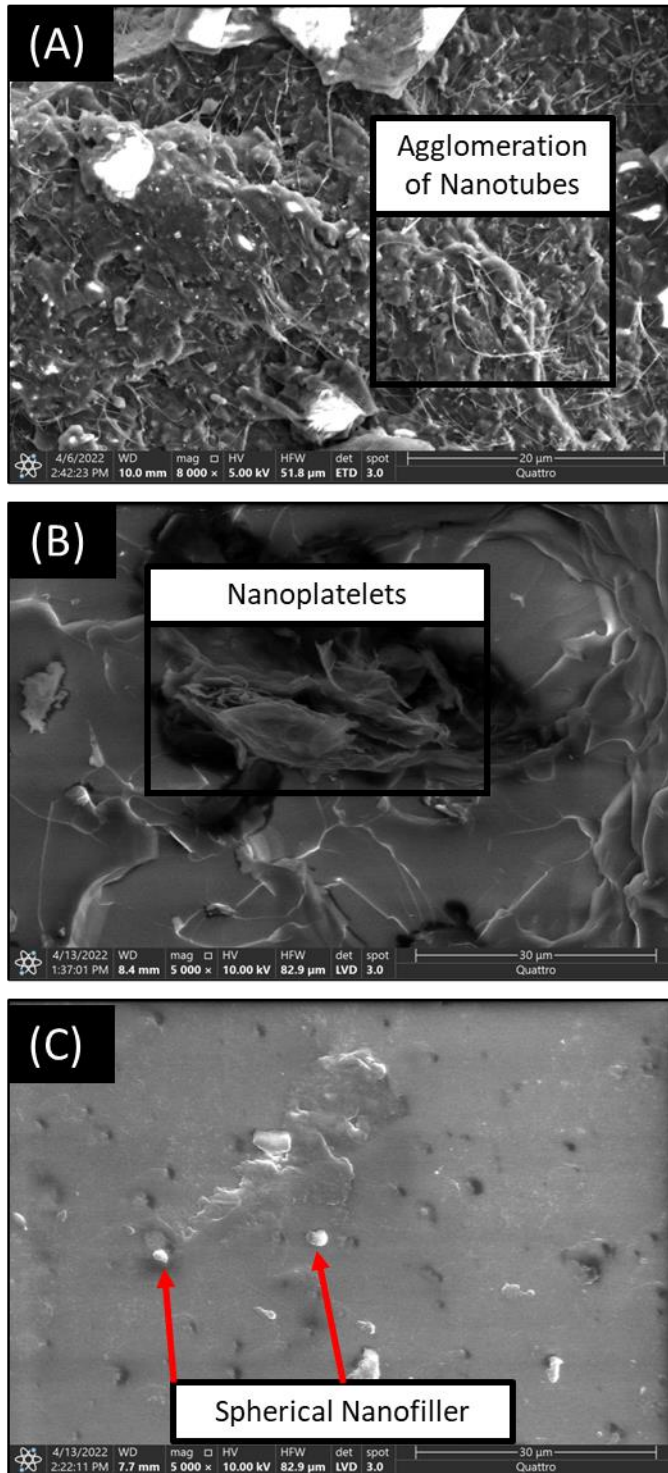


Figure 4.14A – C: SEM Micrographs of E132 OPEFB Nanocomposite (Nanofiller Geometry Variation: A: Tube, B: Platelets, C: Spherical)

4.4.3.2 Tensile Strength of Nanofiller Geometry Variation

Figure 4.15 presents the average tensile strength of OPEFB E132 nanocomposites filled with varying nanofiller geometries (Tube, Platelets and Spherical) alongside neat E132 and E132 reinforced with 0.3125 % of OPEFB, serving as comparison. Among the three varying nanofiller geometries, tube-shaped nanofillers displayed the least tensile strength followed by nanoplatelets, which has an additional improvement of 2.5 MPa, equivalent to a 4.15 % increase in tensile strength. The tensile strength of these composites is also reflected in their surface fracture in Figure 4.13A – B; where composites filled with nanotube contain void thereby reducing their mechanical strength while composites filled with nanoplatelets contain crack branches, indicating a sign of high stress during fracture. Furthermore, with the use of SEM micrographs presented in Figure 4.14A, the presence of agglomerated nanotubes further explains its reduced mechanical performance. It is believed that the agglomerates act as a site weak spot, preventing higher load transfer instead of reinforcing the composites.

Composites filled with spherical carbon nanofillers displayed the highest tensile strength at 59.1 MPa. The incorporation of spherical shaped fillers compared to tubes and platelets display improvements in tensile strength by 1.2 MPa and 3.7 MPa, which are equivalent to 2.07 % and 6.68 % respectively. Spherical shaped nanofillers have been reported to distribute stress more evenly compared to irregular counterparts [199] as there is a lack of protrusion. Observing its surface fracture in Figure 4.13C, it is believed that the use of spherical shaped nanofiller imparted ductility, as a sign of necking behaviour was found on its surface fracture. The presence of crack pinning also suggests it has improved toughness.

By comparing E132 epoxy-based material as a whole, its neat condition poses the lowest tensile strength. The introduction of 0.3125 wt% of OPEFB as microfillers has shown to impart tensile reinforcing ability across the board, even surpassing the strength of tube-shaped nanofillers reinforced composite by 1.8 %. From this study, it is found that incorporation of OPEFB alongside platelets and spherical shaped fillers as a hybrid

nanocomposite, increases the tensile strength of E132 based epoxy by 18.6 % and 21.1% respectively.

Literature has agreed that the filler reinforcing effect is dependent on the aspect ratio of the nanofiller [92, 98], increasing its interfacial bonding, and enabling greater loading transfer. Thus, improving its mechanical properties. It was conceptually believed that tube-shaped nanofillers, particularly SWCNT would yield the desired outcome due to their high aspect ratio. However, the addition of fillers also causes embrittlement, as it hinders the mobility of the particles [194].

Similar research was conducted by Hu et al.[196] in 2021, who simulated the effects of nanofiller shapes/geometries (nanotube and nanoplatelets). It was found that tube-shaped nanofiller in a composite contributes reinforcement only at relatively low stress or elastic regime; having very poor performance in high stress or plastic regime. On the other hand, nanoplatelets were found to have marginally better performance in both elastic and plastic settings. This was attributed to the lower interfacial stress, where nanoplatelets were less susceptible to debonding. Thus, this supports the results obtained in this research for both tube and platelet. It is hypothesized that a higher total surface area per volume fraction of the spherical-shaped filler allowed greater efficiency of stress transfer.

Based on the presented average tensile strength, it was found that the use of spherical nanofiller in E132 polymer matrix resulted in the most effective tensile strength, attaining an average of 59.1 MPa, achieving a total improvement of 21.11 %. By varying the geometries/aspect ratios of the nanofiller, it can observe that the decrease in nanofiller dimension (Tube > Platelets > Spherical) yielded greater tensile strength.

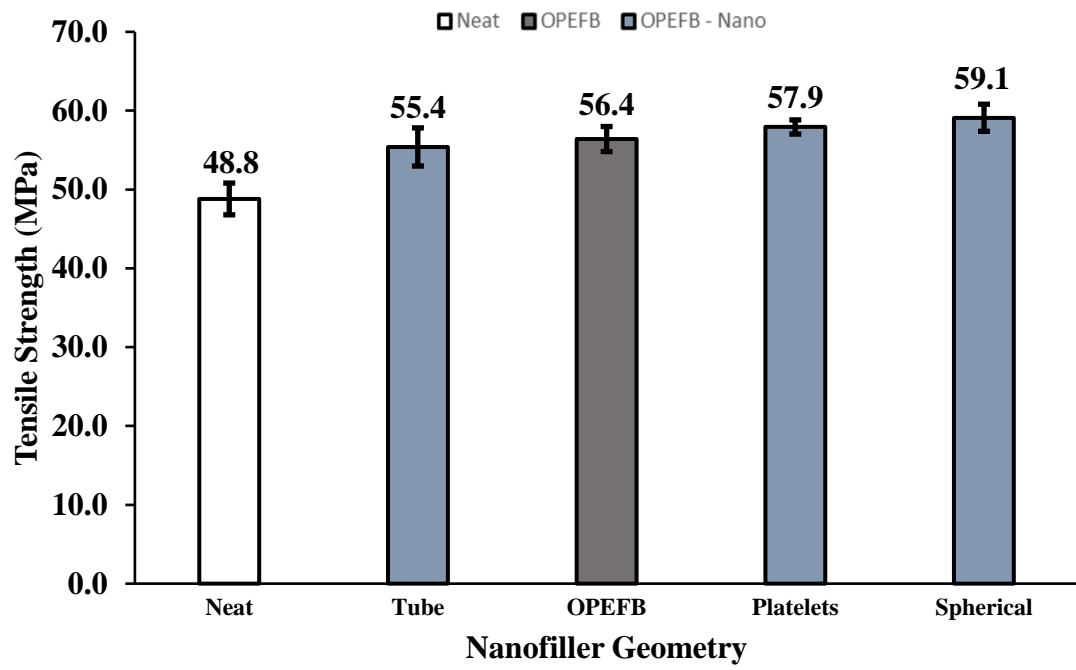


Figure 4.15: Tensile Strength of E132 OPEFB Nanocomposites (Filler Geometry Variation)

4.5 Effects of Matrix Density

4.5.1 Surface Morphology of Matrix Variation

Figure 4.16A-C presents the surface fracture of OPEFB spherical shaped carbon nanopowder under varying polymer matrix density (Tarbender, EpoxAmite 102 and E132). The surface fracture of the fabricated composite samples were analysed under x10 magnification.

The overall fracture surface of the composites appears to vary across different matrices; the changes in matrix density from Tarbender (low) to EpoxAmite 102 (medium) to E132 (high) result in a less granular and smoother surface fracture. Upon closer inspection, these granules are the conical – parabolic markings. Figure 4.16A, composite made from Tarbender (low) presents the highest presence of the smallest sized marking among the three different epoxy matrices. Thus, indicating that it experienced the fastest crack propagation.

Figure 4.16B, composite made from EpoxAmite 102 (medium) presents a surface with two distinct fracture features. The left side is considerably rougher with a higher density of conical parabolic markings. Whereas on the right side, it is observed to be less granular and contains hackles marks. This surface fracture displayed both ductile and brittle surface features, capturing their transitional behaviour. Its transitional behaviour has been separated by a white dashed line. Interestingly, the conical parabolic markings on the left side were observed to be relatively sharper in comparison to the mentioned markings in Figure 4.16A.

Figure 4.16C, composite made from E132 (high) presents a surface fracture that is uniquely different compared to the previous surface fracture; it is comparatively smoother and consists of fewer conical parabolic markings that are also larger, accompanied by spherulitic morphology. This morphology indicates a crack arrest as the energy release rate is insufficient to bypass the spherulite [190]. At a closer inspection, crack pinning can be observed throughout its surface fracture; it is easily identified by the

presence of its characteristic tails [197]. Crack pinning is associated with increased toughness as the particle impedes the propagation of the crack by bowing out the crack front between the particles [197]. In addition, the spherulitic morphology indicated in the figure closely resembles a ductile tear, where the eye of it appears to have a sign of necking behaviour.

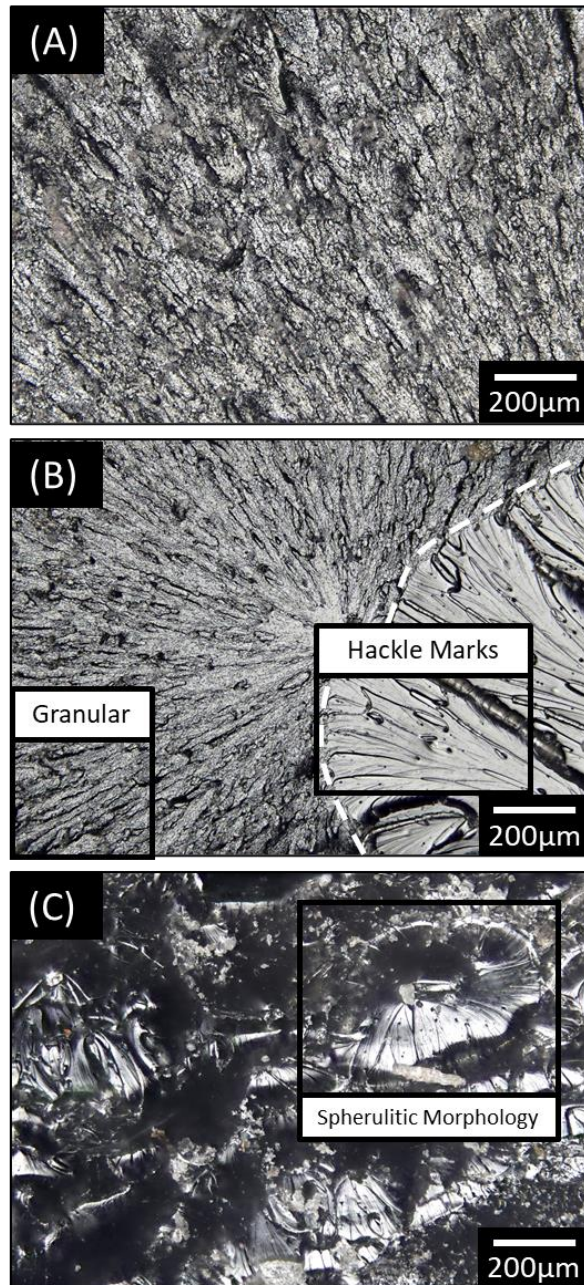


Figure 4.16A – C: Surface Fracture of OPEFB Nanocomposite (Matrix Density Variation: A: Tarbender, B: EpoxAmite 102, C: E132)

Figure 4.17A-C presents the SEM micrographs of OPEFB carbon nanopowder in varying polymer matrix density (Tarbender, EpoxAmite 102 and E132), focusing on the microscopic fracture patterns. These figures further highlight the distinctive fracture patterns of the nanocomposites. The changes from low density to medium to high resulted in a less granular, smoother, and even surface fracture.

In Figure 4.17A, composite made from Tarbender (low) can be observed to contain a high number of microcracks and produced a relatively uneven fracture pattern, indicating the material's brittleness. In addition, even at x2000 magnification, no signs of filler agglomerations were observed. Thus, indicating that both fillers (OPEFB filler and the nanofiller) achieved good dispersion.

In Figure 4.17B, composite made from EpoxAmite 102 (medium) can be observed to have a drastic decrease in the number of microcracks alongside a more even surface. Similarly, both fillers (OPEFB filler and the nanofiller) can be observed to achieve good dispersion. Furthermore, the formation of a conical – parabolic marking can be observed at the bottom right quadrant of the figure; to which the secondary crack nucleated in front of the primary crack.

In Figure 4.17C, composite made from the E132 (high) can be observed to have a drastic decrease in the number of microcracks, alongside a more even surface compared to the other two matrices. As a result of this, a less cluttered surface can be observed. Thus, also making the filler particles in this polymer matrix more distinguishable. It can be observed that the filler particle within this composite did achieve good dispersion as with the other composite. However, it is also shown to result in poorer distribution of the fillers, with lower spatial distribution among the fillers.

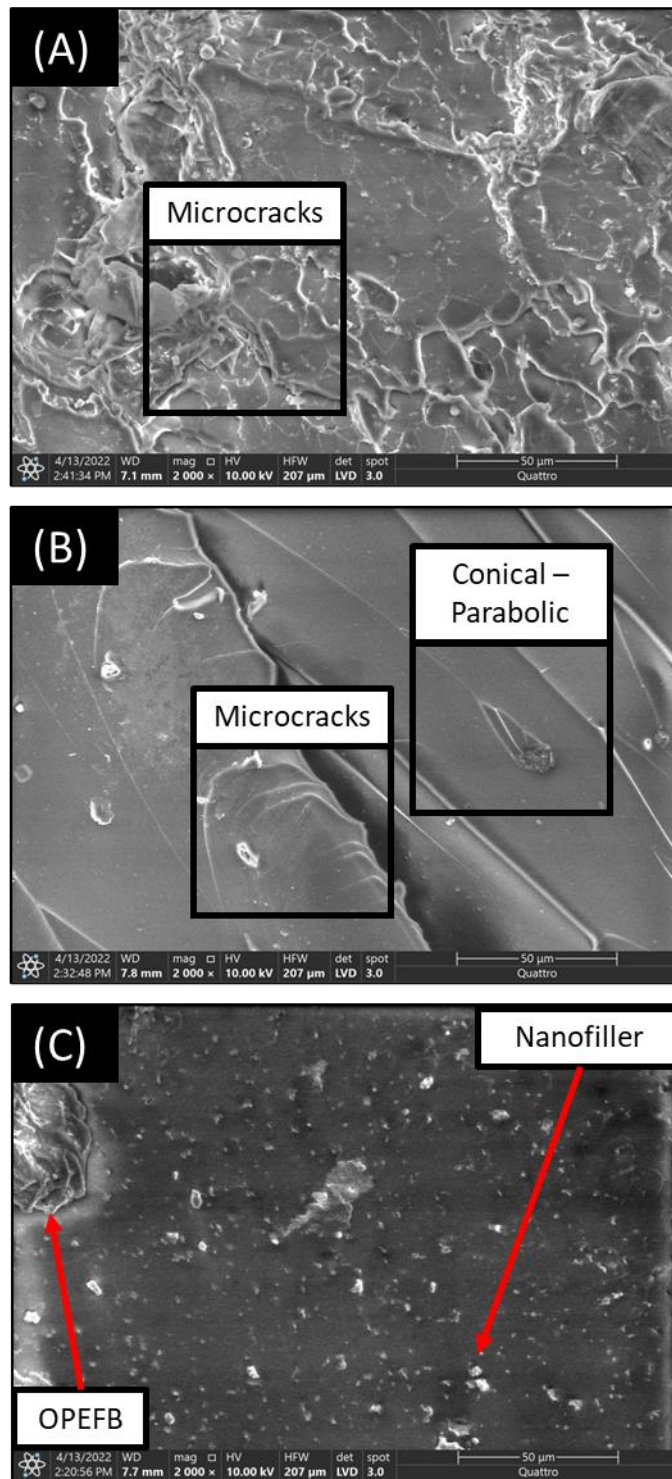


Figure 4.17A – C: SEM micrographs of OPEFB Nanocomposite (Matrix Density Variation: A: Tarbender, B: EpoxAmite 102, C: E132)

Figure 4.18A-C presents the SEM micrographs of OPEFB carbon spherical nano particles in varying polymer matrix density (Tarbender, EpoxAmite 102 and E132) with the focus on the interfacial region between OPEFB filler and the matrix. In Figure 4.18A and B (Tarbender and EpoxAmite 102 respectively), it can be observed that adequate bonding was present due to the absence of fiber pull-out. However, dark regions were spotted along the perimeter of these OPEFB fillers (the interfacial region between the filler and the matrix). It is hypothesized, that the void regions along the interface were formed due to the stress and strain experienced during tensile strength. As the load was transferred from the matrix to the filler particles, the forces it experienced were strong enough to cause the filler to fracture and overcome the adhesion along the perimeter of the filler, thus creating this gap. The presence of this gap contributes to lower tensile performance [200]. The forces applied were insufficient to overcome the overall interfacial bonding between the matrix and filler, as evident by the lack of a pull-out zone.

In Figure 4.18C, it can be observed that the dark region around the interface of the OPEFB filler and matrix is not noticeable. This indicates that good interfacial bonding was achieved, as the forces experienced were not sufficient to overcome its adhesion and bonding. Further inspecting the morphology of the OPEFB filler, it has a significantly rougher texture compared to the specimens. Due to improved adhesion, it is believed that a higher load transfer efficiency was experienced by the OPEFB filler and resulted in a more intense fracture. Thus, resulting in increased surface roughness.

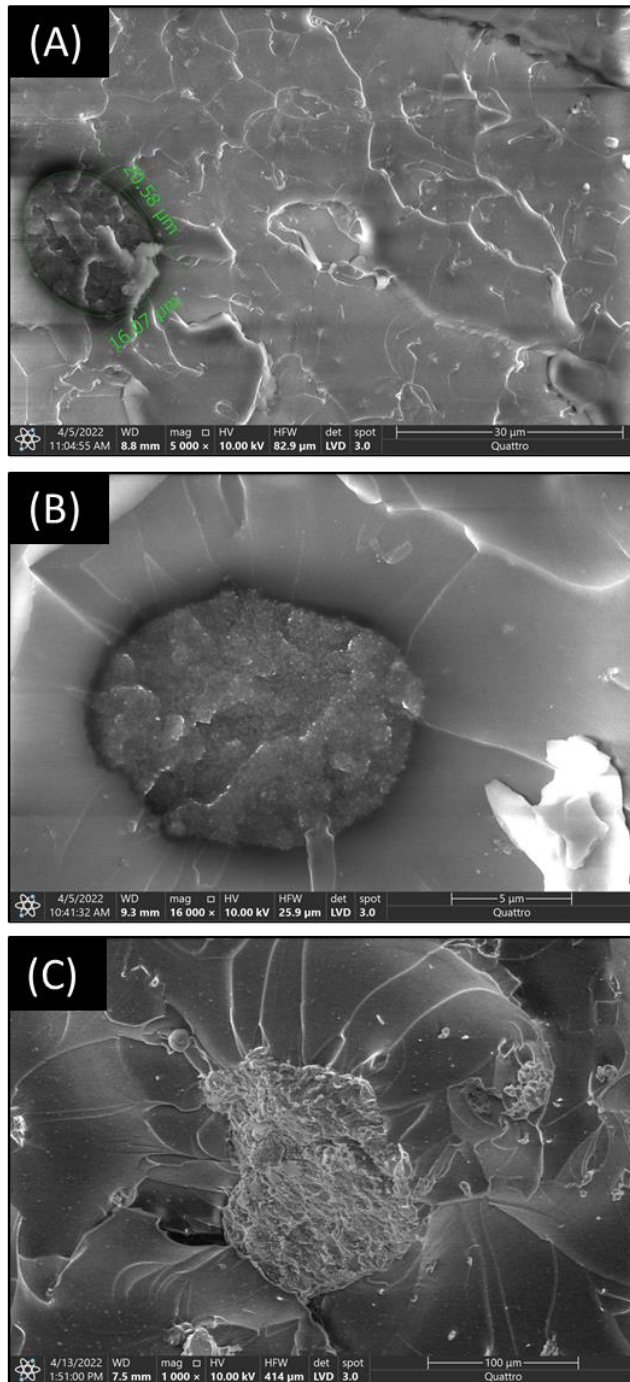


Figure 4.18A – C: SEM Micrographs of OPEFB Nanocomposite (Matrix Density Variation: A: Tarbender, B: EpoxAmite 102, C: E132)

Figure 4.19A-C presents the SEM micrographs of OPEFB carbon spherical nano particles in varying polymer matrix density (Tarbender, EpoxAmite 102 and E132), focusing on the microscopic fracture patterns. In Figure 4.19A, the fracture pattern of Tarbender OPEFB nanocomposites resembles the pattern of fractured tempered glass. Thus, indicating its brittle properties. Unfortunately, upon magnification above x5000, the material started to burn due to a higher concentration of electrons focused within a smaller area. Such burn marks can be found in the shape of a rectangle at the bottom of the figure. This may also be a result usage of high voltage and the lack of conductive coating.

In Figure 4.19B, the fracture pattern of EpoxAmite 102 OPEFB nanocomposites was observed to have its boundary layer peeled off. To further explain it, two different micro size films can be seemed to detach themselves at an angle while still being connected at one end. Upon further inspection, the composites appear to have fractured in layers, where their uneven surface is a result of multiple layers. Interestingly, the observed fracture patterns have neither the traits of brittle nor ductile features. Hence, it is believed the composite has intermediate property.

In Figure 4.19C, the fracture pattern of E132 OPEFB nanocomposites is vastly different compared to the other specimens. This SEM micrograph present plastically deformed regions with well-developed spurs; These features are typical in ductile fractures [201]. Upon closer inspections, a spring shaped / spiral structure can be observed as a result of its fracture.

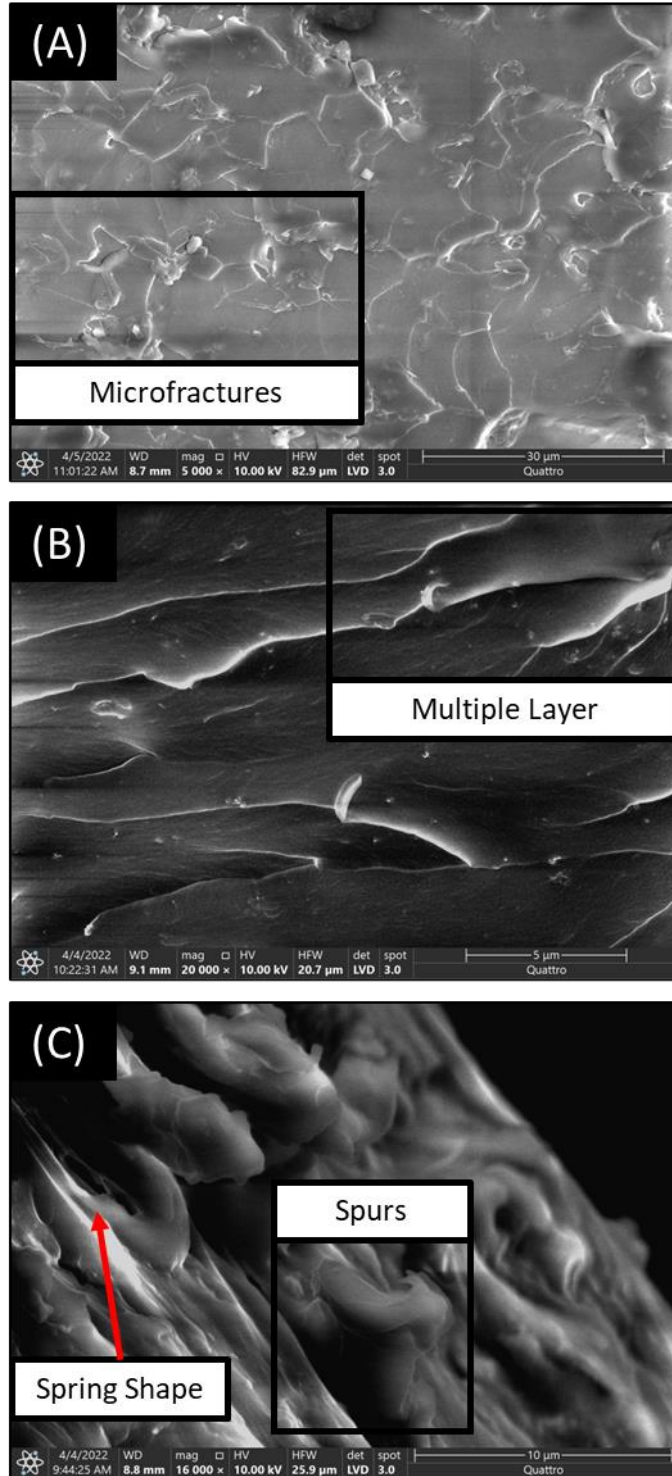


Figure 4.19A – C: SEM Micrographs of OPEFB Nanocomposite (Matrix Density Variation: A: Tarbender, B: EpoxAmite 102, C: E132)

4.5.2 Tensile Strength of Matrix Variation

Figure 4.20 presents the average tensile strength of OPEFB carbon spherical nanoparticles in varying polymer matrix density (Tarbender, EpoxAmite 102 and E132). Composite made of EpoxAmite 102 (medium) displayed the least tensile strength followed by composite made of Tarbender (low), which is 3 MPa higher; equivalent to a 6.06 % increase in tensile strength. The tensile strength of these composites is also reflected in their surface fracture in Figure 4.16A – B; where composites made from EpoxAmite 102 (medium) presented a surface fracture that contains a transitory fracture behaviour with sharper conical - parabolic markings in Figure 4.16B. On the other hand, composite made from Tarbender is more uniform and granular in structure, suggesting that the presence of the parabolic markings and smaller conical shaped cracks found within the said markings restricts the primary crack [187], thus leading to higher tensile performance.

That being mentioned, composite made from E132 (high) displayed the highest average tensile strength at 59.1 MPa. The use of a high-density matrix compared to low density and medium density displays higher tensile strength by 6.6 MPa and 9.6 MPa, which is equivalent to 12.57 % and 19.39 % respectively. Observing their surface fracture, the increase in matrix density results in less granular and smoother surface morphologies. Additionally, it was observed that the high density matrix achieved greater interfacial bonding between the filler and the matrix.

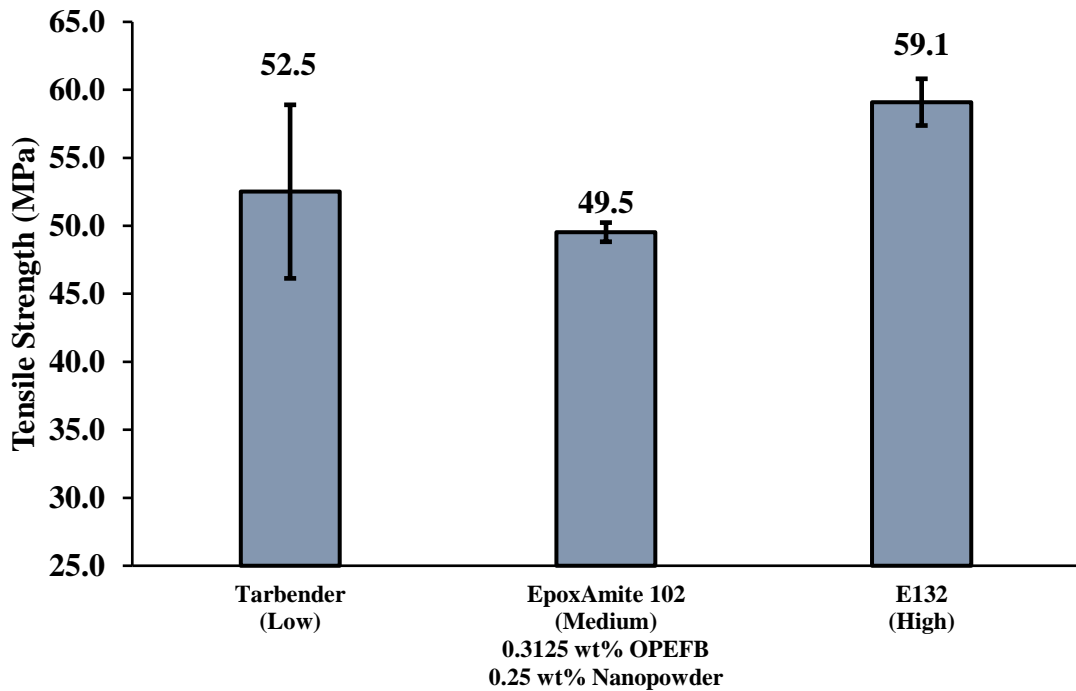


Figure 4.20: Tensile Strength of OPEFB Carbon Nanocomposites (Matrix Density Variation)

The relationship between density (D) and its molecular weight (MM) can be expressed in the form of $D = \frac{n \times MM}{V}$, where n is the number of moles of the substance and V is its volume. Thus, establishing its co-relationship where the greater its molecular weight, the higher its density. From literature, it has been understood that at lower molecular weight, polymer chains are loosely bonded by weak van der Waals forces, allowing the chain to move easily [202]. However, at large molecular weight, the chain becomes larger, resulting in chain entanglement. That being mentioned, the relationship between tensile strength and molecular weight will reach a saturation level [202]. Despite that, fracture toughness has been shown to increase monotonically with a higher value of molecular weight [203].

In thermoset polymers such as epoxy, the presence of cross-links restricts the motion of the chain and increases the strength of the polymer [202]. A highly cross-linked epoxy system was shown to have the least resistance to fracture, crazing and (possibly) plastic deformation [203]. Interestingly, it was found that reduction in polymer

molecular weight allows the transition of failure mode from ductile to brittle failure via chain scission [204]. Thus, suggests that the molecular weight and matrix density influence its failure mode, revolving around crosslink density and the degree of chain entanglements.

Figure 4.21 presents the stress-strain curve of OPEFB carbon nanopowder composites made from varying polymer matrix density (Tarbender, EpoxAmite 102 and E132). This figure shows that Tarbender (low) nanocomposites are very brittle and displayed low toughness. The specimen fractured before necking, absorbing a comparatively low amount of energy. On the other hand, EpoxAmite 102 (medium) nanocomposite was observed to be more ductile and tougher. It experienced more strain before its fracture, producing a larger area under the curve. E132 (high) nanocomposite was observed to be the most ductile and toughest. It experienced the most strain with the largest area under the curve before the fracture occurred. These data indicate that the increase in polymer matrix density allows for higher ductility and higher toughness when applied as a matrix in OPEFB nanocomposite.

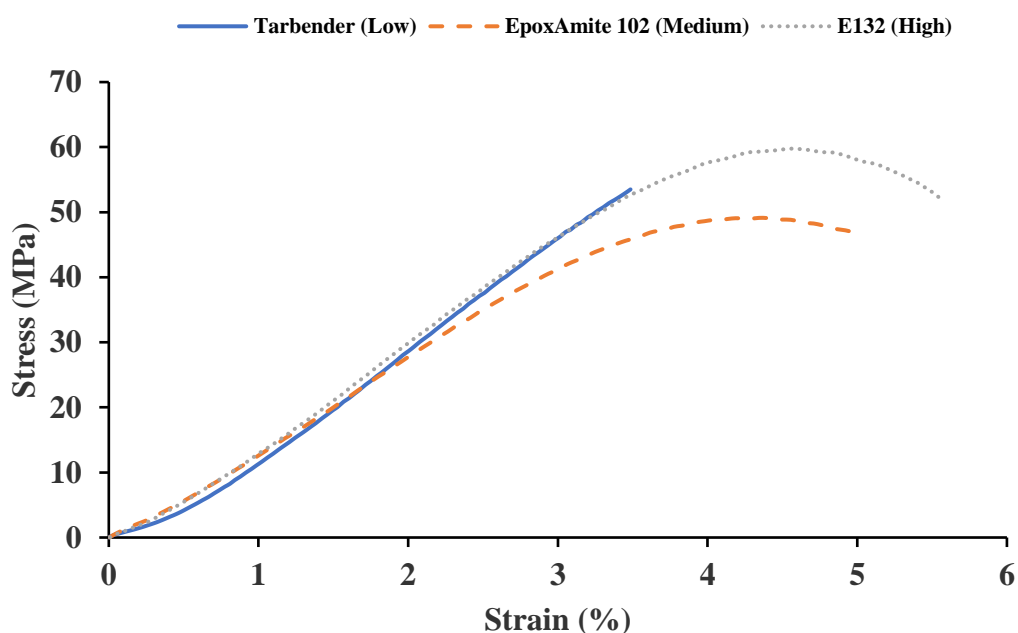


Figure 4.21: Stress-Strain Graph of OPEFB Carbon Nanocomposites (Matrix Density Variation)

4.5.3 Weibull Analysis and Modelling

Based on the tensile strength collected via the UTM tests, the values for Tarbender, EpoxAmite 102 and E132 OPEFB nanocomposites are sorted from the lowest to the highest and then assigned a probability occurrence. The relevant values are presented in Appendix B. With the tabulated values, Weibull analysis can be performed by plotting $\ln \left[\ln \left[\frac{1}{1-P_f(\sigma)} \right] \right]$ against $\ln[\sigma]$.

By performing the Weibull analysis, values such as Weibull Modulus, and Weibull Characteristic Strength can be calculated. Weibull modulus indicates the strength distribution width of the material, where a high value / steep slope is favoured, as the material is more predictable and has a lower tendency to break at a stress much lower than its mean value [205]. In other words, Weibull Modulus reflects the reliability of the material, a larger value indicates higher reliability [177].

Using the tensile strengths obtained experimentally, Weibull analysis can be used as an evaluation method for strength statistics by calculating the characteristics strength of the material. The characteristic strength is analogous to median strength, where 50 % of the fracture would be lower than the median strength. The difference between characteristics strength and average strength lies in the details of the distribution, where it is similar but not equal [206]. The two-parameter Weibull distribution is expressed in Eq1.

Figure 4.22A shows the Weibull plot of OPEFB Nanocomposite made from Tarbender (low). The best fit line drawn is shown to be an acceptable regression model with a good fit, obtaining a coefficient of determination of 0.98. Thus, results in 9.5 for its Weibull Modulus and 55.2 MPa for its Characteristics Strength. Figure 4.22B shows the Weibull plot of OPEFB Nanocomposite made from EpoxAmite 102 (medium). The best fit line drawn is shown to be an acceptable regression model with a good fit, obtaining a coefficient of determination of 0.98. Thus, resulting 82.2 for its Weibull Modulus and 49.8 MPa for its Characteristics Strength. Figure 4.22C shows the Weibull plot of OPEFB Nanocomposite made from E132 (high). It can be observed that the best fit line drawn

did not intercept one of the data points. Hence that point is considered an outlier. One possible explanation for this variation lies within the orientation and size of the critical flaw [207] present within the fabricated sample. Additionally, imperfect nanofillers with vacancy defects can also lead to a poor interface region [208], resulting in reduced tensile strength. The best fit line drawn for the remaining data points is shown to be an acceptable regression model with a good fit, obtaining a coefficient of determination of 0.93. Thus, achieving 183.4 for its Weibull Modulus and 59.9 MPa for its Characteristics Strength. Table 4:12 summarizes the Weibull Moduli and Characteristics Strengths.

It is found that with the increase in polymer matrix density, the higher the Weibull Modulus of the OPEFB Nanocomposite. Thus, indicated that higher polymer density results in a composite material that is more reliable with a lower tendency to break at a stress much lower than its average tensile strength.

Based on the obtained Characteristics Strengths, an effective model of tensile strength against matrix density was developed using MATLAB R2021b. Using the MATLAB basic fitting tool, Equation 4.1 was shown to best fit alongside the 3 data points, where y is the tensile strength and x is the matrix density:

$$y = 4603.1746x^2 - 10396.9841x + 5918.881 \quad \text{Equation (4.1)}$$

Two additional OPEFB carbon nano particle composites of varying matrix density (1.10 g/cm³ and 1.12 g/cm³) were fabricated and tested. Based on the 5 samples for each density, composites made with 1.10 g/cm³ obtained an average tensile strength of 52.0 MPa whereas, composites made with 1.12 g/cm³ obtained an average tensile strength of 48.0 MPa. Using the empirical model developed above, composites made with 1.10 gcm⁻³ and 1.12 gcm⁻³ would yield 52.0 MPa and 48.0 MPa respectively. The experimental and modelled values are presented in Table 4:13.

Comparing both results, the experimental and modelled values are very similar; composites made with 1.10 g/cm³ have a percentage of error of 0% while composites made with 1.12 g/cm³ has a percentage of error of 1.03%. Thus, it can be concluded the model is valid.

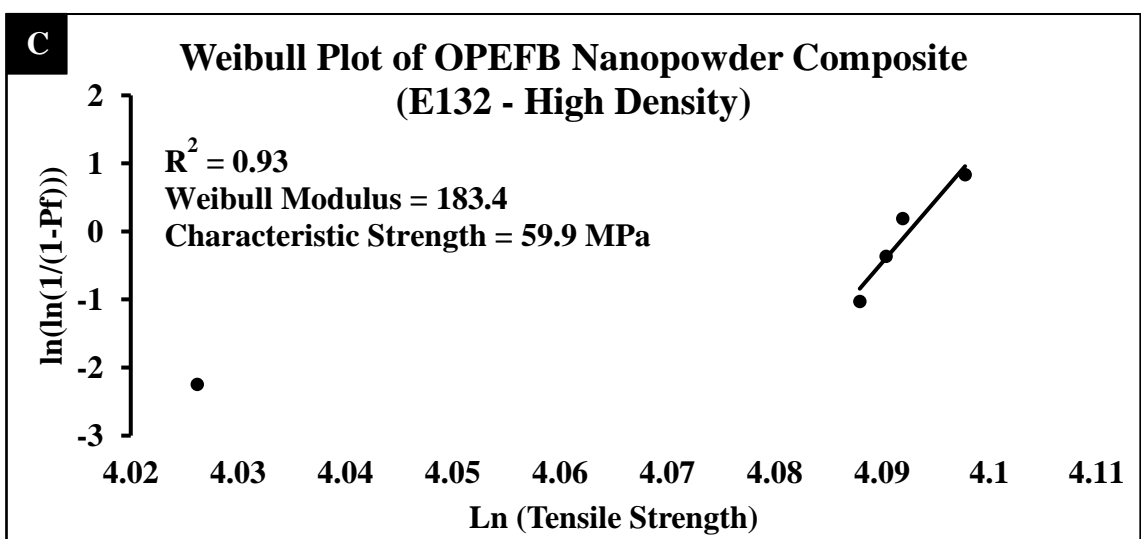
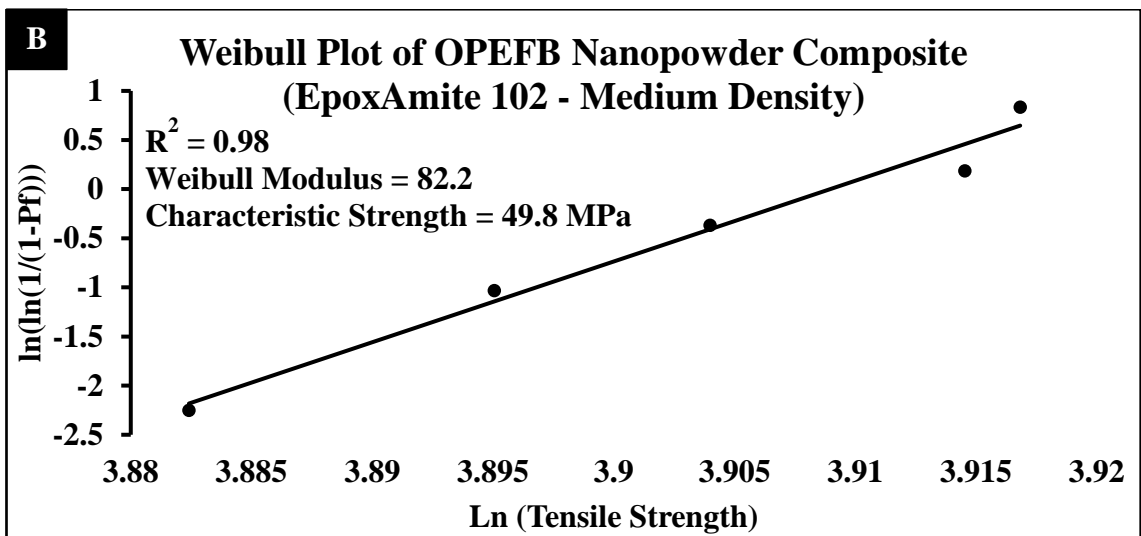
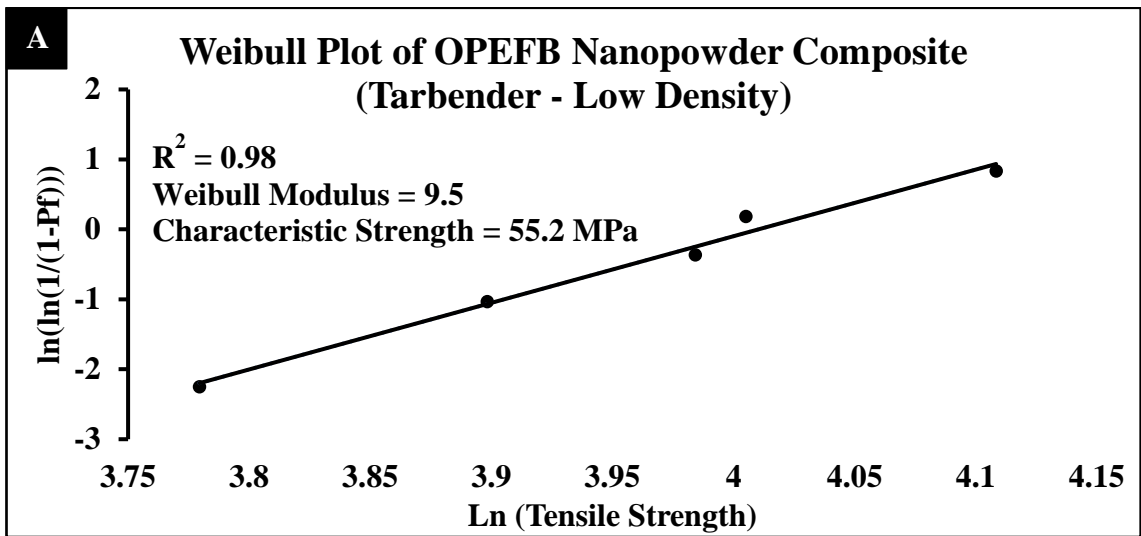


Figure 4.22A – C: Weibull Plot of OPEFB Nanocomposite (Matrix Variation)

Table 4:12: Summary of Weibull Moduli and Characteristic Strengths

Epoxy	Density (g/cm ³)	Weibull Modulus	Characteristic Strength (MPa)
Tarbender	1.09	9.5	55.2
EpoxAmite 102	1.11	82.2	49.8
E132	1.18	183.4	59.9

Table 4:13: Experimental and Modelled Tensile Strength Values

Density (g/cm ³)	Tensile Strength (MPa)		Percentage of Error (%)
	Modelled	Experimental	
1.10	52.0	52.0	0
1.12	48.5	48.0	1.03

4.6 Summary of Results and Discussion

Beginning with the degassing of epoxy, after 5 minutes, a reduction in macro bubbles within the mixture was observed in all processes (hot water, ultrasonic bath and vacuum). It is revealed that a longer duration of degassing process leads to further removing the bubbles present within the epoxy mixture. However, a longer duration of the process resulted in shorter epoxy workability as experienced with 8 minutes of hot water and ultrasonic bath process. This could be due to the additional heat applied to the epoxy mixture in the mentioned process, promoting its curing process. The hot water treated mixture presented a smaller and greater number of bubbles when compared to the ultrasonic bath treated which has larger bubbles and lower numbers. The effective duration of the process for hot water and ultrasonic bath process is identified to be 7 minutes, while on the other hand, the vacuum process displayed the least formation of bubbles and microvoids even for 10 minutes. It was observed that the vacuum process showed the highest reduction of bubbles followed by hot water and then the ultrasonic bath. It is also revealed that the vacuum degassing process resulted in the highest average tensile strength at 48.8 MPa. It is 5.3 MPa and 7 MPa higher than the ultrasonic bath and hot water process.

Moving onto the effects of treating OPEFB fiber, it can be qualitative concluded that the treatment of fiber was successful. The surface morphology of the fiber after treatment presented a consistent and cleaner outlook, with the removal of impurities embedded on the surface of the fiber; a rougher surface is attributed to the removal of hemicellulose and the presence of crater indicates the removal of silica bodies. By using the works of other researchers, it is believed impurities such as natural oils, wax, pectin, silica bodies and hemicellulose were removed. In addition, the presence of fibrillation was also observed. Thus, the treated fiber will allow greater interfacial bonding between the fiber and matrix when it is used as a filler.

With the incorporation of OPEFB filler into the polymer matrix, it was observed that higher loading content led to the formation of darker and less translucent composites. Colour variation can be seen with 0 % ~ 2.5 % OPEFB whereas above 2.5% OPEFB did

not produce any significant difference to the naked eye. However, with the use of an optical microscope, significant variation can be seen at different filler loadings. At neat conditions, a significantly cleaner surface was observed compared to the composites containing OPEFB fillers. With the inclusion of fillers, the presence of white particles was observed. The number of white particles found on the surface of the composite increases with higher loading of OPEFB filler. Thus, indicating the successful addition of the fillers. At 10% OPEFB, poor dispersion of filler and signs of agglomerates within the matrix was observed. Similar to its physical changes, the incorporation of OPEFB fillers from 0.3125 % to 2.5 % has a reinforcing effect on the fabricated composites. Filler loading of 1.25 % achieved the highest average tensile strength of 57.3 MPa, a 17.4 % improvement compared to the neat condition. Additional filler content above 2.5 %, has been found to negatively influence the average tensile strength of the composites; the fillers became harder to disperse homogeneously and were prone to agglomeration, thereby reducing the adhesion between the matrix and filler.

On the topic of sonication, it is revealed that the presence of ice in the sonication process leads to the lower formation of bubbles on the resin and lowered temperature by up to 30.5 °C. In addition, it was found that ice and water immersion condition was more effective at reducing the temperature of the resin at high sonication amplitude, with an average temperature reduction of 26.7 °C at 60 % amplitude. Therefore, water & ice bath condition was selected to be used for future sonication process. On that note, it was also found that increasing the sonication amplitude by 20 % after the initial 20 %, increases the temperature of the resin by 12.5 ± 0.9 °C. Lastly, the increase in sonication duration and amplitude has also been shown to increase the formation of bubbles and alter their physical appearance from clear/translucent to dark brown. Its believed that the changes in chromatics properties are due to the addition of heat and degradation of the polymer structure. From the literature review, the addition of heat alters its conjugation length, thus, affecting the absorption of chromatic wavelength. Another explanation for the colour change can be attributed to the formation of the carbonyl group within the polymer as a result of thermal oxidation. Further investigation will be required to study the effects on mechanical properties.

To recap the addition of nanofillers, it was found that the filler loadings of 0.3125 wt% OPEFB alongside 0.25 wt% nanofiller yielded the most effective tensile strength; achieving an average of 57.9 MPa, with an overall improvement of 18.7 %. In addition, the use of three different nanotube sizes shows that composite incorporating nanotubes <10nm displayed a significant reduction in its tensile strength, by approximately 34.48 %. This was attributed to its higher interfacial stress, which resulted in earlier debonding caused by its high aspect ratio. Furthermore, this study found that altering the geometry of the nanofiller from Tube > Platelets > Spherical yielded greater average tensile strength. This can be attributed to the lower interfacial stress, where nanoplatelets and spherical particles were less susceptible to debonding. It is hypothesized that a higher total surface area per volume fraction of the spherical-shaped filler allows greater efficiency of stress transfer.

Lastly, with the use of three varying matrix density epoxy, OPEFB carbon nanoparticle-based (spherical shaped) nanocomposites were fabricated. Composite made of medium density displayed the least tensile strength followed by composite made of low density and then with high density. It is found that the increase in matrix density increases the ductility and reliability of the nanocomposites. It should also be pointed out that the Weibull analysis conducted in this research is limited with use 5 sample size, and potentially subjected to larger deviation with its Weibull modulus. Observing their surface fracture, the increase in matrix density results in less granular and smoother surface morphologies. In addition, good dispersion of fillers was achieved in all three matrices. However, it should be highlighted that matrix made from high density was observed to have a poorer distribution of fillers. Further supporting through SEM micrographs, it is also revealed that the failure mode transitioned from brittle to intermediate to ductile for low, medium and high density respectively. The result also showed that the tensile strength alongside the interfacial bonding between filler and matrix is greatly affected by the matrix density. Figure 4.23 summarizes both the morphological and tensile behaviour of the nanocomposites.

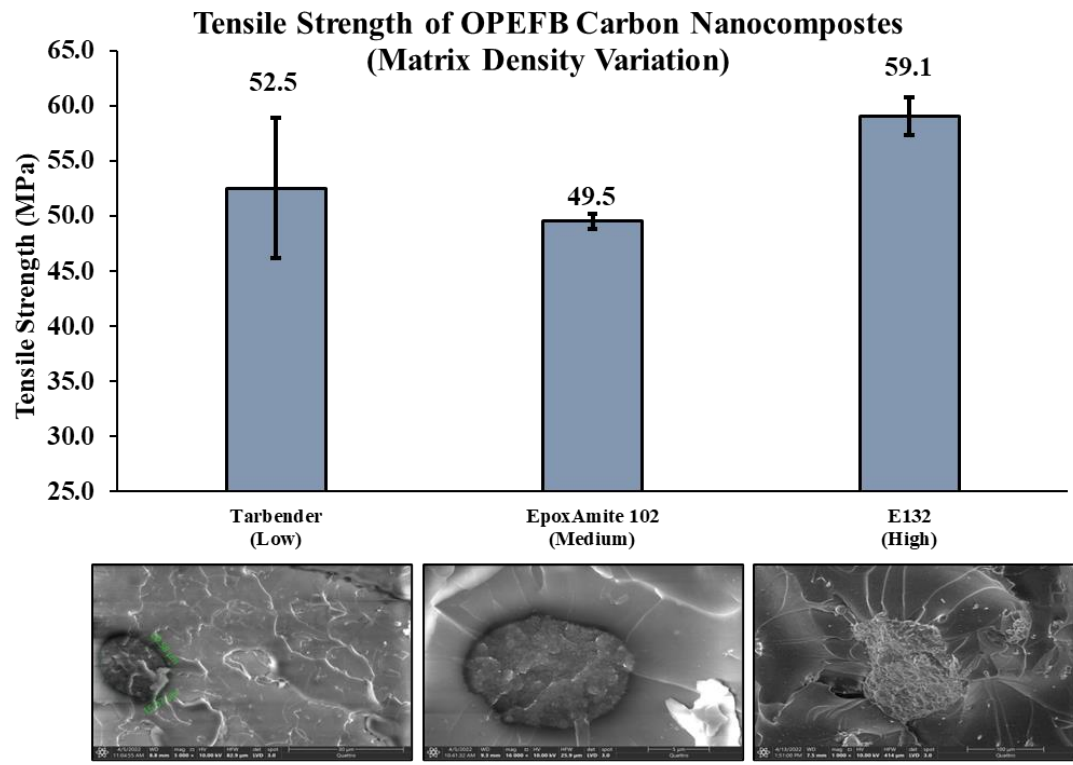
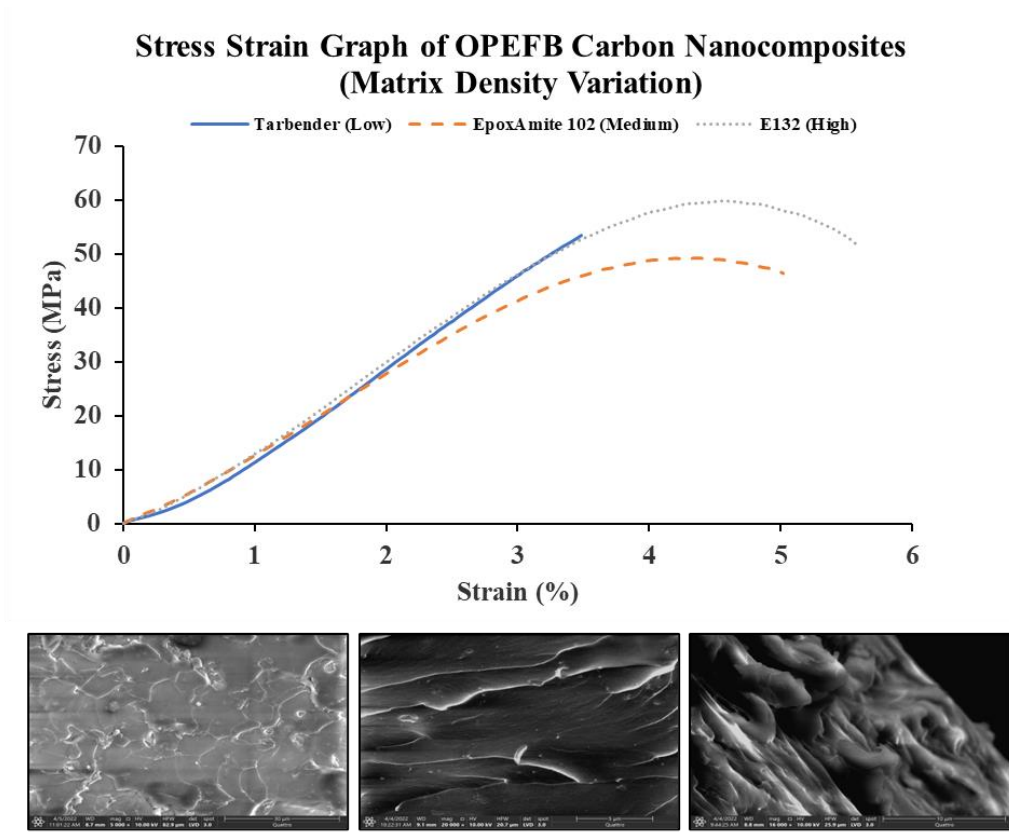


Figure 4.23: Summary of the Morphological and Tensile Behavior of Nanocomposites Under the Influence of Varying Matrix Density

CHAPTER 5

CONCLUSION

5.1 Conclusion

Based on the research conducted, all the objectives of this research were achieved. These include the effects degassing process, OPEFB filler loading, the physical effects of sonication parameters (immersion medium, duration & amplitude), nanofiller parameters (loading, size & geometry) and the matrix density.

This study shows that the presence of voids and poor dispersion of fillers in a composite material will result in reduced mechanical performance. While the use of degassing process and sonication are capable of reducing the formation of such defects, effective parameters in terms of duration and introduction of heat energy should be limited. Furthermore, the nanofillers' loading rate, size and geometry are shown to influence their dispersion behaviour and mechanical reinforcement. In addition, it was discovered that the matrix density significantly affects the nanocomposite fracture characteristic, mechanical performance, and the interfacial bonding between filler and matrix. Lastly, a model was developed and validated based on the empirical data from the experimental works. The findings in this thesis are supported through both quantitative and qualitative analysis.

The following is a list of conclusions that have been made based on the results obtained and discussions presented:

- I. It was established that the most effective degassing process is using the vacuum method for a duration of 10 minutes.
- II. It was observed that epoxy resin is more sensitive toward heat energy degradation (hot water processed) compared to mechanical forces degradation (ultrasonic bath).
- III. It is found that 0.3125 wt% - 2.5 wt% of OPEFB fiber has a reinforcing effect, resulting in up to 17.4% improvement in tensile strength at 57.3 MPa.
- IV. It was shown that ice and water was the most effective immersion condition, capable of reducing the temperature of the resin and formation of bubbles during sonication.
- V. It was presented that higher sonication amplitude and longer duration resulted in greater polymer degradation (higher intensity of chromatic alteration).
- VI. It is revealed that the combination of 0.3125 wt% OPEFB filler and 0.25 wt% carbon nanofillers was the most effective, resulting in up to 18.7 % improvement in tensile strength at 57.9 MPa.
- VII. It is noticed that the size of the nanotubes <30nm is the threshold limit on tensile strength reinforcement.
- VIII. It is observed that the use of spherical shaped nanofiller was the most effective, resulting in the highest average tensile strength at 59.1 MPa.
- IX. It is revealed that the increase in matrix density increases the ductility and reliability of the nanocomposite.
- X. It is indicated that the increase in matrix density also increases the interfacial bonding between the filler and matrix.
- XI. An effective model based on the experimental tensile strength was developed and validated.

5.2 Recommendations

The influence of matrix properties and compatibility of filler in composite material is an area that requires further understanding. For future work in this field of research, the following is a list of recommendations that can be considered.

- I. Study the effects OPEFB carbon nanocomposites degradation due to long-term weathering and fatigue.
- II. Investigate the effects of filler orientation (macro, micro and nano size) to further enhance its reinforcing potential.

REFERENCES

- [1] M. Asyraf, M. Anwar, L. M. Sheng, and M. K. Danquah, "Recent Development of Nanomaterial-Doped Conductive Polymers," *JOM*, vol. 69, no. 12, pp. 2515-2523, 2017.
- [2] A. Mostovoy, A. Bekeshev, L. Tastanova, M. Akhmetova, P. Bredihin, and Y. Kadykova, "The effect of dispersed filler on mechanical and physicochemical properties of polymer composites," *Polymers and Polymer Composites*, 2020.
- [3] V. Arumugaprabu, T. J. Ko, M. Uthayakumar, and R. D. Joel Johnson, "Failure Analysis in Hybrid Composites Prepared Using Industrial Wastes," *Failure Analysis in Biocomposites, Fibre-Reinforced Composites and Hybrid Composites*, M. Jawaid, M. Thariq and N. Saba, eds., pp. 229-244: Woodhead Publishing, 2019.
- [4] R. Scaffaro, and L. Botta, "Nanofilled Thermoplastic–Thermoplastic Polymer Blends," *Nanostructured Polymer Blends*, S. Thomas, R. Shanks and S. Chandrasekharakurup, eds., pp. 133-160, Oxford: William Andrew Publishing, 2014.
- [5] W. He, P. Song, B. Yu, Z. Fang, and H. Wang, "Flame retardant polymeric nanocomposites through the combination of nanomaterials and conventional flame retardants," *Progress in Materials Science*, vol. 114, pp. 100687, 2020.
- [6] S. Debnath, T. Ke Khieng, M. Anwar, A. K. Basak, and A. Pramanik, "Strain Rate Sensitivity of Epoxy Composites Reinforced with Varied Sizes of Bagasse Particles," *Journal of Composites Science*, vol. 4, no. 3, pp. 110, 2020.
- [7] M. Y. Khalid, Z. U. Arif, W. Ahmed, and H. Arshad, "Recent trends in recycling and reusing techniques of different plastic polymers and their composite materials," *Sustainable Materials and Technologies*, vol. 31, pp. e00382, 2022.
- [8] A. Khan, and K. K. Saxena, "A review on enhancement of mechanical properties of fiber reinforcement polymer composite under different loading rates," *Materials Today: Proceedings*, vol. 56, pp. 2316-2322, 2022.

- [9] M. R. Sanjay, G. R. Arpitha, and B. Yogesha, "Study on Mechanical Properties of Natural - Glass Fibre Reinforced Polymer Hybrid Composites: A Review," *Materials Today: Proceedings*, vol. 2, no. 4, pp. 2959-2967, 2015.
- [10] J. Holbery, and D. Houston, "Natural-fiber-reinforced polymer composites in automotive applications," *JOM*, vol. 58, no. 11, pp. 80-86, 2006.
- [11] A. Kumar Sharma, R. Bhandari, C. Sharma, S. Krishna Dhakad, and C. Pinca-Bretotean, "Polymer matrix composites: A state of art review," *Materials Today: Proceedings*, vol. 57, pp. 2330-2333, 2022.
- [12] J. Jung, and H. A. Sodano, "High strength epoxy nanocomposites reinforced by epoxy functionalized aramid nanofibers," *Polymer*, pp. 122438, 2020.
- [13] Momina, and K. Ahmad, "Study of different polymer nanocomposites and their pollutant removal efficiency: Review," *Polymer*, vol. 217, pp. 123453, 2021.
- [14] M. Zhang, G. M. Biesold, W. Choi, J. Yu, Y. Deng, C. Silvestre, and Z. Lin, "Recent advances in polymers and polymer composites for food packaging," *Materials Today*, vol. 53, pp. 134-161, 2022.
- [15] S. Pourhashem, F. Saba, J. Duan, A. Rashidi, F. Guan, E. G. Nezhad, and B. Hou, "Polymer/Inorganic nanocomposite coatings with superior corrosion protection performance: A review," *Journal of Industrial and Engineering Chemistry*, 2020.
- [16] H. Ribeiro, J. P. C. Trigueiro, C. F. Woellner, J. J. Pedrotti, D. R. Miquita, W. M. Silva, M. C. Lopes, G. J. M. Fachine, M. A. Luciano, G. G. Silva, and P. M. Ajayan, "Higher thermal conductivity and mechanical enhancements in hybrid 2D polymer nanocomposites," *Polymer Testing*, vol. 87, pp. 106510, 2020.
- [17] S. Khandelwal, and K. Y. Rhee, "Recent advances in basalt-fiber-reinforced composites: Tailoring the fiber-matrix interface," *Composites Part B: Engineering*, vol. 192, pp. 108011, 2020.
- [18] J. George, and H. Ishida, "A review on the very high nanofiller-content nanocomposites: Their preparation methods and properties with high aspect ratio fillers," *Progress in Polymer Science*, vol. 86, pp. 1-39, 2018.
- [19] N. Patel, and P. Jain, "An investigation on mechanical properties in randomly oriented short natural fiber reinforced composites," *Materials Today: Proceedings*, 2020.

- [20] N. Ramdani, M. Derradji, and E. O. Mokhnache, "Natural Fiber Reinforced Polybenzoxazine Composites: A Review," *Materials Today Communications*, pp. 103645, 2022.
- [21] A. Ganguly, S. Shankar, A. Das, M. Shukla, C. Swaroop, and T. Bhardwaj, "Natural fibre reinforced composites: A review based on additive manufacturing routes and biodegradability perspective," *Materials Today: Proceedings*, 2022.
- [22] T. M. Murugesan, S. Palanisamy, C. Santulli, and M. Palaniappan, "Mechanical characterization of alkali treated Sansevieria cylindrica fibers–Natural rubber composites," *Materials Today: Proceedings*, 2022.
- [23] D. Mohana Krishnudu, D. Sreeramulu, and P. Venkateshwar Reddy, "A study of filler content influence on dynamic mechanical and thermal characteristics of coir and luffa cylindrica reinforced hybrid composites," *Construction and Building Materials*, vol. 251, pp. 119040, 2020.
- [24] A. Sharma, M. Thakur, M. Bhattacharya, T. Mandal, and S. Goswami, "Commercial application of cellulose nano-composites – A review," *Biotechnology Reports*, vol. 21, pp. e00316, 2019.
- [25] R. Vijay, A. Vinod, D. Lenin Singaravelu, M. R. Sanjay, and S. Siengchin, "Characterization of chemical treated and untreated natural fibers from Pennisetum orientale grass- A potential reinforcement for lightweight polymeric applications," *International Journal of Lightweight Materials and Manufacture*, vol. 4, no. 1, pp. 43-49, 2021.
- [26] P. Manimaran, M. R. Sanjay, P. Senthamaraiannan, B. Yogesha, C. Barile, and S. Siengchin, "A new study on characterization of Pithecellobium dulce fiber as composite reinforcement for light-weight applications," *Journal of Natural Fibers*, vol. 17, no. 3, pp. 359-370, 2020.
- [27] C. Vigneswaran, M. Ananthasubramanian, and P. Kandhavadi, "Bioprocessing of synthetic fibres," *Bioprocessing of Textiles*, C. Vigneswaran, M. Ananthasubramanian and P. Kandhavadi, eds., pp. 189-250: Woodhead Publishing India, 2014.

- [28] R. K. Malviya, R. K. Singh, R. Purohit, and R. Sinha, "Natural fibre reinforced composite materials: Environmentally better life cycle assessment – A case study," *Materials Today: Proceedings*, vol. 26, pp. 3157-3160, 2020.
- [29] T. K. Khieng, S. Debnath, E. Ting Chaw Liang, M. Anwar, A. Pramanik, and A. K. Basak, "A Review on Mechanical Properties of Natural Fibre Reinforced Polymer Composites under Various Strain Rates," *Journal of Composites Science*, vol. 5, no. 5, pp. 130, 2021.
- [30] S. Islam, S. Islam, and M. Hasan, "Natural Fiber Reinforced Polymer Composites as Sustainable Green Composites," *Reference Module in Materials Science and Materials Engineering*: Elsevier, 2022.
- [31] T. A. Miliket, M. B. Ageze, M. T. Tigabu, and M. A. Zeleke, "Experimental characterizations of hybrid natural fiber-reinforced composite for wind turbine blades," *Heliyon*, vol. 8, no. 3, pp. e09092, 2022.
- [32] S. M. M. Amir, M. T. H. Sultan, M. Jawaid, S. N. A. Safri, A. U. M. Shah, M. R. Yusof, J. Naveen, S. Mohd, K. A. M. Salleh, and N. Saba, "Effects of layering sequence and gamma radiation on mechanical properties and morphology of Kevlar/oil palm EFB/epoxy hybrid composites," *Journal of Materials Research and Technology*, vol. 8, no. 6, pp. 5362-5373, 2019.
- [33] S. Shinoj, and R. Visvanathan, "Oil Palm Fiber Polymer Composites: Processing, Characterization and Properties," *Lignocellulosic Polymer Composites*, pp. 175-212, 2014.
- [34] N. F. S. M. Azani, M. K. M. Haafiz, A. Zahari, S. Poinsignon, N. Brosse, and M. H. Hussin, "Preparation and characterizations of oil palm fronds cellulose nanocrystal (OPF-CNC) as reinforcing filler in epoxy-Zn rich coating for mild steel corrosion protection," *International Journal of Biological Macromolecules*, vol. 153, pp. 385-398, 2020.
- [35] B. Wang, F. Dong, M. Chen, J. Zhu, J. Tan, X. Fu, Y. Wang, and S. Chen, "Advances in Recycling and Utilization of Agricultural Wastes in China: Based on Environmental Risk, Crucial Pathways, Influencing Factors, Policy Mechanism," *Procedia Environmental Sciences*, vol. 31, pp. 12-17, 2016.

- [36] E. Sarikaya, H. Çallioğlu, and H. Demirel, "Production of epoxy composites reinforced by different natural fibers and their mechanical properties," *Composites Part B: Engineering*, vol. 167, pp. 461-466, 2019.
- [37] T. S. Cheng, D. N. Uy Lan, S. Phillips, and L. Q. N. Tran, "Characteristics of oil palm empty fruit bunch fiber and mechanical properties of its unidirectional composites," *Polymer Composites*, vol. 40, no. 3, pp. 1158-1164, 2019.
- [38] B. D. Richard, A. Wahi, R. Nani, E. Iling, S. Osman, and D. S. H. Ali, "Effect of Fiber Loading on Mechanical Properties of Oil Palm Frond/Urea Formaldehyde (OPF/UF) Composite," *International Journal of Integrated Engineering*, vol. 11, no. 7, 2019.
- [39] A. F. Ahmad, Z. Abbas, S. J. Obaiys, and M. F. Zainuddin, "Effect of untreated fiber loading on the thermal, mechanical, dielectric, and microwave absorption properties of polycaprolactone reinforced with oil palm empty fruit bunch biocomposites," *Polymer Composites*, vol. 39, no. S3, pp. E1778-E1787, 2018.
- [40] M. K. B. Bakri, E. Jayamani, S. K. Heng, and S. Hamdan, "Reinforced Oil Palm Fiber Epoxy Composites: An Investigation on Chemical Treatment of Fibers on Acoustical, Morphological, Mechanical and Spectral Properties," *Materials Today: Proceedings*, vol. 2, no. 4, pp. 2747-2756, 2015.
- [41] N. A. Ramlee, M. Jawaid, E. S. Zainudin, and S. A. K. Yamani, "Tensile, physical and morphological properties of oil palm empty fruit bunch/sugarcane bagasse fibre reinforced phenolic hybrid composites," *Journal of Materials Research and Technology*, vol. 8, no. 4, pp. 3466-3474, 2019.
- [42] T. E. Omoniyi, "Potential of Oil Palm (*Elaeisguineensis*) Empty Fruit Bunch Fibres Cement Composites for Building Applications," *AgriEngineering*, vol. 1, no. 2, pp. 153-163, 2019.
- [43] Y.-C. Miao, D. Xing, X.-Y. Xi, X. Yue, Y.-X. Bai, and P.-C. Ma, "Development of conducting basalt fibre with polymer-based nanocomposite sizing," *Materials Today Communications*, vol. 23, pp. 101170, 2020.
- [44] S. R. Karnati, P. Agbo, and L. Zhang, "Applications of silica nanoparticles in glass/carbon fiber-reinforced epoxy nanocomposite," *Composites Communications*, vol. 17, pp. 32-41, 2020.

- [45] E. Jean Serge, J. P. Alla, P. D. B. Belibi, K. J. Mbadcam, and N. N. Fathima, "Clay/polymer nanocomposites as filler materials for leather," *Journal of Cleaner Production*, vol. 237, pp. 117837, 2019.
- [46] A. Guchait, A. Saxena, S. Chattopadhyay, and T. Mondal, "Influence of Nanofillers on Adhesion Properties of Polymeric Composites," *ACS Omega*, vol. 7, no. 5, pp. 3844-3859, 2022.
- [47] E. Vatansever, D. Arslan, and M. Nofar, "Polylactide cellulose-based nanocomposites," *International Journal of Biological Macromolecules*, vol. 137, pp. 912-938, 2019.
- [48] L. Yue, A. Maiorana, F. Khelifa, A. Patel, J.-M. Raquez, L. Bonnaud, R. Gross, P. Dubois, and I. Manas-Zloczower, "Surface-modified cellulose nanocrystals for biobased epoxy nanocomposites," *Polymer*, vol. 134, pp. 155-162, 2018.
- [49] P. Chindaprasirt, P. Sukontasukkul, A. Techaphatthanakon, S. Kongtun, C. Ruttanapun, D.-Y. Yoo, W. Tangchirapat, S. Limkatanyu, and N. Banthia, "Effect of graphene oxide on single fiber pullout behavior," *Construction and Building Materials*, vol. 280, pp. 122539, 2021.
- [50] S. M. M. Amir, M. T. H. Sultan, M. Jawaid, A. H. Ariffin, S. Mohd, K. A. M. Salleh, M. R. Ishak, and A. U. M. Shah, "Nondestructive testing method for Kevlar and natural fiber and their hybrid composites," *Durability and Life Prediction in Biocomposites, Fibre-Reinforced Composites and Hybrid Composites*, M. Jawaid, M. Thariq and N. Saba, eds., pp. 367-388: Woodhead Publishing, 2019.
- [51] Ö. E. İşmal, and R. Paul, "Composite textiles in high-performance apparel," *High-Performance Apparel*, J. McLoughlin and T. Sabir, eds., pp. 377-420: Woodhead Publishing, 2018.
- [52] V. V. Vasiliev, and E. V. Morozov, "Introduction," *Advanced Mechanics of Composite Materials and Structures (Fourth Edition)*, V. V. Vasiliev and E. V. Morozov, eds., pp. xvii-xxv: Elsevier, 2018.
- [53] R. Lin, B. Villacorta Hernandez, L. Ge, and Z. Zhu, "Metal organic framework based mixed matrix membranes: an overview on filler/polymer interfaces," *Journal of Materials Chemistry A*, vol. 6, no. 2, pp. 293-312, 2018.

- [54] M. Loos, "Composites," *Carbon Nanotube Reinforced Composites*, M. Loos, ed., pp. 37-72, Oxford: William Andrew Publishing, 2015.
- [55] R. Kumar, and A. Anand, "Tribological behavior of natural fiber reinforced epoxy based composites: A review," *Materials Today: Proceedings*, vol. 18, pp. 3247-3251, 2019.
- [56] R. S. M, S. Siengchin, J. Parameswaranpillai, M. Jawaid, C. I. Pruncu, and A. Khan, "A comprehensive review of techniques for natural fibers as reinforcement in composites: Preparation, processing and characterization," *Carbohydr Polym*, vol. 207, pp. 108-121, 2019.
- [57] L. Kerni, S. Singh, A. Patnaik, and N. Kumar, "A review on natural fiber reinforced composites," *Materials Today: Proceedings*, 2020.
- [58] M. M. A. Nassar, R. Arunachalam, and K. I. Alzebdeh, "Machinability of natural fiber reinforced composites: a review," *The International Journal of Advanced Manufacturing Technology*, vol. 88, no. 9, pp. 2985-3004, 2017.
- [59] B. Singh, R. Kumar, and J. Singh Chohan, "Polymer matrix composites in 3D printing: A state of art review," *Materials Today: Proceedings*, 2020.
- [60] L. M. Nicholson, K. S. Whitley, T. S. Gates, and J. A. Hinkley, "Influence of molecular weight on the mechanical performance of a thermoplastic glassy polyimide," *Journal of Materials Science*, vol. 35, no. 24, pp. 6111-6121, 2000.
- [61] F. Li, Y. Gao, C. Zhang, J. Jin, X. Ji, Y. Zhang, X. Zhang, and W. Jiang, "Design of high impact thermal plastic polymer composites with balanced toughness and rigidity: Effect of matrix polymer molecular weight," *Polymer*, vol. 208, pp. 122957, 2020.
- [62] Balani. K, Verma. V, and N. R. Agarwal A, "Physical, Thermal, and Mechanical Properties of Polymers," *Biosurfaces*, pp. 329-344, 2015.
- [63] G. O. Glória, M. C. A. Teles, F. P. D. Lopes, C. M. F. Vieira, F. M. Margem, M. d. A. Gomes, and S. N. Monteiro, "Tensile strength of polyester composites reinforced with PALF," *Journal of Materials Research and Technology*, vol. 6, no. 4, pp. 401-405, 2017.
- [64] S. Venkatraman, H. Yingying, and Y. S. Wong, "Bio-absorbable Cardiovascular Implants: Status and Prognosis," *JOM*, vol. 72, no. 5, pp. 1833-1844, 2020.

- [65] M. Labet, and W. Thielemans, "Synthesis of polycaprolactone: a review," *Chemical Society Reviews*, vol. 38, no. 12, pp. 3484-3504, 2009.
- [66] Y. Ul-Haq, I. Murtaza, S. Mazhar, R. Ullah, M. Iqbal, H. Zeeshan ul, A. A. Qarni, and S. Amin, "Dielectric, thermal and mechanical properties of hybrid PMMA/RGO/Fe₂O₃ nanocomposites fabricated by in-situ polymerization," *Ceramics International*, vol. 46, no. 5, pp. 5828-5840, 2020.
- [67] M. R. M. Jamir, M. S. A. Majid, and A. Khasri, "Natural lightweight hybrid composites for aircraft structural applications," *Sustainable Composites for Aerospace Applications*, M. Jawaid and M. Thariq, eds., pp. 155-170: Woodhead Publishing, 2018.
- [68] M. Raji, H. Abdellaoui, H. Essabir, C.-A. Kakou, R. Bouhfid, and A. e. k. Qaiss, "Prediction of the cyclic durability of woven-hybrid composites," *Durability and Life Prediction in Biocomposites, Fibre-Reinforced Composites and Hybrid Composites*, M. Jawaid, M. Thariq and N. Saba, eds., pp. 27-62: Woodhead Publishing, 2019.
- [69] E. Kayalvizhi Nangai, and S. Saravanan, "Synthesis, fabrication and testing of polymer nanocomposites: A review," *Materials Today: Proceedings*, 2021.
- [70] S. R. Benin, S. Kannan, R. J. Bright, and A. Jacob Moses, "A review on mechanical characterization of polymer matrix composites & its effects reinforced with various natural fibres," *Materials Today: Proceedings*, 2020.
- [71] R. Vanitha, and C. Kavitha, "Development of natural cellulose fiber and its food packaging application," *Materials Today: Proceedings*, 2020.
- [72] D. Bhattacharyya, A. Subasinghe, and N. K. Kim, "Natural fibers: Their composites and flammability characterizations," *Multifunctionality of Polymer Composites*, K. Friedrich and U. Breuer, eds., pp. 102-143, Oxford: William Andrew Publishing, 2015.
- [73] A. Komuriah, N. S. Kumar, and B. D. Prasad, "Chemical Composition of Natural Fibers and its Influence on their Mechanical Properties," *Mechanics of Composite Materials*, vol. 50, no. 3, pp. 359-376, 2014.

- [74] J. Pere, E. Pääkkönen, Y. Ji, and E. Retulainen, "Influence of the hemicellulose content on the fiber properties, strength, and formability of handsheets," *BioResources*, vol. 14, no. 1, pp. 251-263, 2019.
- [75] P. Peças, H. Carvalho, H. Salman, and M. Leite, "Natural Fibre Composites and Their Applications: A Review," *Journal of Composites Science*, vol. 2, no. 4, 2018.
- [76] Yustinah, N. Hidayat, R. Alamsyah, A. M. Roslan, H. Hermansyah, and M. Gozan, "Production of polyhydroxybutyrate from oil palm empty fruit bunch (OPEFB) hydrolysates by *Bacillus cereus* suaeda B-001," *Biocatalysis and Agricultural Biotechnology*, vol. 18, pp. 101019, 2019.
- [77] S. Biswas, S. Kindo, and A. Patnaik, "Effect of fiber length on mechanical behavior of coir fiber reinforced epoxy composites," *Fibers and Polymers*, vol. 12, no. 1, pp. 73-78, 2011.
- [78] H. Wu, X. Lin, and A. Zhou, "A review of mechanical properties of fibre reinforced concrete at elevated temperatures," *Cement and Concrete Research*, vol. 135, pp. 106117, 2020.
- [79] W. Suksong, W. Tukanghan, K. Promnuan, P. Kongjan, A. Reungsang, H. Insam, and S. O-Thong, "Biogas production from palm oil mill effluent and empty fruit bunches by coupled liquid and solid-state anaerobic digestion," *Bioresource Technology*, vol. 296, pp. 122304, 2020.
- [80] P. L. Tang, W. L. Hong, C. S. Yue, and S. Harun, "Palm oil mill effluent as the pretreatment solvent of oil palm empty fruit bunch fiber for fermentable sugars production," *Bioresource Technology*, vol. 314, pp. 123723, 2020.
- [81] W.-Y. Wong, S. Lim, Y.-L. Pang, S.-H. Shuit, W.-H. Chen, and K.-T. Lee, "Synthesis of renewable heterogeneous acid catalyst from oil palm empty fruit bunch for glycerol-free biodiesel production," *Science of The Total Environment*, vol. 727, pp. 138534, 2020.
- [82] Y. G. Thyavihalli Girijappa, S. Mavinkere Rangappa, J. Parameswaranpillai, and S. Siengchin, "Natural Fibers as Sustainable and Renewable Resource for Development of Eco-Friendly Composites: A Comprehensive Review," *Frontiers in Materials*, vol. 6, no. 226, 2019.

- [83] A. Manral, and P. K. Bajpai, "Analysis of properties on chemical treatment of kenaf fibers," *Materials Today: Proceedings*, 2020.
- [84] P. Khalili, K. Y. Tshai, and I. Kong, "Comparative Thermal and Physical Investigation of Chemically Treated and Untreated Oil Palm EFB Fiber," *Materials Today: Proceedings*, vol. 5, no. 1, Part 3, pp. 3185-3192, 2018.
- [85] S. M.R, S. Siengchin, J. Parameswaranpillai, M. Jawaid, C. I. Pruncu, and A. Khan, "A comprehensive review of techniques for natural fibers as reinforcement in composites: Preparation, processing and characterization," *Carbohydrate Polymers*, vol. 207, pp. 108-121, 2019.
- [86] M. K. Faizi, A. B. Shahrman, M. S. Abdul Majid, Z. A. Ahmad, B. M. T. Shamsul, and Y. G. Ng, "The effect of alkaline treatments soaking time on oil palm empty fruit bunch (OPEFB) fibre structure," *Journal of Physics: Conference Series*, vol. 908, pp. 012033, 2017.
- [87] M. Rokbi, H. Osmani, A. Imad, and N. Benseddiq, "Effect of Chemical treatment on Flexure Properties of Natural Fiber-reinforced Polyester Composite," *Procedia Engineering*, vol. 10, pp. 2092-2097, 2011.
- [88] R.W.Siegel, and G.E.Fougere, "Mechanical Properties of Nanophase Metals," *Nanostructured Materials*, vol. 6, pp. 205, 1995.
- [89] M. J. Pitkethly, "Nanomaterials – the driving force," *Materials Today*, vol. 7, no. 12, pp. 20-29, 2004.
- [90] S. Fu, Z. Sun, P. Huang, Y. Li, and N. Hu, "Some basic aspects of polymer nanocomposites: A critical review," *Nano Materials Science*, vol. 1, no. 1, pp. 2-30, 2019.
- [91] M. Rallini, and J. M. Kenny, "Nanofillers in Polymers," *Modification of Polymer Properties*, C. F. Jasso-Gastinel and J. M. Kenny, eds., pp. 47-86: William Andrew Publishing, 2017.
- [92] H. Zhang, R. Ma, D. Luo, W. Xu, Y. Zhao, X. Zhao, Y. Gao, and L. Zhang, "Understanding the cavitation and crazing behavior in the polymer nanocomposite by tuning shape and size of nanofiller," *Polymer*, vol. 188, pp. 122103, 2020.

- [93] E. I. Akpan, X. Shen, B. Wetzel, and K. Friedrich, "Design and Synthesis of Polymer Nanocomposites," *Polymer Composites with Functionalized Nanoparticles*, K. Pielichowski and T. M. Majka, eds., pp. 47-83: Elsevier, 2019.
- [94] Z. Wang, T. Hu, R. Liang, and M. Wei, "Application of Zero-Dimensional Nanomaterials in Biosensing," *Frontiers in Chemistry*, vol. 8, no. 320, 2020.
- [95] R. Verdejo, M. M. Bernal, L. J. Romasanta, F. J. Tapiador, and M. A. Lopez-Manchado, "Reactive Nanocomposite Foams," *Cellular Polymers*, vol. 30, no. 2, pp. 45-62, 2011.
- [96] M. R. M. Vengatesan, V., "Nanoparticle and Nanofiber-Based Polymer Nanocomposites: An Overview," *Spherical and Fibrous Filler Composites*, pp. 1-38, 2016.
- [97] B. L. Li, M. I. Setyawati, L. Chen, J. Xie, K. Ariga, C.-T. Lim, S. Garaj, and D. T. Leong, "Directing Assembly and Disassembly of 2D MoS₂ Nanosheets with DNA for Drug Delivery," *ACS Applied Materials & Interfaces*, vol. 9, no. 18, pp. 15286-15296, 2017.
- [98] S. Pradhan, R. Lach, H. H. Le, W. Grellmann, H.-J. Radusch, and R. Adhikari, "Effect of Filler Dimensionality on Mechanical Properties of Nanofiller Reinforced Polyolefin Elastomers," *ISRN Polymer Science*, vol. 2013, pp. 284504, 2013.
- [99] Y. Huang, N. Li, Y. Ma, F. Du, F. Li, X. He, X. Lin, H. Gao, and Y. Chen, "The influence of single-walled carbon nanotube structure on the electromagnetic interference shielding efficiency of its epoxy composites," *Carbon*, vol. 45, no. 8, pp. 1614-1621, 2007.
- [100] M. R. Ayatollahi, S. Shadlou, M. M. Shokrieh, and M. Chitsazzadeh, "Effect of multi-walled carbon nanotube aspect ratio on mechanical and electrical properties of epoxy-based nanocomposites," *Polymer Testing*, vol. 30, no. 5, pp. 548-556, 2011.
- [101] M. P. Manoharan, A. Sharma, A. V. Desai, M. A. Haque, C. E. Bakis, and K. W. Wang, "The interfacial strength of carbon nanofiber epoxy composite using single fiber pullout experiments," *Nanotechnology*, vol. 20, no. 29, pp. 295701, 2009.

- [102] A. H. Barber, S. R. Cohen, S. Kenig, and H. D. Wagner, "Interfacial fracture energy measurements for multi-walled carbon nanotubes pulled from a polymer matrix," *Composites Science and Technology*, vol. 64, no. 15, pp. 2283-2289, 2004.
- [103] C. Zinge, and B. Kandasubramanian, "Nanocellulose based biodegradable polymers," *European Polymer Journal*, vol. 133, pp. 109758, 2020.
- [104] G. Nichols, S. Byard, M. J. Bloxham, J. Botterill, N. J. Dawson, A. Dennis, V. Diart, N. C. North, and J. D. Sherwood, "A review of the terms agglomerate and aggregate with a recommendation for nomenclature used in powder and particle characterization," *J Pharm Sci*, vol. 91, no. 10, pp. 2103-9, 2002.
- [105] W. Zhang, "Nanoparticle aggregation: principles and modeling," *Adv Exp Med Biol*, vol. 811, pp. 19-43, 2014.
- [106] A. Tessema, D. Zhao, J. Moll, S. Xu, R. Yang, C. Li, S. K. Kumar, and A. Kidane, "Effect of filler loading, geometry, dispersion and temperature on thermal conductivity of polymer nanocomposites," *Polymer Testing*, vol. 57, pp. 101-106, 2017.
- [107] M. C. Tanzi, S. Farè, and G. Candiani, "Organization, Structure, and Properties of Materials," *Foundations of Biomaterials Engineering*, M. C. Tanzi, S. Farè and G. Candiani, eds., pp. 3-103: Academic Press, 2019.
- [108] Y. Chen, L. Xin, Y. Liu, Z. Guo, L. Dong, and Z. Zhong, "A viscoelastic model for particle-reinforced composites in finite deformations," *Applied Mathematical Modelling*, vol. 72, pp. 499-512, 2019.
- [109] D. K. Rajak, D. D. Pagar, P. L. Menezes, and E. Linul, "Fiber-Reinforced Polymer Composites: Manufacturing, Properties, and Applications," *Polymers (Basel)*, vol. 11, no. 10, 2019.
- [110] W. D. Callister, and D. G. Rethwisch, *Materials science and engineering : an introduction*, 2018.
- [111] L. Mohammed, M. N. M. Ansari, G. Pua, M. Jawaid, and M. S. Islam, "A Review on Natural Fiber Reinforced Polymer Composite and Its Applications," *International Journal of Polymer Science*, vol. 2015, pp. 243947, 2015.

- [112] R. D. S. G. Campilho, "Recent innovations in biocomposite products," *Biocomposites for High-Performance Applications*, D. Ray, ed., pp. 275-306: Woodhead Publishing, 2017.
- [113] R. K. Mishra, A. Sabu, and S. K. Tiwari, "Materials chemistry and the futurist eco-friendly applications of nanocellulose: Status and prospect," *Journal of Saudi Chemical Society*, vol. 22, no. 8, pp. 949-978, 2018.
- [114] L. F. C. Nascimento, L. H. L. Louro, S. N. Monteiro, É. P. Lima, and F. S. da Luz, "Mallow Fiber-Reinforced Epoxy Composites in Multilayered Armor for Personal Ballistic Protection," *JOM*, vol. 69, no. 10, pp. 2052-2056, 2017.
- [115] Y. Qing, R. Sabo, J. Y. Zhu, U. Agarwal, Z. Cai, and Y. Wu, "A comparative study of cellulose nanofibrils disintegrated via multiple processing approaches," *Carbohydrate Polymers*, vol. 97, no. 1, pp. 226-234, 2013.
- [116] D. Trache, M. H. Hussin, M. K. M. Haafiz, and V. K. Thakur, "Recent progress in cellulose nanocrystals: sources and production," *Nanoscale*, vol. 9, no. 5, pp. 1763-1786, 2017.
- [117] E. Fortunati, J. M. Kenny, and L. Torre, "Lignocellulosic materials as reinforcements in sustainable packaging systems: Processing, properties, and applications," *Biomass, Biopolymer-Based Materials, and Bioenergy*, D. Verma, E. Fortunati, S. Jain and X. Zhang, eds., pp. 87-102: Woodhead Publishing, 2019.
- [118] A. Widnyana, I. G. Rian, I. W. Surata, and T. G. T. Nindhia, "Tensile Properties of coconut Coir single fiber with alkali treatment and reinforcement effect on unsaturated polyester polymer," *Materials Today: Proceedings*, vol. 22, pp. 300-305, 2020.
- [119] W. Chaiwong, N. Samoh, T. Eksomtramage, and K. Kaewtatip, "Surface-treated oil palm empty fruit bunch fiber improved tensile strength and water resistance of wheat gluten-based bioplastic," *Composites Part B: Engineering*, vol. 176, pp. 107331, 2019.
- [120] F. M. Al-Oqila, and M. S. Salit, "Natural fiber composites," *Materials Selection for Natural Fiber Composites*, F. M. Al-Oqila and M. S. Salit, eds., pp. 23-48: Woodhead Publishing, 2017.

- [121] M. Muneer Ahmed, H. N. Dhakal, Z. Y. Zhang, A. Barouni, and R. Zahari, “Enhancement of impact toughness and damage behaviour of natural fibre reinforced composites and their hybrids through novel improvement techniques: A critical review,” *Composite Structures*, vol. 259, pp. 113496, 2021.
- [122] N. C. Huang, and X. Y. Liu, “Debonding and fiber pull-out in reinforced composites,” *Theoretical and Applied Fracture Mechanics*, vol. 21, no. 3, pp. 157-176, 1994.
- [123] E. Soundrapandian, P. V. Kumar, G. S. Kumar, S. Jagan, and M. M. Raj, “Investigation of mechanical properties of natural fiber reinforced polymer composites,” *Materials Today: Proceedings*, 2021.
- [124] A. Selmi, “Void Effect on Carbon Fiber Epoxy Composites,” in 2nd International Conference on Emerging Trends in Engineering and Technology (ICETET'2014), May 30-31, 2014 London (United Kingdom), 2014.
- [125] M. Mehdikhani, L. Gorbatikh, I. Verpoest, and S. V. Lomov, “Voids in fiber-reinforced polymer composites: A review on their formation, characteristics, and effects on mechanical performance,” *Journal of Composite Materials*, vol. 53, no. 12, pp. 1579-1669, 2018.
- [126] Xueshu Liu, and F. Chen, “A Review of Void Formation and its Effects on the Mechanical Performance of Carbon Fiber Reinforced Plastic,” *Engineering Transactions*, no. 64, pp. 33-51, 2016.
- [127] A. Bajpai, A. K. Alapati, A. Klingler, and B. Wetzel, “Tensile Properties, Fracture Mechanics Properties and Toughening Mechanisms of Epoxy Systems Modified with Soft Block Copolymers, Rigid TiO₂ Nanoparticles and Their Hybrids,” *Journal of Composites Science*, vol. 2, no. 4, pp. 72, 2018.
- [128] S. V. Joshi, L. T. Drzal, A. K. Mohanty, and S. Arora, “Are natural fiber composites environmentally superior to glass fiber reinforced composites?,” *Composites Part A: Applied Science and Manufacturing*, vol. 35, no. 3, pp. 371-376, 2004.
- [129] O. T. Adesina, T. Jamiru, E. R. Sadiku, O. F. Ogunbiyi, and L. W. Beneke, “Mechanical evaluation of hybrid natural fibre–reinforced polymeric composites

- for automotive bumper beam: a review,” *The International Journal of Advanced Manufacturing Technology*, vol. 103, no. 5, pp. 1781-1797, 2019.
- [130] C. S. Boland, R. De Kleine, G. A. Keoleian, E. C. Lee, H. C. Kim, and T. J. Wallington, “Life Cycle Impacts of Natural Fiber Composites for Automotive Applications: Effects of Renewable Energy Content and Lightweighting,” *Journal of Industrial Ecology*, vol. 20, no. 1, pp. 179-189, 2016.
- [131] T. Khan, M. T. B. Hameed Sultan, and A. H. Ariffin, “The challenges of natural fiber in manufacturing, material selection, and technology application: A review,” *Journal of Reinforced Plastics and Composites*, vol. 37, no. 11, pp. 770-779, 2018.
- [132] M. Zaki Abdullah, Y. Dan-mallam, and P. S. M. Megat Yusoff, “Effect of Environmental Degradation on Mechanical Properties of Kenaf/Polyethylene Terephthalate Fiber Reinforced Polyoxymethylene Hybrid Composite,” *Advances in Materials Science and Engineering*, vol. 2013, pp. 671481, 2013.
- [133] P. P. Gohil, V. Chaudhary, and K. Patel, "Challenges in Machining of Natural Fibre Composites," *Manufacturing of Natural Fibre Reinforced Polymer Composites*, M. S. Salit, M. Jawaid, N. B. Yusoff and M. E. Hoque, eds., pp. 139-153, Cham: Springer International Publishing, 2015.
- [134] A. Kasiri, and D. Brabazon, "Materials Used Within Polymer Matrix Composites (PMCs) and PCM Production Via Additive Manufacturing," *Reference Module in Materials Science and Materials Engineering*: Elsevier, 2021.
- [135] S. Jha, V. Bhavsar, and D. Tripathi, “Dielectric properties of MWCNT dispersed conducting polymer nanocomposites films of PVA-CMC-PPy,” *Materials Today: Proceedings*, 2021.
- [136] J. Guan, A. Derdouri, B. Ashrafi, A. Benhalima, K. S. Kim, M. Daroszewska, and B. Simard, “Boron nitride nanotubes reinforced polycarbonate nanocomposites,” *Materials Today Communications*, vol. 20, pp. 100586, 2019.
- [137] Y.-Q. Shen, Y.-J. Zhu, H.-P. Yu, and B.-Q. Lu, “Biodegradable nanocomposite of glycerol citrate polyester and ultralong hydroxyapatite nanowires with improved mechanical properties and low acidity,” *Journal of Colloid and Interface Science*, vol. 530, pp. 9-15, 2018.

- [138] B. Zhu, Y. Wang, H. Liu, J. Ying, C. Liu, and C. Shen, "Effects of interface interaction and microphase dispersion on the mechanical properties of PCL/PLA/MMT nanocomposites visualized by nanomechanical mapping," *Composites Science and Technology*, vol. 190, pp. 108048, 2020.
- [139] T. C. Huang, J. M. Yeh, and C. Y. Lai, "Polymer nanocomposite coatings," *Advances in Polymer Nanocomposites*, F. Gao, ed., pp. 605-638: Woodhead Publishing, 2012.
- [140] U. Kilic, M. M. Sherif, and O. E. Ozbulut, "Tensile properties of graphene nanoplatelets/epoxy composites fabricated by various dispersion techniques," *Polymer Testing*, vol. 76, pp. 181-191, 2019.
- [141] S. B. Jagtap, and D. Ratna, "Effect of molecular weight of curing agents on properties of nanocomposites based on epoxy resin and organoclay with reactive modifier," *Journal of Applied Polymer Science*, vol. 134, no. 11, 2017.
- [142] N. Karak, "Fundamentals of Nanomaterials and Polymer Nanocomposites," *Nanomaterials and Polymer Nanocomposites*, N. Karak, ed., pp. 1-45: Elsevier, 2019.
- [143] C. Nerín, C. Domeño, and J. Salafranca, "Advances in Sample Preparation of Environmental Solid Matrices," *Comprehensive Sampling and Sample Preparation*, J. Pawliszyn, ed., pp. 783-796, Oxford: Academic Press, 2012.
- [144] R. Kumar, "Lipid-Based Nanoparticles for Drug-Delivery Systems," *Nanocarriers for Drug Delivery*, S. S. Mohapatra, S. Ranjan, N. Dasgupta, R. K. Mishra and S. Thomas, eds., pp. 249-284: Elsevier, 2019.
- [145] A. Kaboorani, B. Riedl, and P. Blanchet, "Ultrasonication Technique: A Method for Dispersing Nanoclay in Wood Adhesives," *Journal of Nanomaterials*, vol. 2013, pp. 341897, 2013.
- [146] U. C. Abubakar, K. R. Alhooshani, and T. A. Saleh, "Effect of ultrasonication and chelating agents on the dispersion of NiMo catalysts on carbon for Hydrodesulphurization," *Journal of Environmental Chemical Engineering*, vol. 8, no. 4, pp. 103811, 2020.

- [147] Y. Li, J. Li, S. Guo, and H. Li, "Mechanochemical degradation kinetics of high-density polyethylene melt and its mechanism in the presence of ultrasonic irradiation," *Ultrasonics Sonochemistry*, vol. 12, no. 3, pp. 183-189, 2005.
- [148] B. Singh, and N. Sharma, "Mechanistic implications of plastic degradation," *Polymer Degradation and Stability*, vol. 93, no. 3, pp. 561-584, 2008.
- [149] J. G. Speight, "Monomers, polymers, and plastics," *Handbook of Industrial Hydrocarbon Processes (Second Edition)*, J. G. Speight, ed., pp. 597-649, Boston: Gulf Professional Publishing, 2020.
- [150] O. Agboola, R. Sadiku, T. Mokrani, I. Amer, and O. Imoru, "Polyolefins and the environment," *Polyolefin Fibres (Second Edition)*, S. C. O. Ugbolue, ed., pp. 89-133: Woodhead Publishing, 2017.
- [151] S. Krause, "Polymer Chemistry: An Introduction, 3rd Edition (Stevens, Malcolm P.)," *Journal of Chemical Education*, vol. 77, no. 1, pp. 35, 2000.
- [152] H. Guo, J. Zhang, D. Porter, H. Peng, D. W. P. M. Löwik, Y. Wang, Z. Zhang, X. Chen, and Z. Shao, "Ultrafast and reversible thermochromism of a conjugated polymer material based on the assembly of peptide amphiphiles," *Chemical Science*, vol. 5, no. 11, pp. 4189-4195, 2014.
- [153] K. Król-Morkisz, and K. Pielichowska, "Thermal Decomposition of Polymer Nanocomposites With Functionalized Nanoparticles," *Polymer Composites with Functionalized Nanoparticles*, K. Pielichowski and T. M. Majka, eds., pp. 405-435: Elsevier, 2019.
- [154] X. Colin, and J. Verdu, "Thermal ageing and lifetime prediction for organic matrix composites," *Plastics, Rubber and Composites*, vol. 32, no. 8-9, pp. 349-356, 2003.
- [155] E. Ernault, E. Richaud, and B. Fayolle, "Thermal oxidation of epoxies: Influence of diamine hardener," *Polymer Degradation and Stability*, vol. 134, pp. 76-86, 2016.
- [156] M. Raji, N. Zari, R. Bouhfid, and A. e. k. Qaiss, "Durability of composite materials during hydrothermal and environmental aging," *Durability and Life Prediction in Biocomposites, Fibre-Reinforced Composites and Hybrid*

Composites, M. Jawaid, M. Thariq and N. Saba, eds., pp. 83-119: Woodhead Publishing, 2019.

- [157] A. E. Krauklis, and A. T. Echtermeyer, "Mechanism of Yellowing: Carbonyl Formation during Hygrothermal Aging in a Common Amine Epoxy," *Polymers*, vol. 10, no. 9, pp. 1017, 2018.
- [158] C. V. Oprea, "Mechanochemical degradation of polymers," *Polymer Mechanics*, vol. 14, no. 6, pp. 783-792, 1978.
- [159] L. Q. Reyes, J. Zhang, B. Dao, D. L. Nguyen, and R. J. Varley, "Subtle variations in the structure of crosslinked epoxy networks and the impact upon mechanical and thermal properties," *Journal of Applied Polymer Science*, vol. 137, no. 29, 2020.
- [160] B. A. Patterson, C. E. Busch, M. Bratcher, J. Cline, D. E. Harris, K. A. Masser, A. L. Fleetwood, and D. B. Knorr, "Influence of temperature dependent matrix properties on the high-rate impact performance of thin glass fiber reinforced composites," *Composites Part B: Engineering*, vol. 192, pp. 108009, 2020.
- [161] X. Wang, X. Yuan, M. Wu, F. Gao, X. Yan, K. Zhou, and D. Zhang, "Effect of Epoxy Resin on the Actuating Performance of Piezoelectric Fiber Composites," *Sensors (Basel)*, vol. 19, no. 8, 2019.
- [162] A. Tabatabaeian, and A. R. Ghasemi, "Curvature changes and weight loss of polymeric nano-composite plates with consideration of the thermal cycle fatigue effects and different resin types: An experimental approach," *Mechanics of Materials*, vol. 131, pp. 69-77, 2019.
- [163] N. Azlina Ramlee, M. Jawaid, S. Abdul Karim Yamani, E. Syams Zainudin, and S. Alamery, "Effect of surface treatment on mechanical, physical and morphological properties of oil palm/bagasse fiber reinforced phenolic hybrid composites for wall thermal insulation application," *Construction and Building Materials*, vol. 276, pp. 122239, 2021.
- [164] A. H. S. Nur Athirah Mohamad Radzi, and S. S. Jamari, "Structural Studies of Surface Modifeid Oil Palm Empty Fruit Bunch with Alkaline Pre- Treatment as Potential Filler for the Green Composite," *Jurnal Tribologi*, vol. 26, pp. 75-83, 2020.

- [165] T. O. Suoware, S. O. Edelugo, and I. C. Ezema, "Effect of flame retardants on flame propagation and flammability properties of oil palm fibre reinforced polyester composite," *Fire and Materials*, vol. 43, no. 7, pp. 811-820, 2019.
- [166] A. Corigliano, "Damage and Fracture Mechanics Techniques for Composite Structures," *Comprehensive Structural Integrity*, I. Milne, R. O. Ritchie and B. Karihaloo, eds., pp. 459-539, Oxford: Pergamon, 2003.
- [167] N. Saba, M. Jawaid, O. Y. Alothman, and Z. Almutairi, "Evaluation of dynamic properties of nano oil palm empty fruit bunch filler/epoxy composites," *Journal of Materials Research and Technology*, vol. 8, no. 1, pp. 1470-1475, 2019.
- [168] S. Mahalingam, V. Gopalan, H. Velivela, V. Pragasam, Prashanth, and V. Suthenthiraveerappa, "Studies on Shear Strength of CNT/Coir Fibre/Fly Ash Reinforced Epoxy Polymer Composites," *Emerging Materials Research*, vol. 9, no. 1, pp. 1-14, 2020.
- [169] L. Amoroso, E. L. Heeley, S. N. Ramadas, and T. McNally, "Crystallisation behaviour of composites of HDPE and MWCNTs: The effect of nanotube dispersion, orientation and polymer deformation," *Polymer*, vol. 201, pp. 122587, 2020.
- [170] F. Najafi, G. Wang, S. Mukherjee, T. Cui, T. Filleter, and C. V. Singh, "Toughening of graphene-based polymer nanocomposites via tuning chemical functionalization," *Composites Science and Technology*, vol. 194, pp. 108140, 2020.
- [171] N. I. Khan, S. Halder, S. Das, and M. S. Goyat, "Graphitic nanoparticles functionalized with epoxy moiety for enhancing the mechanical performance of hybrid carbon fiber reinforced polymer laminated composites," *Polymer Composites*, vol. 42, no. 2, pp. 678-692, 2020.
- [172] A. A. Tarhini, and A. R. Tehrani-Bagha, "Graphene-based polymer composite films with enhanced mechanical properties and ultra-high in-plane thermal conductivity," *Composites Science and Technology*, vol. 184, pp. 107797, 2019.
- [173] "ASTM D638-14, Standard Test Method for Tensile Properties for Plastics," ASTM International, 2014.

- [174] K. Upadhyay, R. Dwivedi, and A. K. Singh, "Determination and Comparison of the Anisotropic Strengths of Fused Deposition Modeling P400 ABS," *Advances in 3D Printing & Additive Manufacturing Technologies*, D. I. Wimpenny, P. M. Pandey and L. J. Kumar, eds., pp. 9-28, Singapore: Springer Singapore, 2017.
- [175] S. Pimenta, "Fibre failure modelling," *Numerical Modelling of Failure in Advanced Composite Materials*, P. P. Camanho and S. R. Hallett, eds., pp. 193-224: Woodhead Publishing, 2015.
- [176] P. Jiang, Y. Xing, X. Jia, and B. Guo, "Weibull Failure Probability Estimation Based on Zero-Failure Data," *Mathematical Problems in Engineering*, vol. 2015, pp. 1-8, 2015.
- [177] Q. Fu, "Bioactive Glass Scaffolds for Bone Tissue Engineering," *Biomedical, Therapeutic and Clinical Applications of Bioactive Glasses*, G. Kaur, ed., pp. 417-442: Woodhead Publishing, 2019.
- [178] K. Ono, "A Simple Estimation Method of Weibull Modulus and Verification with Strength Data," *Applied Sciences*, vol. 9, no. 8, 2019.
- [179] J. Campbell, "Solidification Structure," *Complete Casting Handbook (Second Edition)*, J. Campbell, ed., pp. 163-222, Boston: Butterworth-Heinemann, 2015.
- [180] D. G. Eskin, "Ultrasonic degassing of liquids," *Power Ultrasonics*, J. A. Gallego-Juárez and K. F. Graff, eds., pp. 611-631, Oxford: Woodhead Publishing, 2015.
- [181] Y. Gu, M. Li, Z. Zhang, and Z. Sun, "Void formation model and measuring method of void formation condition during hot pressing process," *Polymer Composites*, vol. 31, no. 9, pp. 1562-1571, 2010.
- [182] L. Wu, S. V. Hoa, and M.-T. Ton-That, "Effects of water on the curing and properties of epoxy adhesive used for bonding FRP composite sheet to concrete," *Journal of Applied Polymer Science*, vol. 92, no. 4, pp. 2261-2268, 2004.
- [183] S. Palamae, P. Dechatiwongse, W. Choorit, Y. Chisti, and P. Prasertsan, "Cellulose and hemicellulose recovery from oil palm empty fruit bunch (EFB) fibers and production of sugars from the fibers," *Carbohydrate Polymers*, vol. 155, pp. 491-497, 2017.
- [184] T. A. Negawo, Y. Polat, F. N. Buyuknalçaci, A. Kilic, N. Saba, and M. Jawaid, "Mechanical, morphological, structural and dynamic mechanical properties of

- alkali treated Ensete stem fibers reinforced unsaturated polyester composites,” *Composite Structures*, vol. 207, pp. 589-597, 2019.
- [185] D.-H. Kim, and S.-H. Park, “Evaluation of Resin Composite Translucency by Two Different Methods,” *Operative Dentistry*, vol. 38, no. 3, pp. E76-E90, 2013.
- [186] Y.-K. Lee, “Influence of filler on the difference between the transmitted and reflected colors of experimental resin composites,” *Dental Materials*, vol. 24, no. 9, pp. 1243-1247, 2008.
- [187] W. J. Cantwell, and H. H. Kausch, "Fracture behaviour of epoxy resins," *Chemistry and Technology of Epoxy Resins*, B. Ellis, ed., pp. 144-174, Dordrecht: Springer Netherlands, 1993.
- [188] M. D. Hayes, D. B. Edwards, and A. R. Shah, "Fractography Basics," *Fractography in Failure Analysis of Polymers*, M. D. Hayes, D. B. Edwards and A. R. Shah, eds., pp. 48-92, Oxford: William Andrew Publishing, 2015.
- [189] J. Berry, “The morphology of polymer fracture surfaces,” *Journal of Polymer Science Part C: Polymer Symposia*, vol. 3, no. 1, pp. 91-101, 1963.
- [190] J.-B. Kopp, and J. Girardot, “Dynamic fracture in a semicrystalline biobased polymer: an analysis of the fracture surface,” *International Journal of Fracture*, vol. 226, no. 1, pp. 121-132, 2020.
- [191] M. Ragoubi, D. Bienaimé, S. Molina, B. George, and A. Merlin, “Impact of corona treated hemp fibres onto mechanical properties of polypropylene composites made thereof,” *Industrial Crops and Products*, vol. 31, no. 2, pp. 344-349, 2010.
- [192] T. Hielscher, “Ultrasonic Production Of Nano-Size Dispersions And Emulsions,” *Dans European Nano Systems Workshop*, 2007.
- [193] L. Zeng, X. Huang, X. Li, R. Li, Y. Li, and Y. Xiong, “A gelatin-treated carbon nanofiber/epoxy nanocomposite with significantly improved multifunctional properties,” *Materials Today Communications*, vol. 24, pp. 101006, 2020.
- [194] N. Saravanan, V. Yamunadevi, V. Mohanavel, V. K. Chinnaiyan, M. Bharani, P. Ganeshan, K. Raja, and A. Karthick, “Effects of the Interfacial Bonding Behavior on the Mechanical Properties of E-Glass Fiber/Nanographite Reinforced Hybrid Composites,” *Advances in Polymer Technology*, vol. 2021, pp. 6651896, 2021.

- [195] G. Kritikos, and K. Karatasos, "Effect of Nanofiller Size on the Mechanical Properties of Poly(acrylic acid)/Graphene Oxide Nanocomposites," *Macromolecules*, vol. 54, no. 9, pp. 4164-4175, 2021.
- [196] Y. Hu, J.-L. Ding, and Y. Chen, "Effects of nanofiller geometries and interfacial properties on the mechanical performance of polymer nanocomposites—A numerical study," *Polymers and Polymer Composites*, vol. 29, no. 9_suppl, pp. S19-S35, 2021.
- [197] A. Zotti, S. Zuppolini, M. Zarrelli, and A. Borriello, "Fracture Toughening Mechanisms in Epoxy Adhesives," *Adhesives: Applications and Properties*, A. Rudawska, ed., pp. pp237-269, 2016.
- [198] R. A. Riggleman, G. Toepperwein, G. J. Papakonstantopoulos, J. L. Barrat, and J. J. de Pablo, "Entanglement network in nanoparticle reinforced polymers," *J Chem Phys*, vol. 130, no. 24, pp. 244903, 2009.
- [199] M. Mutar, "Synthesis and characterization of novel nanocomposites with nanofillers particles and their applications as dental materials," vol. 7, pp. 1512-1538, 2019.
- [200] R. Porebska, A. Rybak, B. Kozub, and R. Sekula, "Polymer matrix influence on stability of wood polymer composites," *Polymers for Advanced Technologies*, vol. 26, no. 9, pp. 1076-1082, 2015.
- [201] L. Lapčík, M. Vašina, B. Lapčíková, M. Staněk, M. Ovsík, and Y. Murtaja, "Study of the material engineering properties of high-density poly(ethylene)/perlite nanocomposite materials," *Nanotechnology Reviews*, vol. 9, no. 1, pp. 1491-1499, 2020.
- [202] K. Balani, Verma, V., Agarwal, A. and Narayan, R, "Physical, Thermal, and Mechanical Properties of Polymers," *Biosurfaces*, pp. 329-344, 2014.
- [203] R. Rahul, and R. Kitey, "Effect of cross-linking on dynamic mechanical and fracture behavior of epoxy variants," *Composites Part B: Engineering*, vol. 85, pp. 336-342, 2016.
- [204] P. Lin, Q. Xu, S. Cheng, X. Li, Z. Zhao, S. Sun, C. Peng, A. Joy, and S.-Q. Wang, "Effects of Molecular Weight Reduction on Brittle–Ductile Transition and Elastic

- Yielding Due to Noninvasive γ Irradiation on Polymer Glasses,” *Macromolecules*, vol. 50, no. 6, pp. 2447-2455, 2017.
- [205] J. B. Quinn, and G. D. Quinn, “A practical and systematic review of Weibull statistics for reporting strengths of dental materials,” *Dental materials : official publication of the Academy of Dental Materials*, vol. 26, no. 2, pp. 135-147, 2010.
- [206] D.-L. Nguyen, D.-K. Thai, T.-T. Ngo, T.-K. Tran, and T.-T. Nguyen, “Weibull modulus from size effect of high-performance fiber-reinforced concrete under compression and flexure,” *Construction and Building Materials*, vol. 226, pp. 743-758, 2019.
- [207] S. Patibanda, V. J. Nagda, J. Kalra, G. Sivakumar, R. Abrahams, and K. N. Jonnalagadda, “Mechanical behavior of freestanding 8YSZ thin films under tensile and bending loads,” *Surface and Coatings Technology*, vol. 393, pp. 125771, 2020.
- [208] J. A. Palacios, and R. Ganesan, “Reliability evaluation of Carbon-Nanotube-Reinforced-Polymer composites based on multiscale finite element model,” *Composite Structures*, vol. 229, pp. 111381, 2019.

Every reasonable effort has been made to acknowledge the owners of copyright material. I would be pleased to hear from any copyright owner who has been omitted or incorrectly acknowledge.

APPENDIX A: SUMMARY OF CRITIAL REVIEW

Authors	Method	Outcome
<p>Reyes, Larry Q. Zhang, Jane Dao, Buu Nguyen, Duc L. Varley, Russell J. [159]</p>	<p>Materials: DGEBA, DGEMF, DGEMB, BisPA, BisMA, TPE-R, and MDA.</p> <p>The resins were first degassed at 100°C under vacuum for 1 hour then mixed with its hardener at a ratio of 1:1. The mixture was then poured into its molds allow underwent multiple curing treatments; at 150°C for 2 hours, followed by 177°C for 4 hours and lastly at 205°C for 2 hours.</p>	<p>It was concluded that isopropyl linkages present in BisPA and BisMA better improves stiffness and reduces molecular mobility / segmental motion compared to methylene linkages in MDA. On the other hand, ether linkages in TPE-R reduces its mechanical performance due to the increase in flexibility, allowing greater molecular rearrangement.</p>
<p>Patterson, Brendan A. Busch, Casey E. Bratcher, Matthew Cline, Julia Harris, Doug E. Masser, Kevin A. Fleetwood, Adam L.</p>	<p>Materials: EPON 825, D230, D400, and D200.</p> <p>The resins were initially preheated to 60°C then degassed for 10 – 20 minutes under vacuum. The composite was cured at 80°C for 2 hours followed</p>	<p>It was reported that the short beam strength of D2000 and D400 were 56% and 27% higher than D230 at -60°C respectively. It was concluded that the increase in M_c improve the toughness of the polymer.</p>

Authors	Method	Outcome
Knorr, Daniel B. [160]	by 150°C for 8 hours; then fabricated Vacuum assisted resin transfer molding method. The specimens were later then cut using water jet with abrasive.	
Cheng, Teo Siew Uy Lan, Du Ngoc Phillips, Steven Tran, Le Quan Ngoc [37]	Materials: PP, PLA, DER 331, and OPEFB. Both PP and PLA composites were processed using compression molding while epoxy composite was fabricated using vacuum assisted resin infusion. The epoxy was cured at room temperature for 24 hours and underwent a post curing at 80°C for 16 hours.	It was found that the incorporation of OPEFB in epoxy matrix resulted in the most effective enhancement in longitudinal flexural strength. In addition, the epoxy composite was given the highest efficiency factor followed by PLA and PP. It was concluded that OPEFB was only an effective filler when accompanied by PLA and epoxy as PP resulted in poor interfacial adhesion and poor wetting on OPEFB.
Xiao Wang, Xi Yuan, MingLiang Wu, Feng Gao, Xuemei Yan, Kechao Zhou, Dou Zhang [161]	Materials: Araldite 2020, DP460, and DP490. Piezoelectric fiber was filled with the resin to form the composite layer, undergoing a cure at 80°C for 2 hours. It was then	It was reported that the high viscosity of DP490 made it difficult to uniformly fill the fiber even after subjected to a vacuum environment. It can be concluded that the fluidity of an epoxy resin can affect the drive

Authors	Method	Outcome
	thinned to 200µm with a lapping machine. During the encapsulation process, the sample was heated to 80°C and kept for 0.5 hours using a self-made packaging platform.	performance of piezoelectric composite due to the presence of air.
Jagtap, Siddheshwar B. Ratna, Debdatta [141]	Materials: LY556, D400, D600, ED900, and Nanoclay The nanocomposite was prepared by mixing 3 wt% modified clay in acetone and epoxy resin. The mixture was sonicated for 20 minutes using a probe sonicator and degassed for 10 minutes.	It was found that composite with higher molecular weight curing agent displayed better dispersion with better platelets separation. However, it significantly reduces its tensile strength and modulus. In conclusion, higher molecular weight curing agent results in better dispersion and elongation a break.
Tabatabaeian, Ali Ghasemi, Ahmad Reza [162]	Materials: ML506, KER 822, MWCNT, and E glass fiber The composites were fabricated using hand lay-up method. The incorporated glass fibers were cut with arbitrary dimension.	The addition of MWCNT was shown to reduce the curvature of the laminate with the epoxy system of lower density and viscosity. It was concluded that each epoxy system has distinctive properties and curing reactions and further investigation is required. In

Authors	Method	Outcome
		<p>addition, the presence of nanoparticles was shown to reduce the weight loss percentage of the nanocomposite after being subjected to thermal cycle fatigue condition.</p>
<p>Ramlee, Nor Azlina Jawaid, Mohammad Zainudin, Edi Syams Yamani, Shaikh Abdul Karim [163]</p>	<p>Materials: OPEFB, SCB, Silane, Hydrogen Peroxide, and Distilled Water</p> <p>The fibers are treated using 2% v/v silane and 4% v/v hydrogen peroxide, it is then repeatedly washed with water until a pH value of 7 is achieved. The fibers were then kept in distilled water for 24 hours before being dried at 100°C. The composites were fabricated using the hand lay-up method and compressed using hot press molding machine.</p>	<p>It was reported that silane treated composites displayed better tensile strength compared to hydrogen peroxide treated composite. In addition, silane treated composites displayed lower void content as compared to hydrogen peroxide treated. Lastly, SCB composites displayed lower void content compared to OPEFB composites.</p>

Authors	Method	Outcome
<p>Chaiwong, Wantani Samoh, Nabil Eksomtramage, Theera Kaewtatip, Kaewta [119]</p>	<p>Materials: Wheat Gluten, NaOH, and OPEFB</p> <p>The raw palm fiber was first washed thoroughly then soaked in 90°C water for 90 minutes to remove residual surface materials such as waxes and hemicellulose. The hot water treated fibers were then soaked in NaOH solution (1 w/v% and 5 w/v%) in room temperature for 2 hours followed by a wash with distilled water. All treated fibers were then dried in a hot oven at 105 °C for 24 hours. Finally, these fibers were cut and were passed through a 250um sieve. Wheat -gluten bioplastic and fillers were mixed for 3 minutes in a two-roll mill at room temperature. The mixtures were then heated for 3 minutes at 140°C then compressed for 7 minutes using compression molding machine with 300 Pa of pressure at 140°C.</p>	<p>It was found that the use of alkali treatment eliminates natural oil, waxes, pectin and hemicellulose which prevents the interactions between the hydroxyl group and the matrix. In addition, fibers treated with 5 w/v% NaOH solution presented a rougher surface compared to 1 w/v% NaOH solution. The rougher surface of the fiber improved the wetting ability with the matrix and allowed the effect of mechanical interlocking to take place. Furthermore, it was reported that the composite loaded with 15 wt% palm fibers treated with 5 w/v% NaOH resulted in the highest reinforcement when compared to hot water treated and 1 w/v% NaOH.</p>

Authors	Method	Outcome
<p>Nur Athirah Mohamad Radzi, Azizul Helmi Sofian, Saidatul Shima Jamari [164]</p>	<p>Materials: OPEFB, and NaOH.</p> <p>The fibers were soaked in NaOH solution for 99 minutes and underwent an ultrasonic bath at 80°C. It was then washed with deionized water and dried at 70 °C for 8 hours. Lastly, the fibers were then sieved to the length between 2 – 5mm.</p>	<p>It was found that using 1 to 3 w/v% NaOH, large sum of silica remains present in the fibers. By increasing the concentration to 4 and 5 w/v% NaOH, silica components were found to be completely removed. At 5 w/v% NaOH, a rougher fiber surface of OPEFB was observed as hemicellulose components were removed.</p>
<p>Ahmad, Ahmad F. Abbas, Zulkifly Obaiys, Suzan J. Zainuddin, Mohamad Faiz [39]</p>	<p>Materials: OPEFB, and Polycaprolactone</p> <p>The fibers were washed with distilled water for 24 hours then dried in an oven at 80°C. The dried fibers are crushed then sieved through a 250 µm laboratory test sieve. The matrix and filler were mixed for 20 minutes using a blending machine then preheated for 10 minutes at a temperature of 80°C. The composites were then allowed a breathing time for 10s to release</p>	<p>It was reported that the highest elongation and tensile strength were achieved with a filler loading of 12.2 %. Further increase in filler loading was shown to reduce the tensile strength and elongation of composites, where it was attributed to the weak interfacial interactions.</p>

Authors	Method	Outcome
	bubbles before being pressured for 10 minutes under 100kg/cm ² and allowed to cool at room temperature.	
Richard, Beatrice Dimah Wahi, Azizah Nani, Rozie Iling, Elisha Osman, Shahril Ali, Dayang Siti Hazimmah [38]	<p>Materials: Oil Palm Frond, and Urea Formaldehyde.</p> <p>The fiber and polymer matrix were mechanically stirred until homogenous. The mixture was then poured into a mold followed by undergoing hot press process at 5 MPa. The composites were hot pressed for 1200s at 175 °C then cold presses for 1200s at 28 °C.</p>	It was concluded that additional 10.0 wt% (at 50 wt%) untreated oil palm frond into its urea formaldehyde composite has been reported to increase its tensile strength and flexural strength by 40.0 % and 2.5% respectively. The authors indicated that use of untreated fibers and poor dispersion may have contributed to the low mechanical properties of the composite as fiber breakage / pullout
Suoware, Timine O. Edelugo, Sylvester O. Ezema, Ikechukwu C. [165]	<p>Materials: Polyester, NaOH, and OPEFB</p> <p>The fibers were first washed using hot water then soaked in n-Hexane for 12 hours. The fibers were then treated with 5% NaOH solution for 2 hours</p>	The inclusion of 10.0 wt% fiber loading has shown to increase the composites' impact strength by 22.3 % and reduce their flame propagation by 10.5 %. In addition, the inclusion of aluminium tri-hydroxide (ATH) into the composite has also

Authors	Method	Outcome
	<p>and washed with distilled water before being dried under the sun for 3 days. The composites were fabricated using hand layup compression molding.</p>	<p>shown to lower its impact strength.</p>
<p>Azlina Ramlee, Nor Jawaid, Mohammad Abdul Karim Yamani, Shaikh Syams Zainudin, Edi Alamery, Salman [163]</p>	<p>Materials: OPEFB, SCB, and Phenolic Resin, OPEFB fiber was dried in the oven at 40°C for 24 hours. On the other hand, SCB was immersed in tap water for 24 hours then rinsed with hot water. SCB fiber was then dried in the oven at 60 °C for 48 hours before being crushed to size of ~13mm. Fiber and fillers were mixed manually for 15 minutes before being spread into the mold. The composites were then compressed for 10 minutes at 150 °C with a pressure of 40 tons. It was later then cold pressed for 5 minutes before being cut.</p>	<p>It was found that pure OPEFB fiber composite displayed better tensile strength and tensile modulus compared to pure SCB fiber composite. However, OPEFB fiber composite showed higher water absorption, resulting in greater thickness swelling. The authors have also reported that the use of untreated fiber results in weak dispersion and adhesion as impurities on the surface of the fiber present a difficulty for the resin to cover it.</p>

Authors	Method	Outcome
Saba, N. Jawaid, M. Alothman, Othman Y. Almutairi, Zeyad [167]	Materials: OPEFB, DER 331 and Jointmine 905-3S. The nanocomposites were fabricated using the hand lay – up technique. The resin was mixed with nano OPEFB using a high-speed mechanical stirrer for 60 minutes.	It was reported that the addition of 3 % nano OPEFB filler composite was the most effective as it improved the storage modulus and loss modulus. In addition, the use of nano OPEFB in the composites has also been shown to lower its damping factor as it restricts the polymeric chain movement. Furthermore, Agglomerations and voids in the composites evident at higher filler loading.
Mahalingam, Sivakumar Gopalan, Venkatachalam Velivela, Hemanth Pragasam, Vignesh Prashanth, Suthenthiraveerappa, Vimalanand [168]	Materials: LY556, coir fiber, CNTs, and Fly Ash. CNT were first added with the epoxy then stirred for 1 hour with the use of a mechanical stirrer. Coir fibers and fly ash were then added to mixture and stirred again for 1 hour. It was later poured into the mould and cooled at room temperature.	It was found that with increasing content of CNT in 1 wt% of coir fiber and fly ash composite, it decreases its shear modulus. In addition, the increase in coir and fly ash result in higher shear modulus while the increase of CNT only marginally improves its.

Authors	Method	Outcome
<p>Amoroso, Lorena Heeley, Ellen L. Ramadas, Sivaram Nishal McNally, Tony [169]</p>	<p>Materials: HDPE and MWCNT.</p> <p>HDPE pellets were first grounded to fine powder and dried in a vacuum over at 40 °C for 12 hours. The powders were then mixed with MWCNT before being fed to a 16mm co – rating parallel twin – screw extruder; between the temperature of 135 °C to 155 °C a speed of 100 rpm. The extruded strands were made into pellet form and dried for 8 hours. The standard dumbbell shaped tensile bars were fabricated using piston injection mold system at a temperature of 160 °C, pressure of 450 bar and mold temperature of 50 °C.</p>	<p>It was found that the addition of MWCNT up to 0.5 wt% resulted in reduced tensile strength, indicating that polymer chains stretched in the direction of the applied load. The addition of 3 wt% MWCNT resulted in the highest tensile strength. The presence MWCNT - polymer network formed a high resistance for the polymer chain to orientate, stiffening the matrix.</p>
<p>Najafi, Farzin Wang, Guorui Mukherjee, Sankha Cui, Teng Filleter, Tobin</p>	<p>Materials: Graphene and PMMA.</p> <p>Graphene samples underwent UV/Ozone treatment for a duration of</p>	<p>It was found that higher functionalization degree leads to an excessively strong interfacial bonding, induces greater rigidity that ultimately results in higher</p>

Authors	Method	Outcome
Singh, Chandra Veer [170]	0.5 hours up to 5 hours. It is later then exfoliated then deposited on a silicon wafer with 300 nm thick oxide layer. The silicon wafer was then spin coated with PMMA which was later then soaked in NaOH solution to etch the silicon oxide.	brittle behavior. 1 – 2 hours of treatment was reported to result I higher concentration of hydroxyl groups on the graphene. However, longer duration of treatment imparts the reduction of oxidized graphene, decreasing the presence of hydroxyl groups.
Kilic, Ugur Sherif, Muhammad M. Ozbulut, Osman E. [140]	Materials: GNP, 635 Thin Epoxy System and EPOTUF 37-40. The use of ultrasonication and high shear mixing were used for the dispersion of GNPS. The samples were prepared by mixing the 0.25% nanofiller in both epoxy system using a probe sonicator at 40% amplitude for a duration of 30 minutes, 1 hours, 2 hour and 3 hours. The “ductile epoxy” was degassed inside a vacuum oven at 90 C for 20 minutes whereas	It was found that the increase is sonication time resulted in a decrease of particle size of GNPs. In addition, dispersing GNP into the hardener resulted in lower tensile properties. It was reported that only 0.25 % GNP in “brittle epoxy” increased the tensile strength and the longer sonication duration of 2 hours only marginally improved it. On the other hand, the tensile strength of ductile epoxy composite increased with increasing GNP content up to 1% loading and higher loading decrease its strength. In contrast to the brittle epoxy, higher

Authors	Method	Outcome
	<p>“brittle” epoxy did not undergo degassing as it resulted in foams.</p>	<p>tensile strength was achieved with the shorter sonication duration at 1% GNP in ductile epoxy.</p>
<p>Khan, Nazrul Islam Halder, Sudipta Das, Subhankar Goyat, Manjeet S. [171]</p>	<p>Materials: GrNP, LY 556, HY906, Epichlorohydrin and Carbon Fiber GrNP) at 0.5 wt% of epoxy resin were blended with the curing agent via 1500 rpm high speed mechanical agitator for 15 minutes, followed by then sonication at 60% amplitude for 1 hour. The resin and accelerator were later then added into the mixture and blended once more for 15 minutes. The end mixture was then degassed and poured into a silicon mold. Precuring and post curing were carried in an oven at 120°C for 2 hours and 160°C for 8 hours respectively.</p>	<p>It was found that the addition graphene increased the tensile strengths of composites as compared to neat epoxy. The effect of functionalization improved its tensile performance with the use P- GrNP, followed by E- GrNP, and the highest with G- GrNP. These improvement in strength in attributed better interaction between filler and matrix as the fillers restricts the crack propagation along the crack path. Furthermore, surface functionalization of the GrNP instilled stronger interfacial adhesion between the filler matrix and dispersion of fillers. Thus, improving the loading transferability, resulting in superior strength.</p>

Authors	Method	Outcome
<p>Tarhini, A. A. Tehrani-Bagha, A. R. [172]</p>	<p>Materials: GNF, PVDF-HFP and DMF.</p> <p>The composite films were fabricated using simple film formation process.</p> <p>The matrix was first dissolved in hot DMF while GNF were dispersed in DMF with varying content via sonication at 35 °C for 35 minutes. The solutions were the mixed using a magnetic stirrer until the exact volume of graphene was obtained; every 5 minutes 2 ml of GNP dispersion was added into 25ml of PVDF – HE. The whole solution was stirred for an additional 10 – 15 minutes before being poured into a silicon mold. It was later then placed in an oven at 90 °C for 24 hours.</p>	<p>It was found that increasing concentration of GNF in the composite improves its tensile strength. In addition, the composite films presented high electrical conductivity due to the presence of graphene layers.</p>

APPENDIX B: SUMMARY OF WEIBULL ANALYSIS

Matrix (Classification)	Tensile Strength (MPa)	P	$\ln \left[\ln \left[\frac{1}{1 - P_f(\sigma)} \right] \right]$	$\ln[\sigma]$
Tarbender (Low)	43.793	0.1	-2.250367327	3.779473987
	49.317	0.3	-1.030930433	3.898268849
	53.748	0.5	-0.366512921	3.984306457
	54.882	0.7	0.185626759	4.005185426
	60.853	0.9	0.834032445	4.10846112
EpoxAmitte 102 (Medium)	48.541	0.1	-2.250367327	3.8824088
	49.159	0.3	-1.030930433	3.8950599
	49.600	0.5	-0.366512921	3.9039908
	50.126	0.7	0.185626759	3.9145398
	50.241	0.9	0.834032445	3.9168314
E-132 (High)	56.047	0.1	-2.250367327	4.02619062
	59.616	0.3	-1.030930433	4.08792399
	59.763	0.5	-0.366512921	4.09038674
	59.855	0.7	0.185626759	4.09192497
	60.204	0.9	0.834032445	4.0977388